In presenting the dissertation as a partial fulfillment of the requirements for an advanced degree from the Georgia Institute of Technology, I agree that the Library of the Institute shall make it available for inspection and circulation in accordance with its regulations governing materials of this type. I agree that permission to copy from, or to publish from, this dissertation may be granted by the professor under whose direction it was written, or, in his absence, by the Dean of the Graduate Division when such copying or publication is solely for scholarly purposes and does not involve potential financial gain. It is understood that any copying from, or publication of, this dissertation which involves potential financial gain will not be allowed without written permission.

_____

_____

7/25/68

EFFECTS OF STRAIN RATE ON MECHANICAL PROPERTIES OF METALS IN THE PRESENCE OF STRESS CONCENTRATORS

A THESIS

Presented to

The Faculty of the Graduate Division

by

Hugh Stephen Pearson

In Partial Fulfillment

of the Requirements for the Degree

Master of Science in Metallurgy

Georgia Institute of Technology

June, 1969

EFFECTS OF STRAIN RATE ON MECHANICAL PROPERTIES OF METALS
IN THE PRESENCE OF STRESS CONCENTRATORS

Approved:

Chairman

Date approved by Chairman: May 29-69

ACKNOWLEDGMENTS

The research described herein was funded by Lockheed-Georgia Company Independent Research Authorization 2320. The investigation was conducted with the guidance of the Department of Metallurgy, Georgia Institute of Technology, and was in partial fulfillment of the requirements for a Master of Science in Metallurgy degree. The author is indebted to Dr. E. E. Underwood, Associate Director of Research, Materials Sciences of Lockheed-Georgia Company, for his interest and support, and to J. S. Owens and D. D. Stamps also of Lockheed-Georgia Company, and to Dr. P. F. Packman of Vanderbilt University, for their many helpful comments. The author also expresses his thanks to Dr. Niels N. Engel, his thesis advisor, for his help and inspiration, and to Dr. E. A. Starke, Jr. and Dr. B. G. LeFevre, members of the reading committee.

TABLE OF CONTENTS

TABLE OF CONTENTS (Continued)

LIST OF TABLES

LIST OF FIGURES

LIST OF FIGURES (Continued)

LIST OF FIGURES (Continued)

LIST OF FIGURES (Continued)

LIST OF SYMBOLS

P - Applied load

Ψ - Cross sectional area

σ - Engineering stress, $\frac{P}{\Psi}$

σ_{tu} - Ultimate tensile stress

σ_{ty} - Yield stress determined by the 0.2 percent offset method

σ_{lty} - Stress at the lower yield point

σ_{uty} - Stress at the upper yield point

σ_{max} - Peak local stress

σ_{nom} - Average stress

σ_c - Stress required for failure

σ_f - Value of σ_{nom} required for failure

ϵ - Strain, change in gage length/initial gage length

$\dot{x}$ - Rate of change of x

Δx - Change in x between two designated values

φ - A critical value of the Zener-Holloman parameter

σ^* - A critical value of stress above which brittle failure occurs

^oF - Degrees Fahrenheit

^oK - Degrees Kelvin

RT - Room temperature

KSI - 1000 pounds per square inch

NSR - Notch strength ratio, $\frac{\sigma_f}{\sigma_{tu}}$

pcf - Plastic constraint factor, $\frac{\sigma^*}{\sigma_{ty}}$ (corrected for rate effect)

K_t - Stress concentration factor, $\frac{\sigma_{max}}{\sigma_{nom}}$

K_{Ic} - Plane strain stress intensity factor, defined in Appendix A

B - Thickness of material

T - Temperature

T_D - Ductile-brittle transition temperature

A - Constant

D - Diameter

F - Frequency factor

K_p - Plastic stress concentration factor, Equation (6)

E_s - Secant modulus at maximum load

E - Modulus of elasticity

$\dot{\epsilon}_p$ - Plastic strain rate, $K_p \dot{\epsilon}$

SUMMARY

The behavior of materials subjected to various strain rates and stress concentrations was studied by means of tensile tests on smooth and notched specimens of 1010 steel, a known strain-rate-sensitive material, and 7075-T6 aluminum alloy, a rate-insensitive material. Specimens containing stress concentrators (K_t = 1,2,6, and 13) were tested at universal testing machine head travel rates between 0.002-inch per minute and 3000 inches per minute. Graphs of mechanical properties versus stress concentration factor and versus the logarithm of the head travel rate are presented for each material. It has been verified that the lower yield point of mild steel varies linearly with the logarithm of strain rate for particular regions of the temperature-strain rate spectrum, and it was found that other mechanical properties behave similarly. The linear dependency of strength properties versus log of strain rate also applies for the aluminum alloy.

Mechanical property data, plotted as a function of stress concentration factor, appear to be an indication of the rate sensitivity of a material. That is, if a strengthening effect results from a notch, the material should exhibit a higher failure load with increasing strain rate, and if the notch causes a reduction in a mechanical property, an increasing strain rate will further reduce the property. It is proposed that mechanical property data as a function of stress concentration and strain rate be obtained and used in design, since these variations are not predictable from existing material properties.

The rate dependency of a mechanical property can be small enough to be obscured by scatter in the test data.

CHAPTER I

INTRODUCTION

In 1909, Ludwik[1] reported an empirical logarithmic dependence of yield strength upon strain rate. Numerous research and development programs have since been conducted to develop theories or to collect data for use in design under varying strain rates. Although many theoretical questions remain unanswered regarding the phenomena of strain rate effects, there are sufficient data available to determine empirically the strain rate sensitivity of most engineering materials under simple stress conditions.

The following conclusions are generally accepted:

1. Strain-rate sensitivity changes with test temperature and usually displays minimum sensitivity at an elevated temperature[2].

2. While the tensile strength of pure aluminum varies logarithmically with strain rate ($\sigma_{tu} \propto \log \dot{\epsilon}$), some heat-treated aluminum alloys demonstrate a linear variation[3,4]. The alloy 7075-T6 is essentially unaffected by changes in strain rate.

3. Low-strength steels appear to be more strain-rate-sensitive than high-strength steels[2,5,6].

4. The strain-rate sensitivity of titanium and titanium alloys follows a logarithmic relationship, $\sigma_{tu} \propto \log \dot{\epsilon}$, with pure titanium and annealed alloys being the most sensitive[7].

5. The strain-rate sensitivity of beryllium is complex. A re-

duction in stress with increasing strain rate is attributed to notch sensitivity[8].

Curves showing the typical strain-rate dependency of materials are shown in references 7, 9, and 10 for titanium alloys, aluminum alloys, and general metallics.

The materials designer is faced with two conflicting facts. First, he must design his structure using as little material as possible, both for economy and efficiency of operation; and second, he must ensure that the part will function satisfactorily through the anticipated lifetime. This is normally accomplished by using standard design methods and material properties as presented in documents such as Military Handbook 5[11]. Present design handbocks are lacking in any methods of treating rate of loading. Since most engineering materials are believed to be strengthened by increasing loading rate, it is common to neglect strain rate effects. Cowell[12] recommends this design philosophy for 6061-T6, 6065-T5, and 5456-H321 aluminum alloys.

This problem is made more complex when the material has stress concentrators that perturbate the local stress state. Designing to compensate for the presence of notches is a well known technique[13] (discussed in Chapter II). For conventional materials containing mild notches, any design using this procedure will be conservative. However, this conservative design only applies to materials subjected to nominal loading rates. When high strain rates are encountered the design may not be conservative.

Previous research in this area has been limited to conventional impact tests which are usable only in comparing materials, and precracked

tests analyzed by fracture mechanics. There is no way at present to combine stress concentration theory with strain rate behavior to predict mechanical behavior under combinations of these conditions. These conditions do occur, for example, in landing gears of aircraft. Therefore, it is necessary to determine the mechanical behavior of materials containing stress concentrators subjected to high rates of loading to insure that adverse combinations of these conditions will not cause failure. Two materials representing the extremes in strain-rate sensitivity were selected for evaluation. These materials are 1010 cold-rolled steel which is strain-rate sensitive, and 7075-T6 aluminum which is insensitive to changes in strain rate. Edge-notched tensile specimens were tested in universal testing machines at head-travel rates between 0.002-inch and 3000 inches per minute. The mechanical properties were evaluated versus the loading rates and stress concentration factors.

CHAPTER II

THEORY

To understand the combination of strain rate and stress concentration, three general areas must be discussed: (1) stress concentration theory, (2) temperature influence, and (3) strain rate effects. It is also helpful to understand linear elastic fracture mechanics (i.e., stress analysis of a material containing a crack) since fracture mechanics parameters are affected by strain rate variations. A brief discussion of this subject is presented in Appendix A.

Stress Concentration

Consider a large plate of uniform thickness under uniaxial loading. The nominal stress is given by the usual engineering expression, $\sigma = \frac{P}{\Psi}$, where Ψ is the cross-sectional area normal to the load P. This stress is distributed uniformly throughout the width of the plate. If a small hole is cut in the center of the plate, the local stress distribution in the vicinity of the cutout is changed. At distances far from the discontinuity, the stresses remain essentially the same as those found before the hole was cut. The introduction of a discontinuity in the plate produces a localized concentration of stresses in the vicinity of the cutout. The ratio of the peak local stress σ_{max}, to the average stress σ_{nom}, is defined as the elastic stress concentration factor, K_t:

$$K_t = \frac{\sigma_{max}}{\sigma_{nom}} \quad , \tag{1}$$

where

σ_{max} = maximum stress at the crack tip

σ_{nom} = stress determined from elementary formulas.

The theoretical analysis of K_t values for general discontinuities involves finding a solution for the Airy stress function that satisfies the boundary conditions at the discontinuity and at the points of loading. Neuber[14] and Savin[15] published comprehensive theoretical analyses for many common configurations. Most of the analyses involve lengthy calculations primarily because of the difficulty involved in formulating the boundary conditions on the periphery of the cutout. Frocht[16] and Durelli and Riley[17] have written books on techniques, and Peterson[13] has compiled solutions for numerous commonly used discontinuities into the most complete single source for stress concentration factors.

If failure occurs prior to yielding, Equation (1) is valid up to failure, and σ_{max} can be equated to the stress required for failure σ_c. The nominal stress that would cause failure, σ_f, is calculated for any K_t value from Equation (1):

$$\sigma_f = \frac{\sigma_c}{K_t} \quad . \tag{2}$$

The notch strength ratio, NSR, is defined as follows:

$$NSR = \frac{\sigma_f}{\sigma_{tu}} \quad , \tag{3}$$

where σ_{tu} is the ultimate tensile strength of the unnotched material.

Substituting for σ_f from Equation (2),

$$NSR = \frac{\sigma_c}{K_t \sigma_{tu}} \quad . \tag{4}$$

For ideally brittle materials, $\sigma_c = \sigma_{tu}$; consequently, the NSR for an ideally brittle material equals $\frac{1}{K_t}$.

Since engineering materials are normally ductile, when σ_{max} reaches the proportional limit plastic deformation occurs at the notch tip and the stress state becomes more complicated. Although many excellent references are available, the plasticity theory is not sufficiently developed to account for the deviations from $\frac{1}{K_t}$ observed in engineering materials. One method of accounting for plasticity in the presence of discontinuities is to determine NSR experimentally as a function of K_t for the material, thus effectively modifying the elastic K_t value. Sachs and Sessler[18] developed curves of this type (see Figure 1) and showed that many conventional materials are actually strengthened by mild notches when compared with $\frac{1}{K_t}$. Packman[19] showed that a brittle alloy of titanium behaved according to the $\frac{1}{K_t}$ curve in Figure 1. Therefore, the failure stress of a part can be established by determining the K_t associated with the geometry of the part and using the experimental NSR versus K_t curve to determine when that K_t will cause the part to fail.

Theoretical K_t determination is for a two dimensional configuration, i.e., thickness is not considered. Also, only relative dimensions enter into the calculations; actual size is not considered. These factors do not affect the value of the theoretical elastic stress concentration

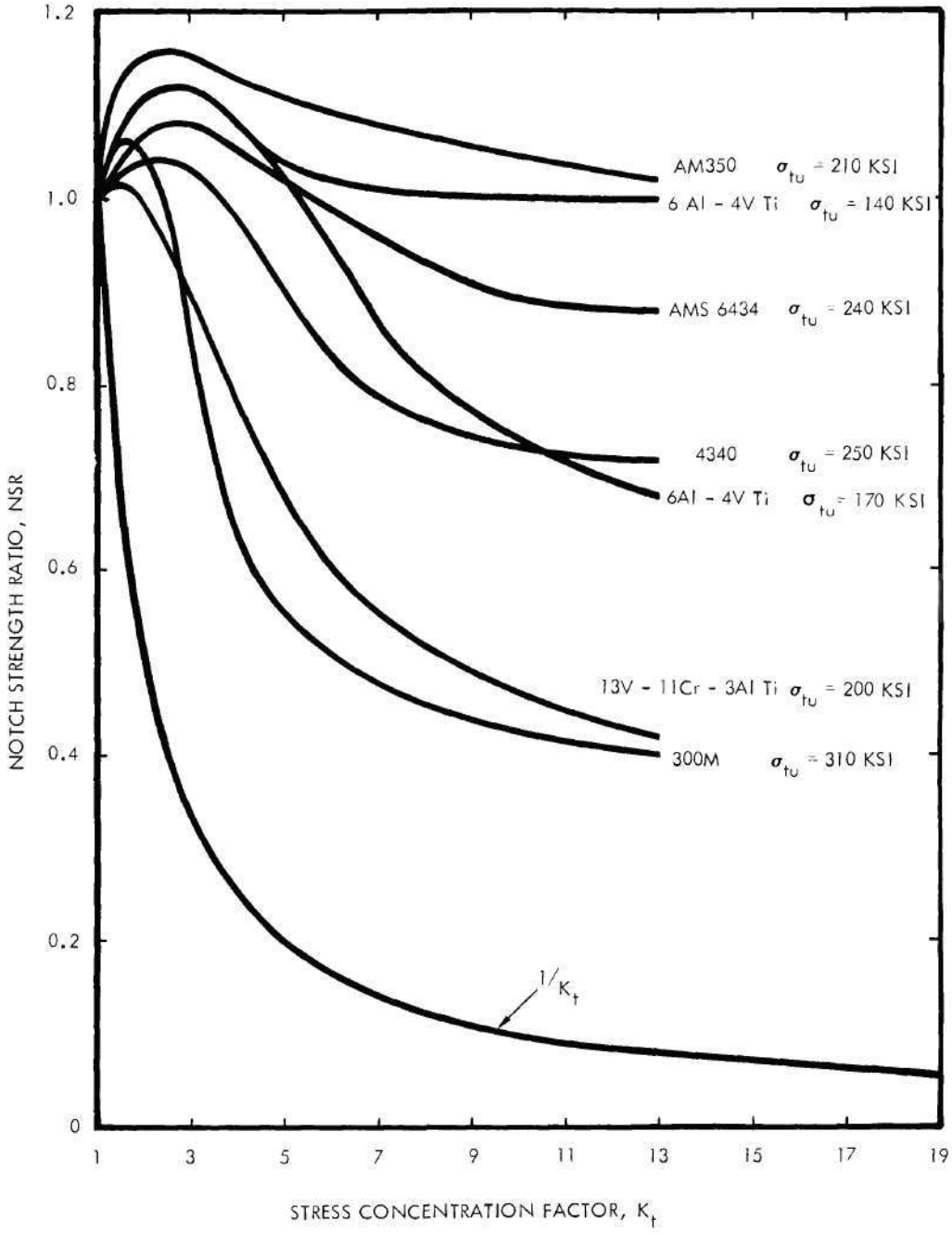

Figure 1. Effect of Stress Concentration on Notch Strength Ratio of 0.0063-inch Thick Sheet Specimens of Several Titanium Alloys and Steels at Room Temperature (From Sachs and Sessler[18])

factor given only in terms of the geometry but have a complicated effect on the actual failure behavior. Weiss, et al.[20] reported significant reductions in the NSR value with constant K_t as the specimen width increased.

The thickness of the specimen influences the stress condition at the notch tip, and consequently the failure stress. The thickness effect is discussed more thoroughly in Appendix A, Lindear Elastic Fracture Mechanics. These geometrical variables must be taken into consideration when the designer is using NSR as a function of K_t.

Temperature Influence and Strain Rate Effects

In 1944 Zener and Holloman[21,22,23,24] suggested that the effect of temperature and strain rate were related. Trozera, Sherby, and Dorn[3] showed that identical stress-strain curves are obtained for constant values of the Zener-Holloman parameter within a given range of strain rate and temperature. The activation energy calculated agreed with the self-diffusion activation energy for their test material. Above a critical value of the Zener-Holloman parameter, φ, the activation energy appeared to decrease with increasing strain rate. It was suggested that several different mechanisms were contributing to the yielding process. They further suggested that the controlling mechanism below this critical value φ was dislocation climb.

Considerable effort has been expended on determining the dislocation mechanisms that apply to the temperature-strain rate effects[25-30]. Some dislocation mechanisms can account for at least part of the effects observed as a function of temperature and strain rate. Rosenfield and Hahn[30] suggest that at least three different types of flow mechanisms and

two different types of fracture mechanisms are operating in the strain rate range between 10^{-4} to 10^{4} sec^{-1} for temperatures between 0° and $300^{\circ}K$. Four characteristic regions of mechanical response were proposed for plain carbon steels (see Figure 2).

Region I: Ambient temperatures and conventional testing speeds. In this region the strain rate effect is small. The controlling mechanism suggested is the edge dislocation mobility. The type of fracture is that normally seen in cup and cone failures.

Region II: Temperature $\gtrsim 100^{\circ}K$ and strain rates between 10^{-1} and 10^{5} sec^{-1}. Here the yield stress is more strain-rate-dependent, but this strain-rate dependency is apparently independent of the temperature. The motion of screw dislocations limited by the Peierls stress and thermally aided kink nucleation was proposed as the strain rate controlling process. Fracture is more brittle, but cup and cone fractures are still shown with brittle behavior in the lower temperature region.

Region III: Temperature 0° to $170^{\circ}K$ and strain rate between 10^{-4} and 10^{5} sec^{-1}. The yield stress is characterized by a diminished strain rate and temperature dependence. Fracture is brittle cleavage. Twining deformation was suggested as the controlling mechanism. The negative temperature and strain-rate dependency of the critical twining stress, and metallographic evidence of twining at the onset of Region III tend to support this suggestion.

Region IV: Strain rates $\gtrsim 10^{5}$ sec^{-1}. This region is more difficult to discuss, primarily because of the problems involved

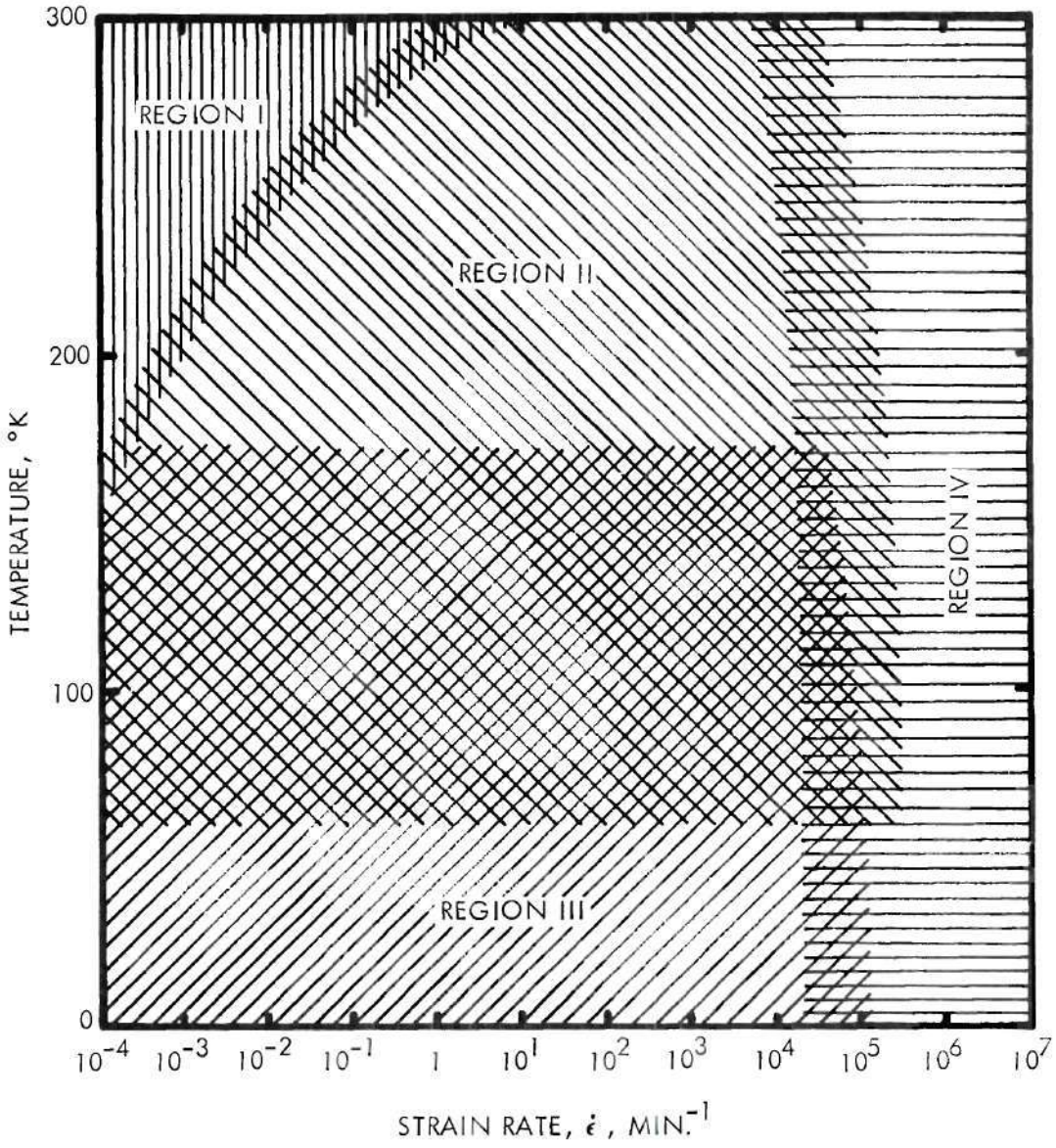

Figure 2. Regions of the Temperature-Strain Rate Spectrum of Low Carbon Steel that Reflect Different Mechanisms of Yielding (From Rosenfield and Hahn[30])

in instrumenting tests, and the limited number of tests available. Extreme strain-rate sensitivity appears to characterize this region. Glass, et al.[31] reported that dislocations could not move with velocities required for them to keep up with the passage of a shock pulse; consequently, dislocations probably played no important role in the deformation of metals under high intensity shocks. Dorn, Mitchell, and Hauser[32] discuss dislocation damping processes which occur as a result of high-velocity shock waves and suggest that these processes become limiting when the dislocation velocity becomes very high.

The approach of Rosenfield and Hahn is very promising in developing useful engineering data relating the effect of temperature and strain rate on mechanical properties of materials. They plotted $\Delta\sigma_{lty}$ as a function of ln $\dot{\epsilon}$, where $\Delta\sigma_{lty}$ is the difference in tensile lower yield strength for specimens tested at the experimental rate and a nominal rate. Several empirical formulations were evaluated in an attempt to determine which was best suited to describe the observed relationship. They found that the Zener-Holloman temperature-independent equation best fit the test data in either Region I or Region II (Figure 2). In Region II, the fit was not very accurate and extrapolations to absolute zero yielded values that were infinite. The final result was a series of semi-empirical equations, one describing the behavior in each region. Each equation predicted a linear relationship within the regions. The available deformation theories could not predict the rate sensitivity from other material properties without the use of experimentally determined constants.

This method of presenting rate sensitivity data (stress as a func-

tion of the logarithm of strain rate) has been used by many researchers (references 2, and 6 through 10), although most data are simply in the form of curves rather than equations.

Leslie and Sober[33] use the semi-logarithmic strain rate relationship as suggested by Rosenfield and Hahn[30] to evaluate the flow stress of ferritic and martensitic steels. They report a wide range of slopes for the steels tested, including some negative slopes. In most cases, a change in the strain rate sensitivity occurred within their evaluation range of 10^{-1} to 10^{-4} sec^{-1}.

Combination of Stress Concentration, Temperature Influence, Strain Rate Effects, and Linear Elastic Fracture Mechanics

Rosenfield, Votava, and Hahn[34] present a detailed summary of the current knowledge of the interaction of these various parameters. Data from Knott[35], Gilbert and Wilcox[36], and Hendrickson, Wood, and Clark[37] are offered in support of a failure criterion based on a critical stress, σ^*, which is more dependent on relaxation, microstructure, and slip mode than on temperature and strain rate effects. The data of Gilbert and Wilcox (shown in Figure 3) show that brittle failures occur above a certain stress level, and ductile failures occur below this stress level. These data were obtained using three different strain rates and several temperatures. Therefore, the concept of a critical stress, independent of temperature and strain rate appears reasonable.

To understand the combined effect of temperature, stress concentration, and strain rate on the behavior of a material, consider first a smooth bar (K_t=1) tested at different temperatures with a constant strain rate. The yield stress, plotted versus temperature, increases

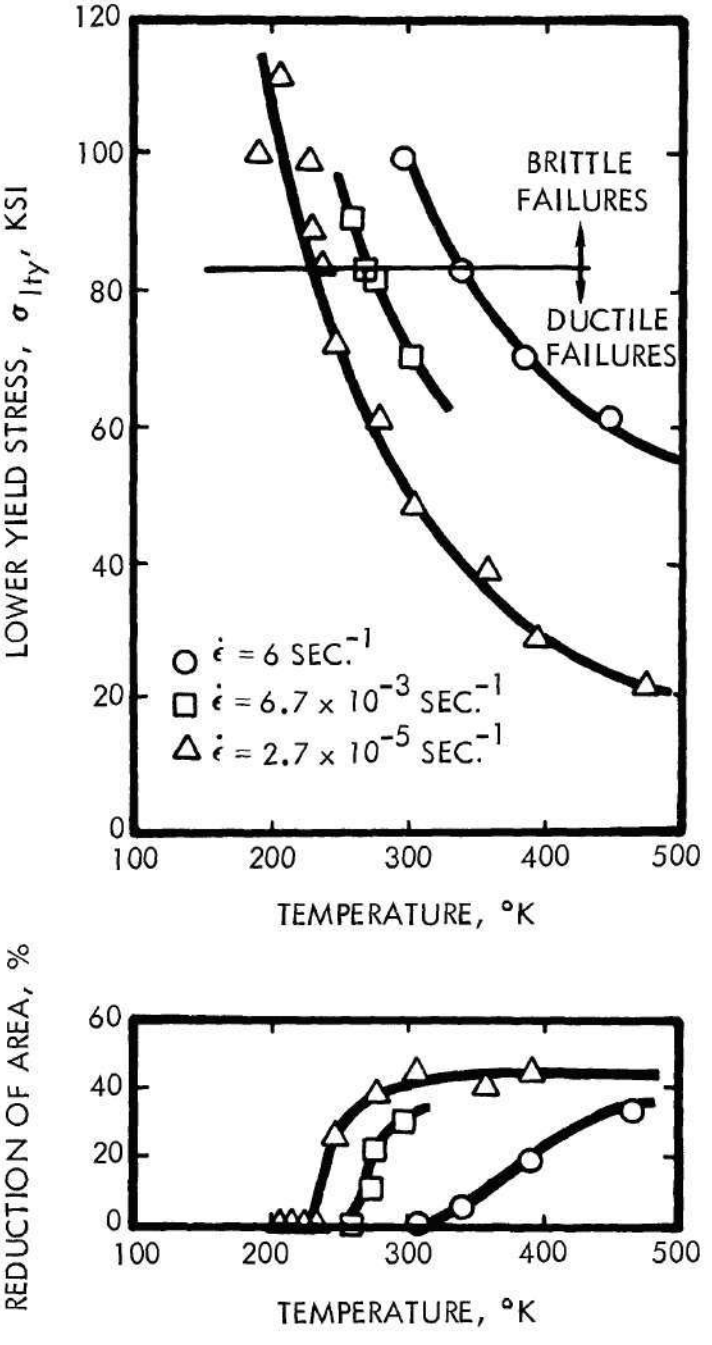

Figure 3. Variation of Lower Yield Stress of Mild Steel with Temperature and Strain Rate Compared with Variation of Reduction of Area Measurements on the Same Specimens (From Gilbert and Wilcox[36])

with decreasing temperature. This is shown schematically in Figure 4a. Below some temperature value or above some σ_{ty} value, the failure mode changes from ductile to brittle. This degree of ductility at fracture is depicted on a reduction of area versus temperature curve shown in Figure 4a. Below the nil ductility temperature, T_1, brittle failures occur. The nil ductility temperature corresponds to the temperature where the yield stress exceeds the critical stress σ^*. At a slightly higher temperature, T_D, the normal ductile-brittle transition occurs. In Figure 4b, again for a $K_t = 1$, a higher strain rate, ϵ_2, raises the yield stress at each test temperature. The result is that the critical stress, σ^*, is exceeded at a higher temperature and the nil ductility temperature is effectively increased with an increase in strain rate.

The presence of a sharp notch, $K_t > 1$, affects the transition temperature as shown in Figure 4c. The yield stress is raised by a plastic constraint factor, pcf, such that if pcf times the yield stress exceeds σ^*, failure will occur. The plastic constraint factor is actually an experimentally determined stress concentration factor that reflects the plasticity at the notch tip. Rosenfield, et al.[34] report pcf values taken from Krafft ranging from 1.0 to 2.7, depending on the plastic zone size and the notch geometry. The net effect in increasing the notch sharpness is an increase in nil ductility temperature from T_1 to T_3. Weiss and Sessler[38] investigated the variation of notch strength ratio (NSR $\propto$ pcf) with testing temperature. They reported a decrease in notch sensitivity with increasing temperature. This indicates that the plastic constraint factor is reduced with increasing temperature.

Rosenfield, et al.[34] report fracture toughness data, taken from

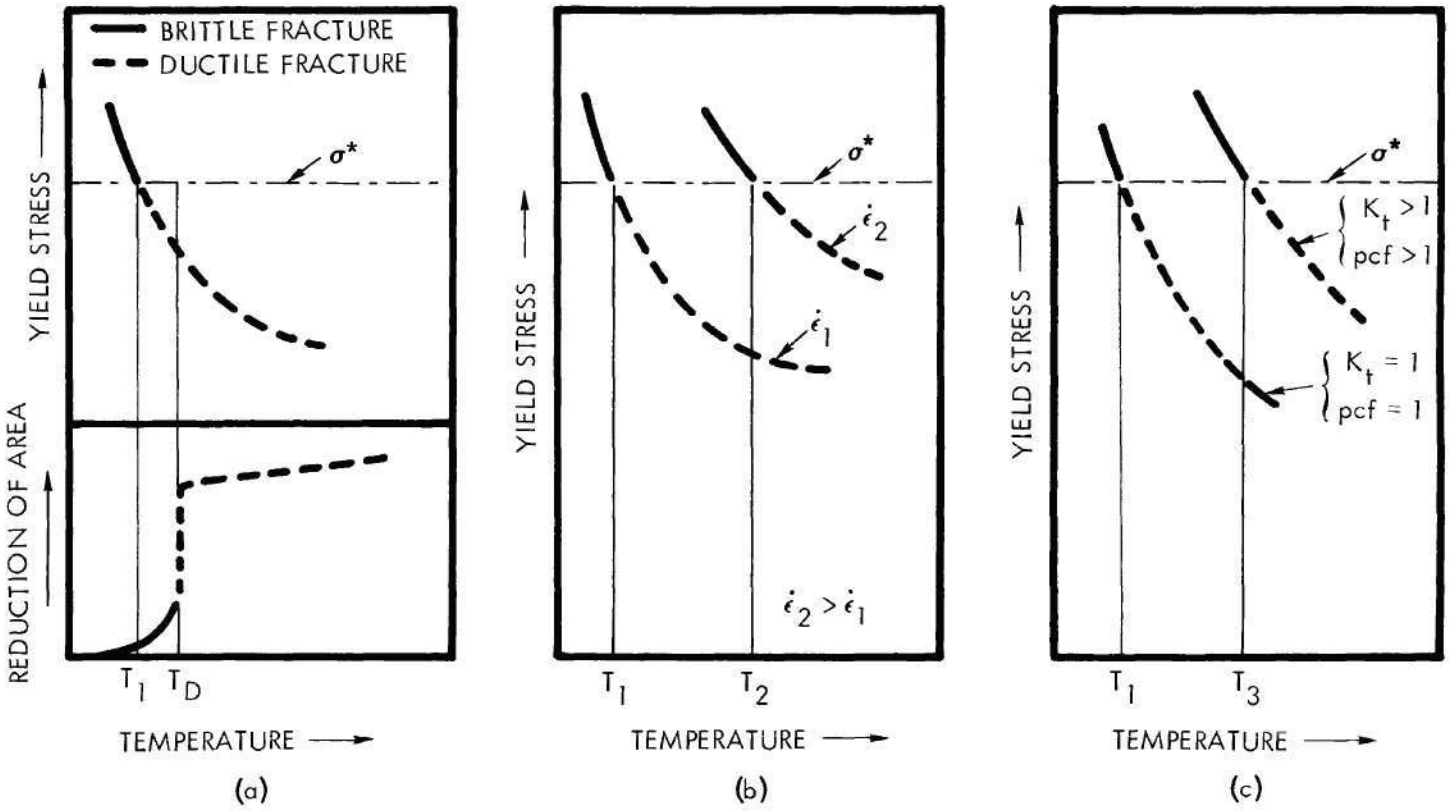

Figure 4. Ductile-Brittle Transition Temperature as Affected by Strain Rate and Stress Concentrators

(a) Comparison of Ductile-Brittle Transition Temperature as Determined by Brittle Fracture Criteria and Reduction of Area Criteria

(b) Ductile-Brittle Transition as Affected by Strain Rate

(c) Ductile-Brittle Transition as Affected by Stress Concentrators

Krafft, indicating that K_{Ic} is not a function of temperature or strain rate (Figure 5a). Replotting the data as a function of $\frac{K_{Ic}}{\sigma_{ty}}$ (see Figure 5b), indicates that the variation in K_{Ic} is due to the change in the yield stress as a function of time and temperature.

Corten and Shoemaker[39], using data of Krafft and Sullivan[40], show that K_{Ic} is a function of a temperature-rate parameter, $T \ln \frac{F}{\dot{\epsilon}}$, where T is temperature and F is a frequency factor. The variation of K_{Ic} with the rate parameter, shown in Figure 6, agrees with the general trend of mechanical property variation with strain rate. This is especially so since T and F can be considered as constants, (the rate parameter could be written A ln $\dot{\epsilon}$, where A is a constant) and K_{Ic} is a function of the stress and the crack configuration.

Corten and Shoemaker[39] evaluated the strain rate at a fixed point ahead of the crack tip and at the elastic-plastic boundary of the plastic zone based on a plastic strain distribution and found only constant differences. The equation of Corten and Shoemaker for fixed point elastic analysis is as follows:

$$\dot{\epsilon}_y = 2.5 \sqrt{D} \left(\frac{\dot{\sigma}_{nom}}{E} \right) \quad , \tag{5}$$

where

$\dot{\epsilon}$ = a function of the specimen diameter, D, the modulus, E, and the rate of change of the nominal stress, $\dot{\sigma}_{nom}$.

For constant diameter specimens, it appears that use of a nominal strain rate based on head travel and specimen gage length to determine the local strain rate at the tip of a notch or crack would only differ

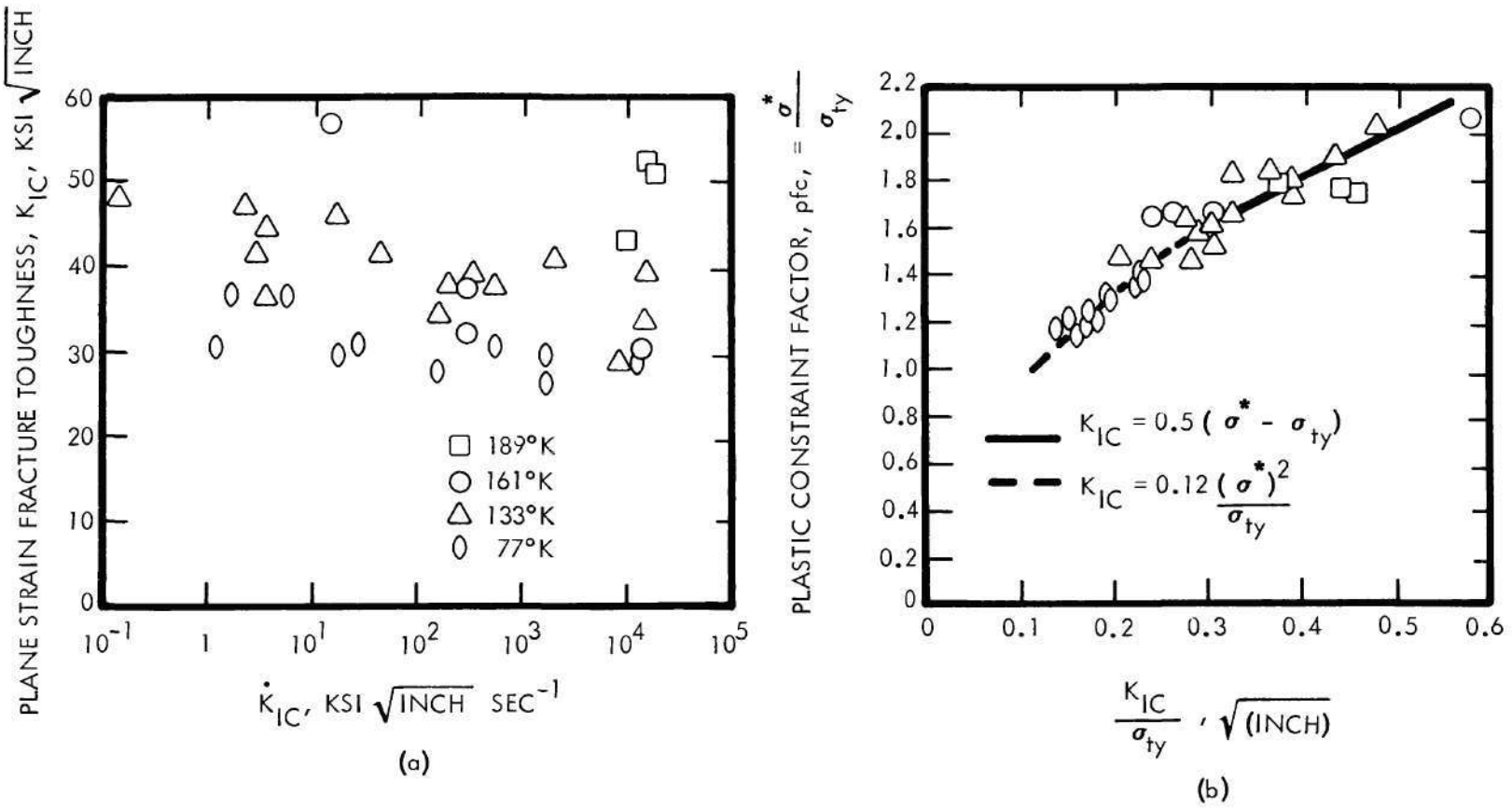

Figure 5. Effect on Plane Strain Fracture Toughness of Loading Rate, Yield Stress and Temperature on Mild Steel Plate (From Rosenfield et al.[30])

(a) Influence of Loading Rate and Temperature on Plane Strain Fracture Toughness (No Correlation Obvious)

(b) Plastic Constraint Factor, σ^*/σ_{ty}, Shown as a Function of K_{Ic}/σ_{ty}. This indicates that the variation of the yield stress with temperature and loading is responsible for variations shown in plane strain fracture toughness.

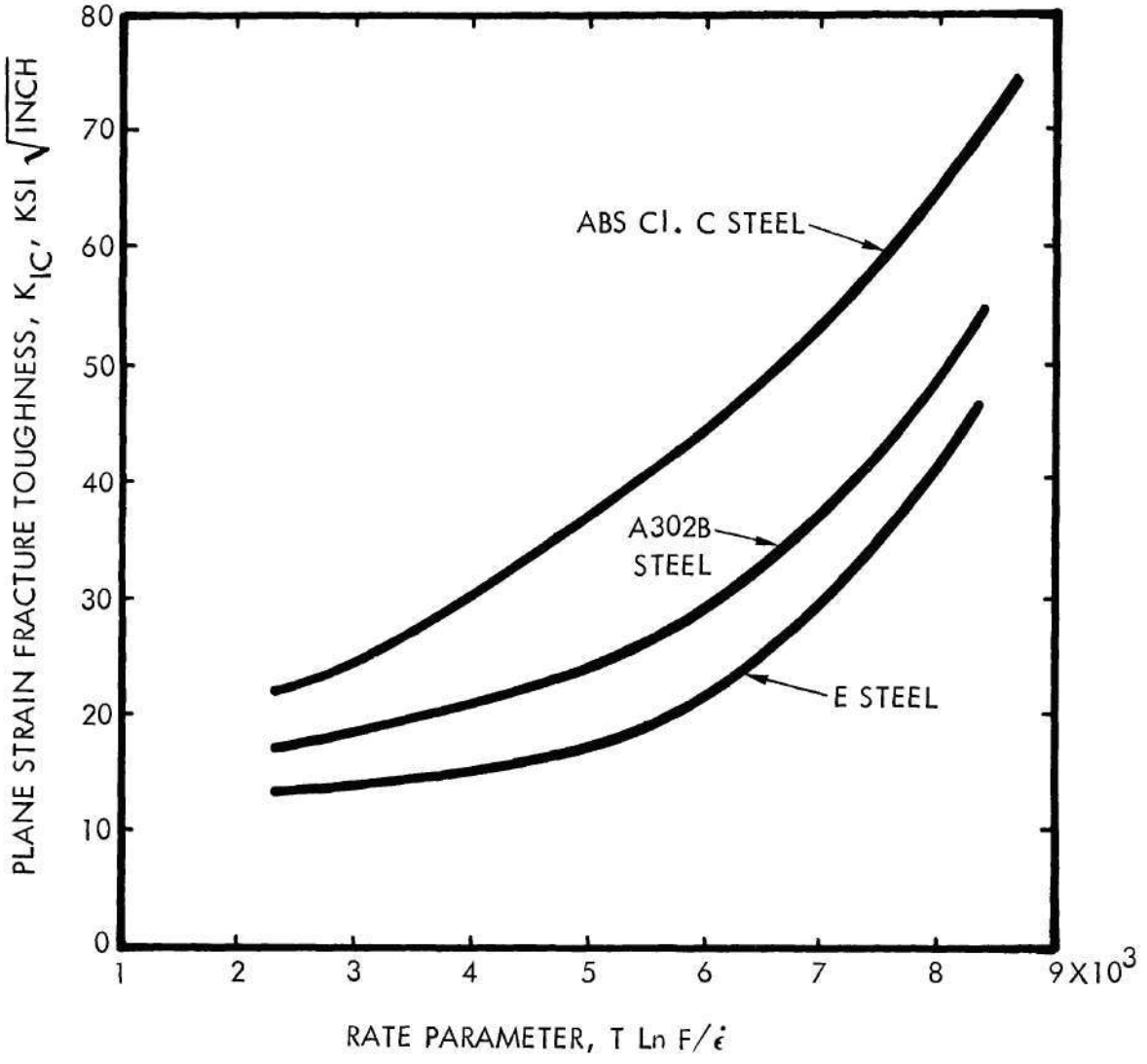

Figure 6. Variation of the Plane Strain Fracture Toughness with the Rate Parameter, T ln F/$\dot{\epsilon}$, for Three Steels (From Corten and Shoemaker[39])

from Equation (5) by a constant. Corten and Shoemaker's methodology compares with the semi-empirical relationships used by Rosenfield and Hahn. Corten and Shoemaker's data are fitted to curves (Figure 6); Rosenfield and Hahn use straight lines for each region.

Irwin[41] postulated that a strain-rate-sensitive material should have a minimum plane-strain stress intensity, called "crack arrest toughness," that is, a function of strain rate at a fixed temperature and plate thickness. Irwin's concept is not in conflict with the linear logarithmic dependency of stress on strain rate. Strain-rate sensitivity in Region I was reported to be very low[30], and the crack arrest toughness might vary slightly with strain rate.

Hendrickson, Wood, and Clark[37] studied the effects of loading rate versus failure stress at various temperatures using a hyperbolic notch in a brittle material. They were successful in predicting the failure stress of the notched specimens by using stress concentration theory and assuming that K_t was a stress-rate multiplier. Their analysis methods assumed negligible amounts of plasticity at the notch tip before failure, i.e., brittle failure was a prerequisite for use of the analysis. They suggested that the theory would have to be modified for engineering materials.

Theoretical Summary

Elastic stress concentration theory is well defined and can be utilized in failure analysis of brittle material, but notched materials deforming plastically require the use of some correction factor such as the notch strength ratio, NSR, for analysis of failure.

Temperature influence and strain rate effects on materials are explainable by theory. At the present time, mechanical behavior of materials is predicted from theoretical formulas in which empirical constants are included.

Research in strain-rate sensitivity of materials containing notches has been limited primarily to conventional impact tests and to a fracture mechanics analysis of precracked specimens. Impact tests have resulted in the ductile-brittle transition concept with changing temperature. Precracked fracture mechanics tests only evaluate the limiting notch in a material. The size of this limiting notch is a function of the material grain size, and stress concentration factors for a crack cannot be accurately determined. Therefore, the available information is insufficient for a determination of material behavior of a notched specimen subjected to different strain rates.

CHAPTER III

EXPERIMENTAL APPROACH

Two alloys were selected for use in this investigation. Cold-rolled 1010 steel is a strain-rate-sensitive material, and 7075-T6 bare aluminum is reported to be insensitive to changes in strain rate. The chemical compositions of both alloys are given in Table 1. Both were obtained in sheet form, nominally 0.125-inch thick. Specimens containing notches of the configurations shown in Figures 7 and 8 were machined from each material. The different notch configurations represented stress concentrations of $K_t = 1$ (smooth specimen), $K_t = 2$, $K_t = 6$, and $K_t = 13$. The stress concentration factors were calculated according to reference 13 (the method of calculation is outlined in Appendix B).

The smooth specimen, $K_t = 1$, and the specimen with $K_t = 2$ were fabricated using standard machining practices. The two sharpest notches were cut by grinding on a modified thread grinding machine using the following procedure: first, the grinding wheel was shaped to the approximate size and a sample specimen cut and examined on a shadowgraph. The wheel was then reshaped to correct errors and a new test cut was made and examined. The procedure was repeated until the notch configuration was as close as possible to that required. The dimensions of each specimen were examined before another specimen was cut to monitor wheel wear. The grinding wheel was reshaped as required.

All notch radii and all distances between notches were measured

Table 1. Chemical Composition of 7075-T6 Aluminum and 1010 Steel Used in Strain-Rate-Sensitivity Tests

Material	Composition, Percent							
	Zn	Fe	Cr	Cu	Mn	Mg	Al	C
7075-T6 aluminum	5.46	0.24	0.16	1.6	0.16	2.5	Bal.	
Alcoa Standard AS21	5.68	0.29	0.16	1.6	0.064	2.5	Bal.	
1010 steel		Bal.			0.394			0.081
AISI Specifications		Bal.			0.3-0.6			0.08-0.13

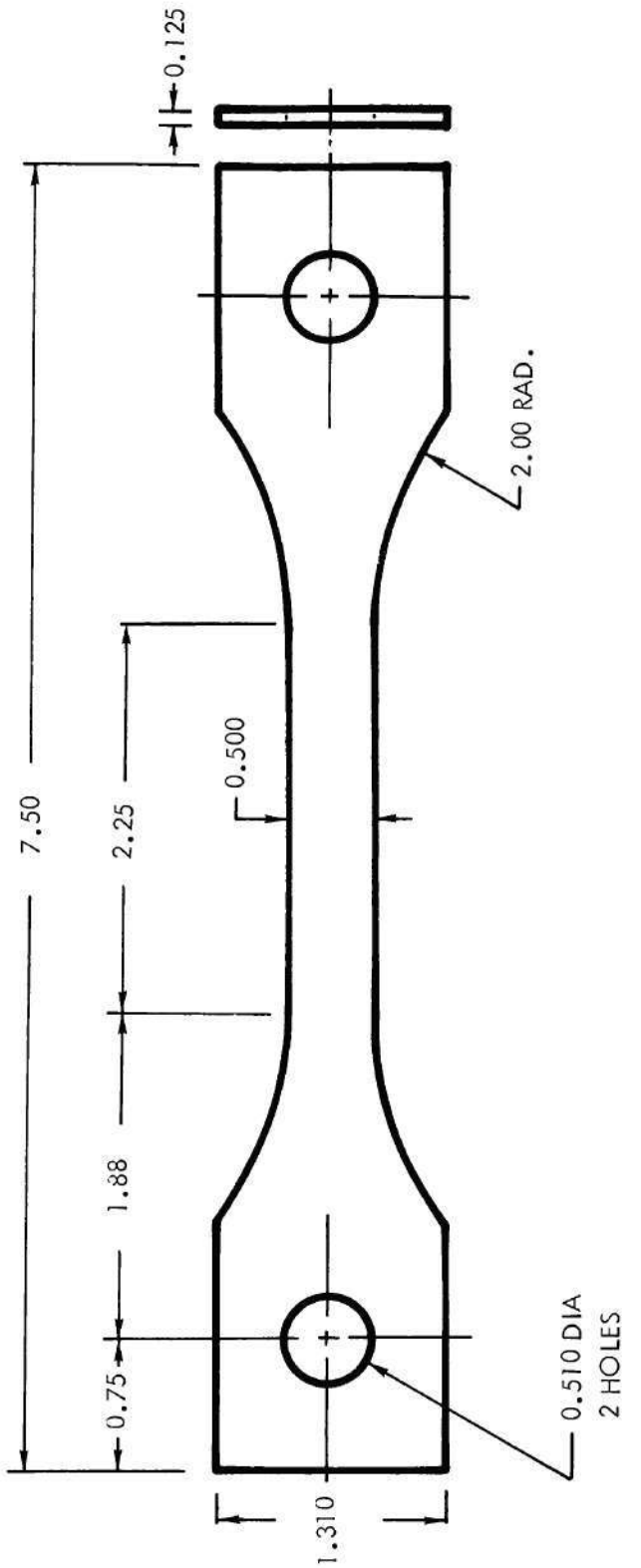

Figure 7. Specimen Configuration Used to Determine Effect of Strain Rate on Mechanical Properties of Materials with $K_t = 1$

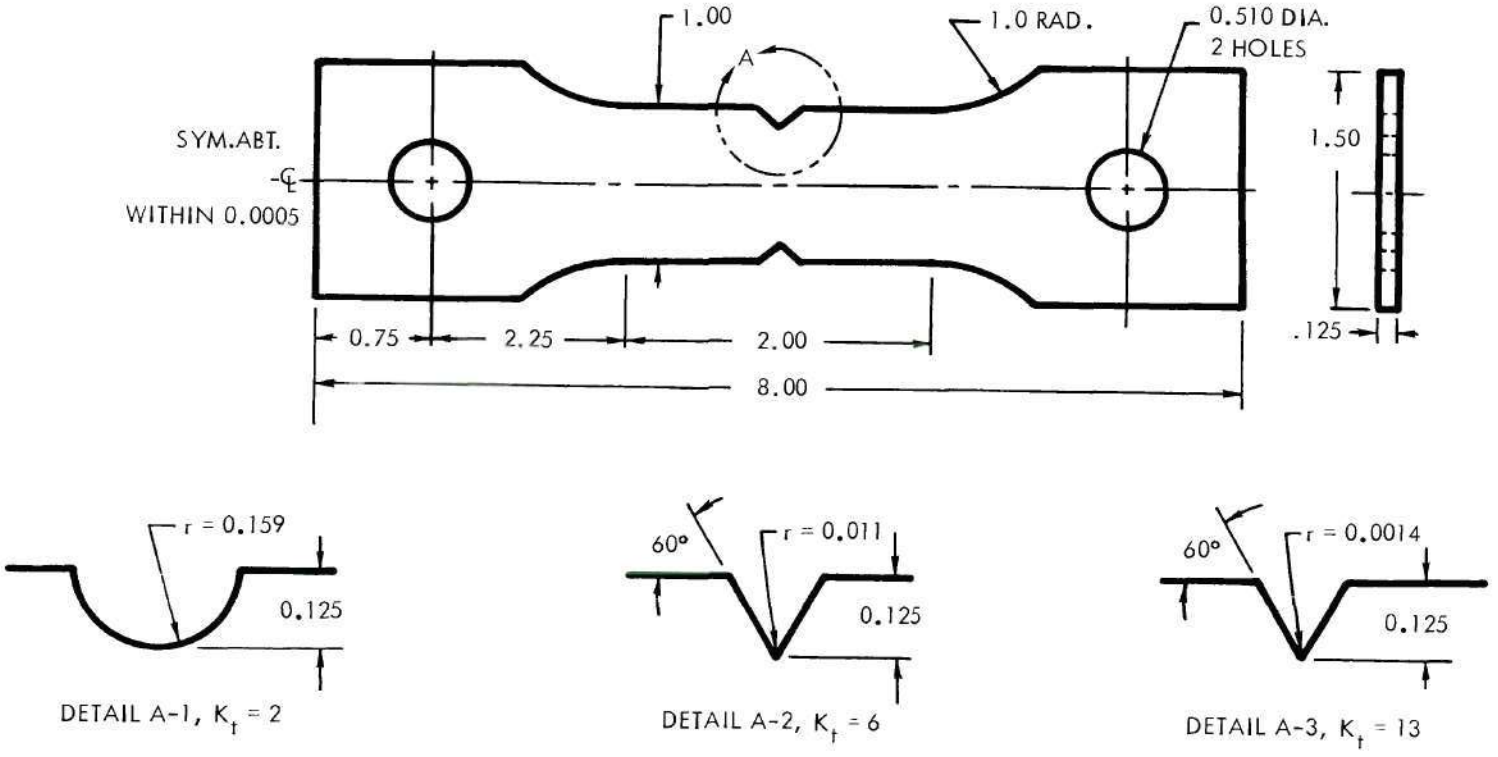

Figure 8. Specimen Configurations Used to Determine Effect of Strain Rate and Stress Concentration, K_t, on Mechanical Properties of Materials

using the shadowgraph, since conventional measurement was impractical. A magnification of 500X was used in measurement of the width and notch radii of the specimens containing the smallest radii, and a magnification of 250X was used for the specimens containing the intermediate notch radii. Specimens containing the largest notch were measured at 100X for the width, and the notch was measured at 20X.

Loading rates selected for the testing procedure were 0.002, 0.5, 2, 100, 400, and 3000 inches per minute. Loading rates between 0.002 and 2 inches per minute were obtained using a Model TTCL Instron Universal Testing Machine with fixed crosshead speeds (Figure 9). Loading rates of 100 and 400 inches per minute were produced by a closed-loop hydraulic universal testing machine manufactured by Riehle Testing Division, AMETEK, Inc. (Figure 10). A closed-loop hydraulic universal testing machine manufactured by MTS Systems Corporation (Figure 11) was used to obtain the loading rate of 3000 inches per minute.

A time base was used on all load-deformation curves. Although higher accuracy would have been obtained for the lower strain rate tests by using a conventional extensometer and measuring deflection over a 2-inch gage length, a conventional extensometer could not be used at the faster rates. (Reynolds Aluminum Company[42] is evaluating the design of a suitable extensometer for high rates using an MTS system, but it is not available for purchase.) The design and fabrication of a high-rate extensometer was considered to be beyond the scope of the program since if identical specimens were used and head deflections were measured, any error due to the specimen shoulders would be consistent and would affect the results only by some constant. This is consistent with the results

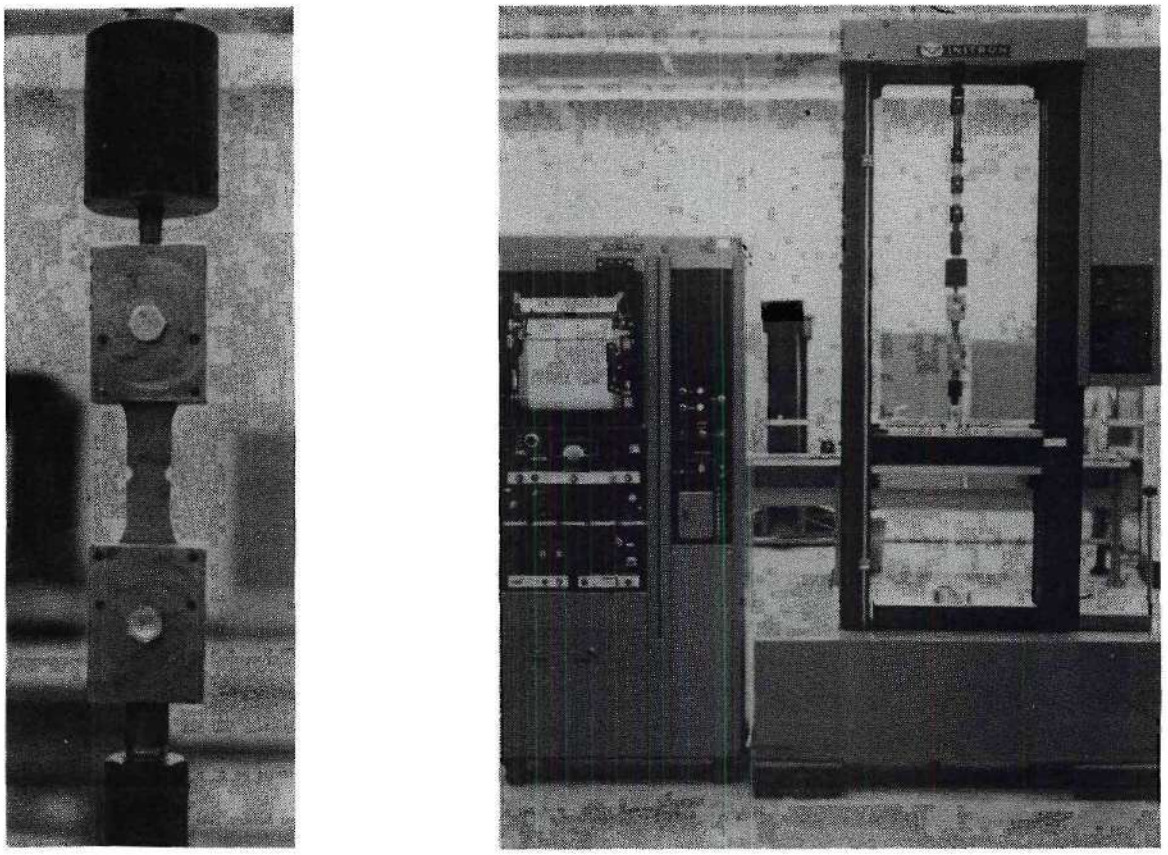

Figure 9. Test Setup for Speeds Between 0.002 and 2.0 Inches per Minute Using an Instron Model TTCL Universal Testing Machine. The closeup shows the specimen, grips, and and slack grip assembly.

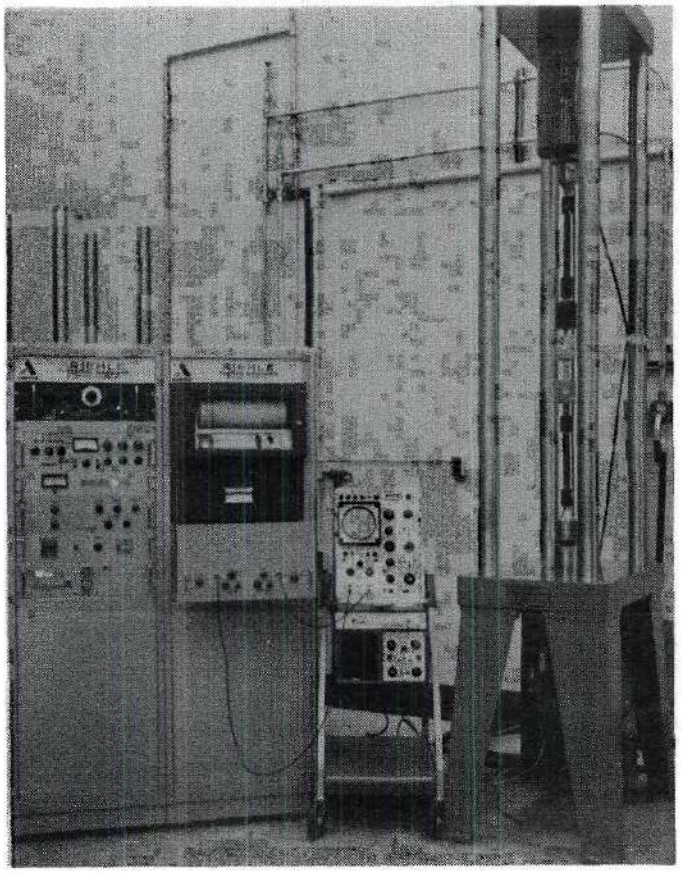

Figure 10. Test Setup for Speeds of 100 and 400 Inches per Minute Using a Riehle Closed-Loop Universal Testing Machine

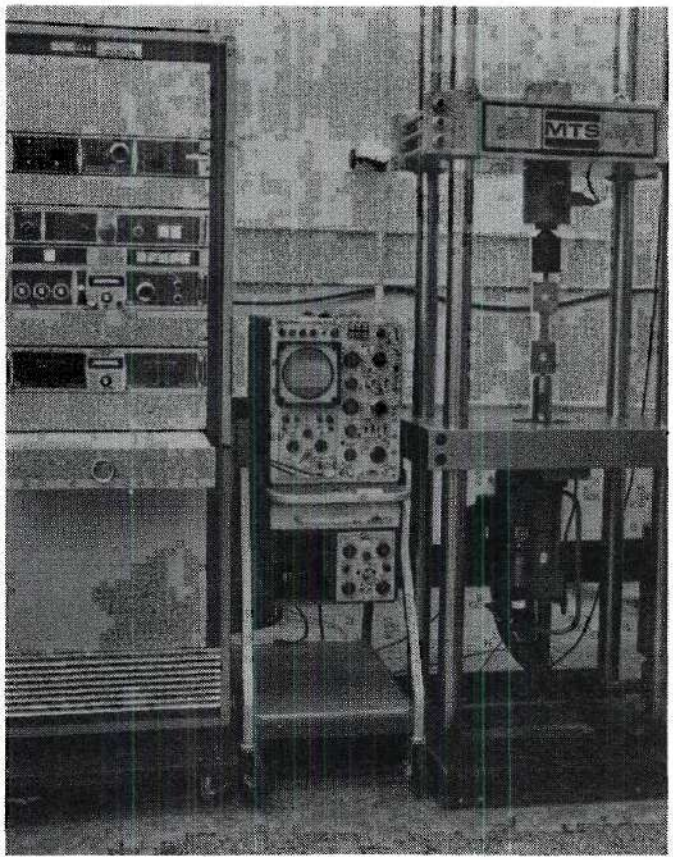

Figure 11. Test Setup for a Speed of 3000 Inches per Minute Using a MTS Closed-Loop Universal Testing Machine

of Corten and Shoemaker[39] (cf. Equation (5)).

The load and head travel were measured on the Instron universal testing machine using the standard recorder. Calibration was accomplished using proving rings certified by the National Bureau of Standards. The accuracy was within ± 1 percent. A special system was developed to record load and deflection for the faster tests. A Tektronix type 549 Storage Oscilloscope was used to record load versus time and deflection versus time. The testing machine was calibrated to ± 1 percent; however, when the oscilloscope was used in the system the overall accuracy was considered to be ± 3 to 4 percent.

Slack grips were used with all specimens to allow the machine to attain the required speed before contact with the specimen. One inch free travel was allowed for the faster rates. The oscilloscope was set to trigger with a small load application (about 10 percent of failure load) so that friction in the slack travel would not trigger the oscilloscope and preempt the load and deformation curves. Also, to display the full load curve over the majority of the screen, time scales as fast as 0.0002 second per cm were required. These fast recordings required that automatic triggering be used.

The oscilloscope was set to record a single trace and the storage feature was used to record the tests. Polaroid pictures were taken of all stored curves. A standard oscilloscope and camera arrangement could have been used for the actual tests, but during the test set-up, especially the set-up of the triggering, the storage feature was quite valuable.

The faster rate tests presented additional problems. At 400 and 3000 inches per minute, ringing was encountered when the slack grip

assembly was first contacted. Reynolds Aluminum Company[42] also encountered this difficulty and partially compensated for it by using a shock absorber in the slack grip and an electronic filter. Several types of shock absorbers were tried for use in this program, and the best results were obtained with 1/8-inch thick silicone rubber (45 Durometer). The load cell was also insulated from the testing machine head with the same rubber.

The amplitude of the ringing was reduced considerably by changing the slack grip assembly from the load cell end to the hydraulic cylinder end of the loading arrangement. This reduced the ringing effect practically to zero for testing the aluminum, but ringing still occurred in the steel specimen tests. After an electronic filter was added to the system, the ringing was reduced to a total amplitude less than the line width, which was considered satisfactory.

CHAPTER IV

EXPERIMENTAL RESULTS

Evaluation of Results for 1010 Steel

All test results are summarized in Table 2 for 1010 steel specimens. The variation of failure stress with stress concentration factor is shown in Figure 12. (In this and all other figures, the averages shown in the tables are plotted.) An average of three specimens were used for each point.

The strain rate sensitivity of 1010 cold-rolled steel is evidenced by the increase in failure stress, shown in Figure 12, for the smooth specimens (K_t=1). Increasing the K_t by the presence of a notch does not significantly alter the strain-rate-sensitivity of the material. The increase in the failure stress of the notched specimen (K_t=13) is about 36 percent larger than the increase in the smooth specimens for similar loading rate changes.

These values of failure stress are replotted in Figure 13 as a function of the logarithm of the strain rate. The data for smooth specimens show that this material is very sensitive to strain rate changes. It is observed that as the notch radius decreases the general shape of the curves is not changed. Therefore, increasing the stress concentration factor only alters the curves by a constant. The displacement of the curves along the stress axis for each K_t value is approximately equal to the percentage change in stress due to K_t as determined from a slow

Table 2. Test Data for 1010 Steel, Cold-Rolled Sheet

Loading Rate, Inches Per Minute	$K_t = 1$					$K_t = 2$				
	Spec. No.	σ_{uty} KSI	σ_{lty} KSI	σ_{tu} KSI	Elong. in 2 inch %	Spec. No.	σ_{uty} KSI	σ_{lty} KSI	σ_{tu} KSI	Elong. in 2 inch %
0.002	A_o4	33.1	29.3	42.4	34.0	$A_1$31	32.4	--	47.4	12.5
	A_o5	32.0	29.8	42.7	33.5	$A_1$32	32.2	--	47.7	12.5
	A_o6	30.9	29.8	42.8	35.0	$A_1$33	31.8	--	46.5	12.5
	Avg.	32.0	29.6	42.6	34.2	Avg.	32.1	--	47.2	12.5
0.5	A_o1	40.0	33.2	45.8	38.0	$A_1$34	39.1	39.0	51.9	14.0
	A_o2	34.1	32.9	45.2	36.0	$A_1$35	38.7	38.7	51.6	14.0
	A_o3	38.0	32.2	45.4	38.5	$A_1$36	38.8	38.8	51.2	14.0
	Avg.	37.4	32.8	45.5	37.5	Avg.	38.9	38.8	51.6	14.0
2.0	A_o7	37.5	33.4	46.4	37.5	$A_1$37	41.9	41.7	52.6	14.0
	A_o8	36.2	33.4	45.8	36.8	$A_1$38	41.8	41.4	52.5	14.0
	A_o9	38.3	33.6	46.4	36.0	$A_1$39	41.1	40.6	52.7	14.5
	Avg.	37.3	33.5	46.2	36.8	Avg.	41.6	41.2	52.6	14.2
100	S-6	49.2	37.3	49.7	40.0	$A_1$40	52.3	49.8	55.7	13.5
	S-7	49.2	39.3	49.7	40.5	$A_1$41	51.0	47.1	54.8	--
	S-10	49.4	38.5	49.6	47.5	$A_1$50	54.2	51.3	59.4	--
	A_o18	50.9	40.0	51.4	43.0					
	A_o19	49.5	40.9	--	45.5					
	Avg.	49.6	39.2	50.1	43.3	Avg.	52.5	49.4	56.4	13.5
400	S-8	48.9	40.4	52.1	46.0	$A_1$60	54.9	51.9	55.6	13.0
	S-9	45.6	43.4	51.4	45.0	$A_1$59	57.5	52.5	56.7	13.0
	A_o15	45.7	45.7	53.0	45.5					
	A_o16	47.4	45.7	--	44.0					
	Avg.	46.9	42.5	52.2	45.1	Avg.	56.2	52.2	56.2	13.0

Table 2. (continued)

Loading Rate, Inches Per Minute	$K_t = 1$ Spec. No.	σ_{uty} KSI	σ_{lty} KSI	σ_{tu} KSI	Elong. in 2 inch %	$K_t = 2$ Spec. No.	σ_{uty} KSI	σ_{lty} KSI	σ_{tu} KSI	Elong. in 2 inch %
3000	A_o22	56.2	46.6	54.2	46.0	A_147	64.2	60.8	60.8	11.5
	A_o23	55.8	47.7	53.6	47.0	A_148	64.2	60.0	60.8	12.0
	A_o24	51.7	49.7	52.4	41.0	A_149	60.0	59.3	59.3	12.0
	A_o25	49.8	49.8	53.7	50.0	A_160	54.9	51.9	55.6	13.0
	A_o27	54.2	45.8	51.5	--					
	A_o26	60.7	46.8	55.2	46.0					
	Avg.	54.7	47.7	53.4	46.0	Avg.	60.8	58.0	59.1	18.1
		$K_t = 6$					$K_t = 13$			
0.002	A_29	34.0	--	47.7	10.5	A_336	31.8	--	45.9	10.5
	A_210	32.4	--	47.4	11.0	A_337	32.3	--	46.0	10.5
	A_211	34.1	--	47.6	11.0	A_338	34.8	--	46.0	9.5
	Avg.	33.5	--	47.6	10.8	Avg.	33.0	--	46.0	10.2
0.5	A_212	40.1	38.9	50.9	11.5	A_339	36.6	35.8	48.0	12.0
	A_213	38.6	37.8	50.3	12.0	A_340	38.4	37.8	49.2	11.5
	A_214	39.2	38.5	50.5	11.5	A_341	37.5	36.7	48.1	14.0
	Avg.	39.3	38.4	50.6	11.7	Avg.	37.5	36.8	48.4	12.5
2.0	A_215	41.3	40.4	51.3	12.5	A_342	41.1	40.6	50.5	11.5
	A_216	41.5	40.7	51.7	12.0	A_343	41.9	39.6	50.5	11.5
	A_217	41.4	40.6	52.1	12.5	A_344	41.7	40.1	50.6	11.0
	Avg.	41.4	40.6	51.7	12.3	Avg.	41.6	40.1	50.5	11.3
100	A_24	54.3	50.6	55.8	--	A_331	54.4	51.4	55.4	10.0
	A_25	--	51.3	55.8	--	A_332	54.8	51.3	55.8	10.5
	A_26	54.7	51.9	56.2	10.0	A_345	54.2	50.5	53.7	--
	A_218	56.2	51.2	58.7	--					
	A_225	51.7	47.2	53.3	14.5					
	Avg.	54.2	50.4	56.0	12.3	Avg.	54.5	51.1	55.0	10.3

Table 2. (continued)

Loading Rate, Inches Per Minute	$K_t = 6$					$K_t = 13$				
	Spec. No.	σ_{uty} KSI	σ_{lty} KSI	σ_{tu} KSI	Elong. in 2 inch %	Spec. No.	σ_{uty} KSI	σ_{lty} KSI	σ_{tu} KSI	Elong. in 2 inch %
400	$A_2$7	--	56.6	59.0	10.0	$A_3$34	--	55.3	57.6	10.0
	$A_2$8	--	57.2	59.0	10.0	$A_3$35	--	54.6	57.9	10.0
	$A_2$19	--	56.7	58.1	--	$A_3$46	--	54.8	57.1	9.5
	$A_2$24	--	56.8	59.3	10.5	$A_3$53	55.7	50.7	52.4	12.5
	$A_2$26	51.2	50.6	53.2	14.5	$A_3$55	55.9	52.1	54.2	--
	$A_2$28	57.2	55.6	57.2	--					
	Avg.	54.2	55.4	57.6	11.2	Avg.	55.8	53.5	56.9	10.5
3000	$A_2$20	68.8	58.9	61.9	10.0	$A_3$47	63.9	60.2	61.9	10.0
	$A_2$21	60.3	57.3	58.3	10.5	$A_3$48	63.4	61.1	61.1	9.0
	$A_2$23	65.7	59.0	59.7	12.5	$A_3$49	63.2	61.2	61.2	9.5
						$A_3$50	62.7	59.4	59.7	10.5
	Avg.	64.9	58.4	60.0	11.0	Avg.	63.3	60.5	61.0	9.8

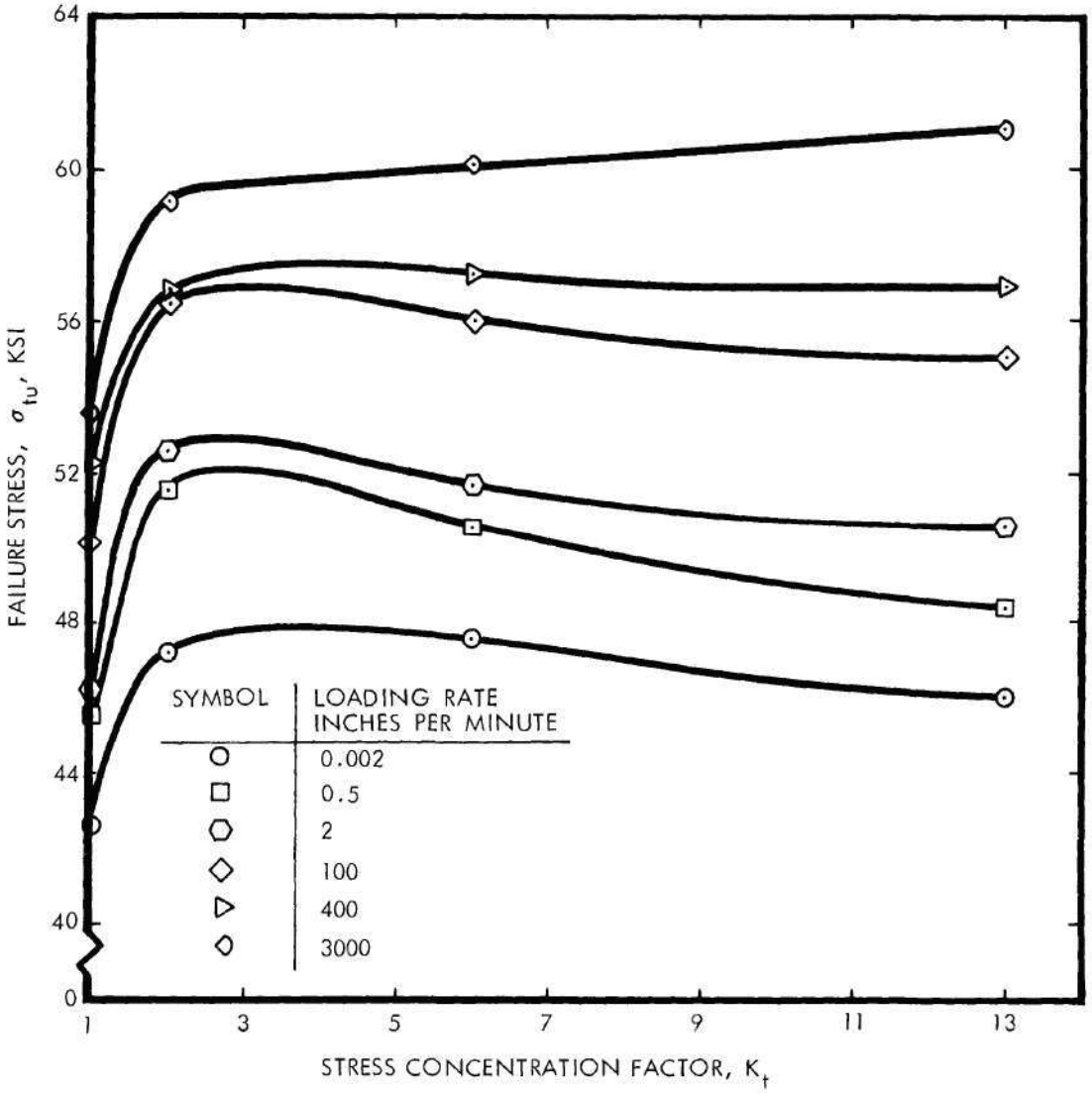

Figure 12. Effect of Stress Concentration and Strain Rate on the Failure Stress of 1010 Steel, Cold-Rolled Sheet

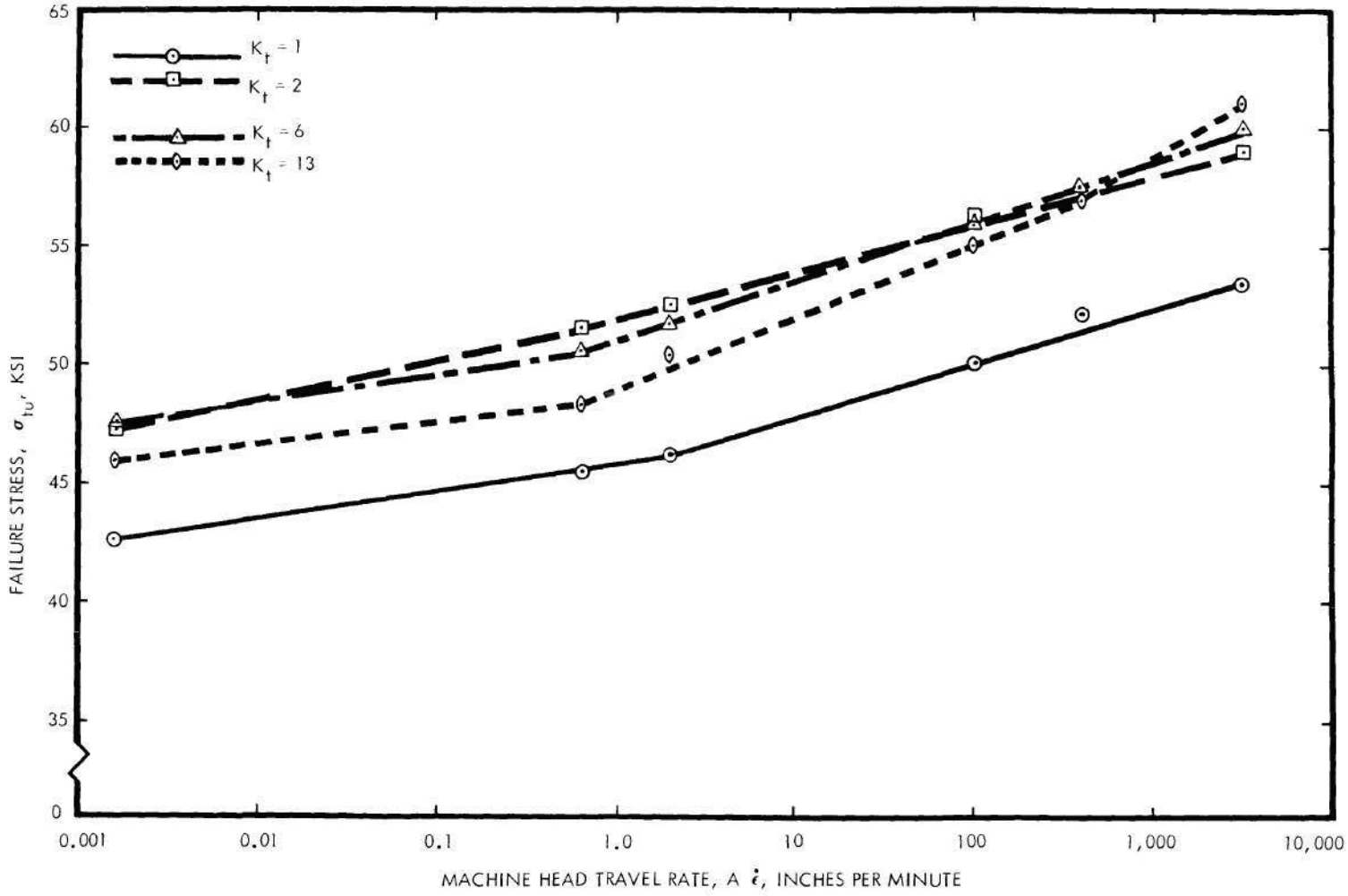

Figure 13. Effect of Stress Concentration and Strain Rate on the Failure Stress of 1010 Steel, Cold-Rolled Sheet

or nominal strain rate curve, shown in Figure 12. A reasonable estimate for the failure stress of a notched specimen tested at any loading rate could be obtained from knowledge of the K_t behavior and the strain rate behavior of a material.

The change in slope of the straight line in the stress versus log strain rate curves (Figure 13) occurs at a loading rate of 2 inches per minute for the smooth specimens and in about 0.5-inch per minute for the notched specimens. The selection of loading rates makes the determination of the change in slope for the notched specimens difficult, but it is apparent that it is at a lower loading rate than for the smooth specimens. This indicates that some form of rate dependency upon K_t exists which may be similar in nature to that suggested by Hendrickson, et al[37].

The change in failure mechanism in Region I to Region II proposed by Rosenfield and Hahn[30] for low carbon steels occurs at a head-travel rate of 12 to 120 inches per minute, while the change in Region II to Region IV occurs at a head-travel rate of 100,000 to 400,000 inches per minute (assuming a 2-inch gage length). The data in Figure 13 agree well with the data in Figure 2. The curve for steel with $K_t = 13$ (Figure 13) indicates a second change in slope between 400 and 3000 inches per minute; this could be an observed change from Region II to Region IV.

The dependency of the upper and lower yield points for 1010 steel on K_t at different strain rates is shown in Figure 14. At a loading rate of 0.002-inch per minute, the difference between the upper and the lower yield phenomena is negligible for all the notched specimens tested. The yield stresses shown in Figure 14 for that speed are the first deviation from linearity of the load-deflection curve. At a loading rate of 0.5-inch

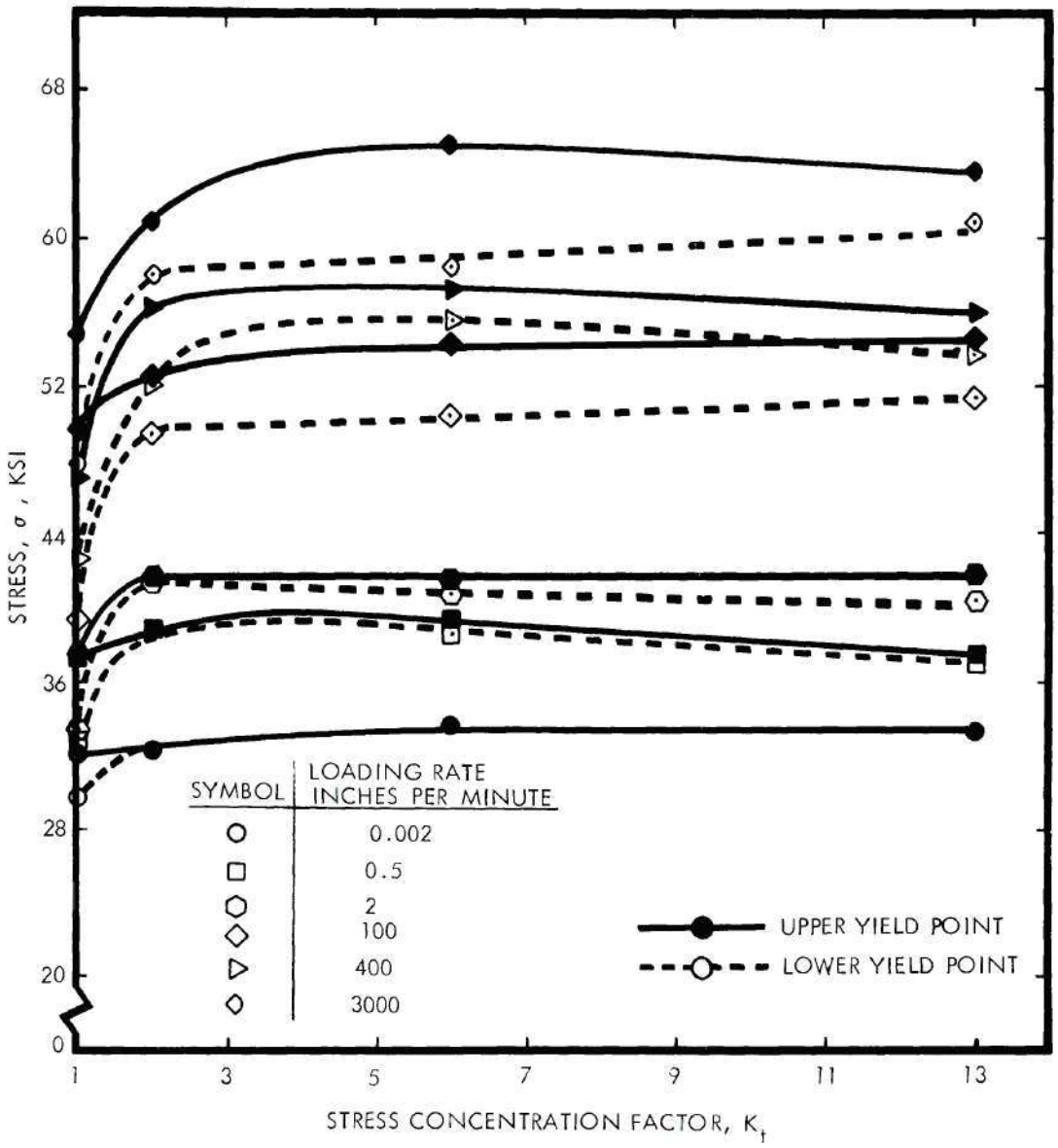

Figure 14. Effect of Strain Rate and Stress Concentration on the Upper and Lower Yield Points of 1010 Steel, Cold-Rolled Sheet

per minute, the upper and lower yield phenomena exist, but the difference between the upper yield stress and the lower yield stress is small and practically non-existent at $K_t = 2$. The stress difference between upper and lower yield points becomes larger with increasing K_t and loading rate.

Evaluation of Results for 7075-T6 Aluminum

All test results for 7075-T6 aluminum are summarized in Table 3. The variations of the failure stress with stress concentration factor are shown in Figure 15. These data appear to indicate that 7075-T6 aluminum is not sensitive to strain rate when a smooth specimen ($K_t=1$) is used; all data for $K_t = 1$ are within experimental error. Introducing a K_t greater than one, however, does change the effect of strain rate on failure stress. With a $K_t = 13$, the alloy exhibits a decreasing failure stress with increasing strain rate from 0.002 to 400 inches per minute. This reduction in failure stress is approximately 11 percent. Further increase in rate to 3000 inches per minute appears to raise the failure stress again for all values of $K_t > 1$.

The aluminum data are replotted in Figure 16 on the basis of stress versus log of strain rate. This presentation shows clearly that there is no measurable effect of strain rate on the failure stress for the smooth specimen and for the specimen with the mildest notch, $K_t = 2$. A decrease in notch strength is shown for the two sharper notches with loading rate up to about 400 inches per minute, then an increase in strength to 3000 inches per minute. If this decrease were in Region I, and the increase in Region II (Figure 2), the behavior would be reason-

Table 3. Test Data for 7075-T6 Bare Aluminum Sheet

Loading Rate, Inches Per Minute	$K_t = 1$				$K_t = 2$				$K_t = 6$				$K_t = 13$			
	Spec. No.	σ_{ty} KSI	σ_{tu} KSI	Elong. in 2 in. %	Spec. No.	σ_{ty} KSI	σ_{tu} KSI	Elong. in 2 in. %	Spec. No.	σ_{ty} KSI	σ_{tu} KSI	Elong. in 2 in. %	Spec. No.	σ_{ty} KSI	σ_{tu} KSI	Elong. in 2 in. %
0.002	A_o4	72.5	78.9	14.5	$A_1 1$	72.9	88.3	2.5	$A_2 33$	70.5	85.9	1.0	$A_3 6$	70.2	77.7	0.5
	A_o5	77.1	82.5	14.0	$A_1 2$	67.5	86.4	2.5	$A_2 34$	69.2	85.6	1.0	$A_3 7$	66.9	76.1	0.4
	A_o6	76.6	82.2	14.0	$A_1 10$	67.4	88.1	3.0	$A_2 35$	68.1	85.8	1.0	$A_3 8$	64.6	78.0	0.5
	Avg.	75.4	81.2	14.2	Avg.	69.3	87.6	2.7	Avg.	69.3	85.8	1.0	Avg.	67.2	77.3	0.5
0.5	A_o1	73.4	80.1	12.5	$A_1 4$	77.5	89.1	2.5	$A_2 36$	56.9	85.2	1.0	$A_3 9$	58.0	70.8	1.2
	A_o2	75.6	81.9	12.5	$A_1 5$	79.9	86.7	2.5	$A_2 37$	56.9	85.2	1.0	$A_3 10$	59.2	68.1	1.0
	A_o3	75.5	81.8	14.5	$A_1 6$	76.5	86.5	2.5	$A_2 38$	56.9	85.1	1.1	$A_3 11$	64.7	73.8	0.5
	Avg.	74.8	81.3	13.2	Avg.	78.0	87.4	2.5	Avg.	56.9	85.2	1.0	Avg.	60.6	70.9	0.9
2.0	A_o7	78.1	83.6	13.0	$A_1 7$	68.3	88.7	2.5	$A_2 39$	58.0	82.8	1.0	$A_3 12$	51.2	71.7	0.6
	A_o8	72.5	79.7	12.5	$A_1 8$	71.7	88.6	2.3	$A_2 40$	69.2	83.3	0.9	$A_3 13$	59.1	68.3	1.0
	A_o9	72.2	79.7	13.0	$A_1 9$	69.8	86.1	2.5	$A_2 41$	68.0	83.4	1.0	$A_3 14$	59.2	71.6	0.5
	Avg.	74.3	81.0	12.8	Avg.	69.9	87.8	2.4	Avg.	65.1	83.2	1.0	Avg.	56.5	70.5	0.7
100	10	79.0	83.6	11.5	$A_1 11$	73.5	88.3	2.0	$A_2 55$	69.2	84.7	1.5	$A_3 1$	66.6	70.3	1.0
	11	79.0	85.2	13.5	$A_1 12$	73.9	88.2	2.5	$A_2 56$	65.7	82.4	1.0	$A_3 2$	71.3	72.1	1.0
	A_o13	72.2	83.1	14.0	$A_1 13$	77.6	89.8	--	$A_2 42$	75.6	83.7	1.0	$A_3 15$	65.6	69.7	1.0
	A_o14	68.1	82.4	13.5												
	Avg.	74.6	83.6	13.1	Avg.	75.0	88.8	2.2	Avg.	70.2	83.6	1.2	Avg.	67.8	70.7	1.0

Table 3. (continued)

Loading Rate, Inches Per Minute	$K_t = 1$				$K_t = 2$				$K_t = 6$				$K_t = 13$			
	Spec. No.	σ_{ty} KSI	σ_{tu} KSI	Elong. in 2 in. %	Spec. No.	σ_{ty} KSI	σ_{tu} KSI	Elong. in 2 in. %	Spec. No.	σ_{ty} KSI	σ_{tu} KSI	Elong. in 2 in. %	Spec. No.	σ_{ty} KSI	σ_{tu} KSI	Elong. in 2 in. %
400	8	75.7	84.8	13.0	$A_1$14	67.8	84.1	2.0	$A_2$31	60.9	77.5	1.5	$A_3$3	66.9	66.9	0.5
	9	75.3	84.7	12.5	$A_1$15	67.8	85.1	2.0	$A_2$32	60.0	81.7	1.5	$A_3$5	57.7	68.2	1.0
	A_o15	69.1	82.9	12.0	$A_1$16	67.0	84.6	2.0	$A_2$43	66.6	81.2	1.0	$A_3$16	69.8	69.8	1.5
	A_o16	71.5	83.8	13.0												
	Avg.	72.9	84.1	12.6	Avg.	67.5	84.6	2.0	Avg.	62.5	80.2	1.3	Avg.	64.8	68.3	1.0
3000	A_o17	--	79.5	13.5	$A_1$17	75.8	88.7	2.5	$A_2$44	80.1	86.7	1.5	$A_3$17	71.0	73.7	1.5
	A_o22	--	81.4	13.5	$A_1$18	71.9	88.2	2.5	$A_2$45	69.5	86.0	1.5	$A_3$18	64.1	72.5	1.5
	A_o23	78.7	81.6	12.0	$A_1$19	57.7	88.9	2.5	$A_2$47	67.1	86.4	1.5	$A_3$19	74.3	74.3	1.0
	A_o24	75.2	81.4	12.5					$A_2$48	80.2	87.9	1.0	$A_3$20	75.9	77.9	1.0
	A_o18	73.5	79.8	13.5												
	A_o21	78.1	83.9	13.5												
	A_o19	67.3	77.4	14.0												
	Avg.	74.6	80.7	13.2	Avg.	68.5	86.6	2.5	Avg.	74.2	86.8	1.4	Avg.	71.3	74.6	1.2

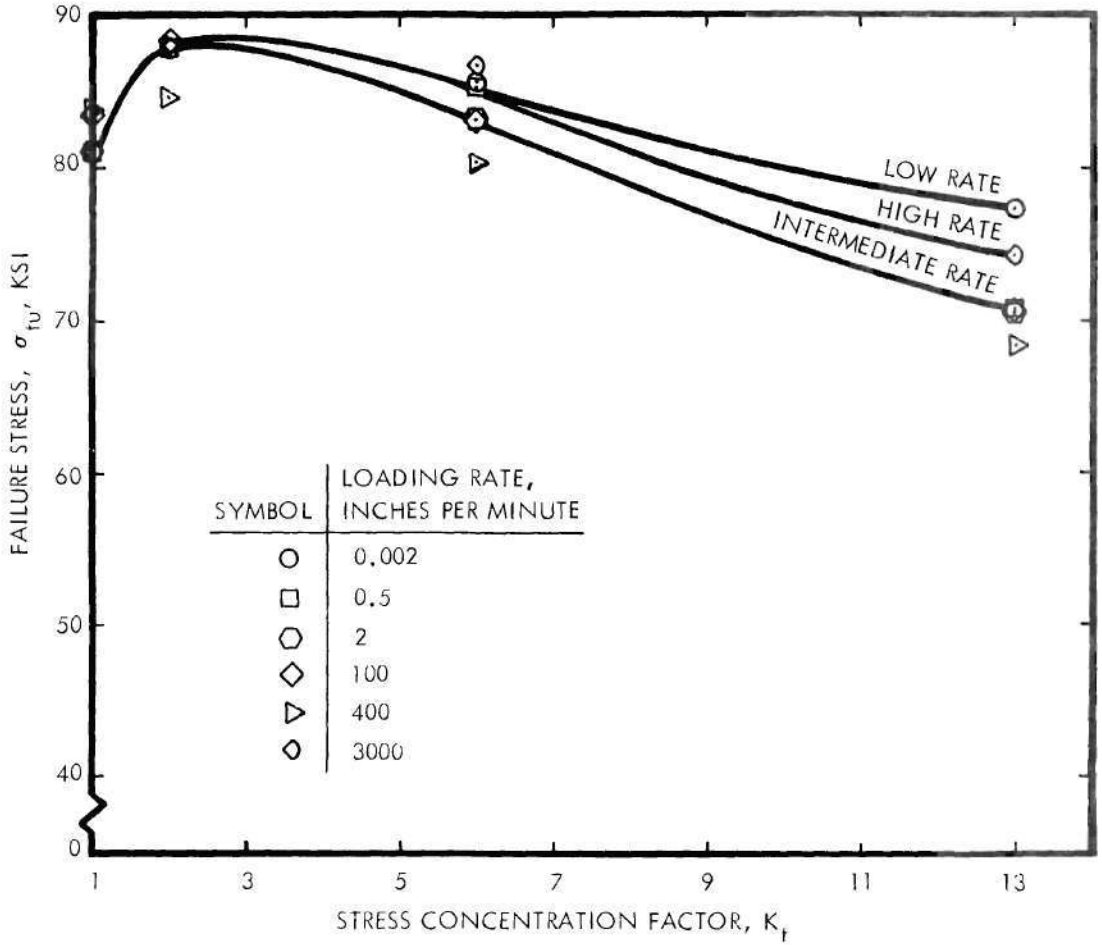

Figure 15. Effect of Stress Concentration and Strain Rate on the Failure Stress of 7075-T6 Bare Aluminum Sheet

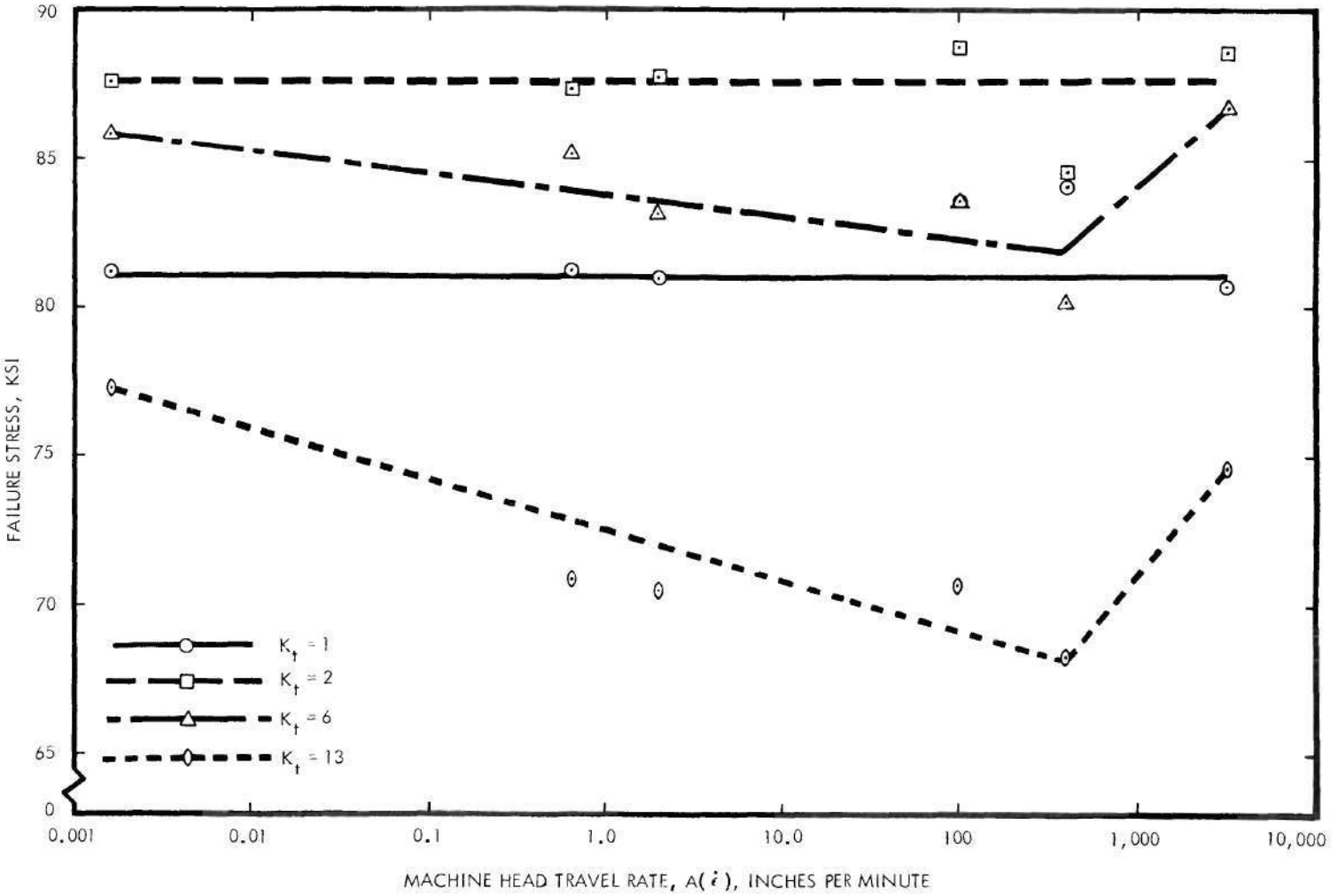

Figure 16. Effect of Stress Concentration and Strain Rate on the Failure Stress of 7075-T6 Bare Aluminum Sheet

able, except that the reversal of negative to positive slope is not readily explainable. Leslie and Sober[33] report negative slopes for steel under certain conditions. Their explanation for this was dynamic effects (strain aging) in martensite.

Yield stress measurements for the aluminum were made, but no yield points were present, and analysis of the data was complicated because of inaccuracies in the offset measurement. The use of head-travel measurements and oscilloscope recordings precluded the availability of the high magnification required for easily discernible 0.2 percent offset yield stress. As the yield stress was highly dependent on analysis technique, the yield stress curves for aluminum are not shown.

Comparison of Results for Steel and Aluminum

By comparing the failure stress versus stress concentration factor curves for steel and aluminum (Figures 12 and 14), it is seen that at a high K_t the failure stress of aluminum is decreased with increasing strain rate, while the failure stress of the steel is increased with increasing strain rate. It is evident from Figure 12 that for all rates of loading the aluminum is strengthened by a mild notch; then, when the K_t exceeds about 7, the failure stress is reduced by the presence of the notch. On the other hand, the steel (Figure 14) is strengthened to a maximum with a mild notch; then, as the notch severity is increased the failure stress decreases but never reduces to the value obtained for the smooth specimen within the K_t limits examined, i.e., no notch sensitivity (NSR > 1).

It is suggested that if the NSR versus K_t behavior shows a reduc-

tion, NSR < 1, the strength will be reduced further by increasing strain rate. If a strengthening effect is shown by NSR > 1, the result would be an increasedfailure stress with increasing strain rate.

The presence or absence of an apparent rate effect on smooth specimens is not a true indicator of the material behavior in the presence of a notch,as evidenced by the aluminum test data.

Load-Deformation Curves

Typical load-deformation curves for both steel and aluminum are shown in Figures 17 through 20 for the 0.002-inch per minute loading rate, Figures 21, 22, and 23 for the intermediate loading rates of 0.5 and 2.0 inches per minute, and in Figures 24 through 29 for the 100, 400, and 3000 inches per minute loading rates. The smooth specimen tested at 0.002-inch per minute developed a curve typical of that expected for aluminum (Figure 17). There are no yield points present in 7075-T6 aluminum. Curves for the notched aluminum specimens tested at 0.002-inch per minute are shown in Figure 18. A failure load comparison is not convenient between notched and unnotched specimens because of differences in cross-section area, but the deflection (time) scales are identical, and it is clear that increasing notch acuity decreases failure, as would be expected. The general shapes of the curves obtained from aluminum specimens are otherwise similar except for the loss in ductility with increasing K_t.

A comparison of the load-deformation curves for steel notched and unnotched specimens tested at 0.002-inch per minute shown typically in Figure 19 and Figure 20 show distinct differences. The smooth specimen

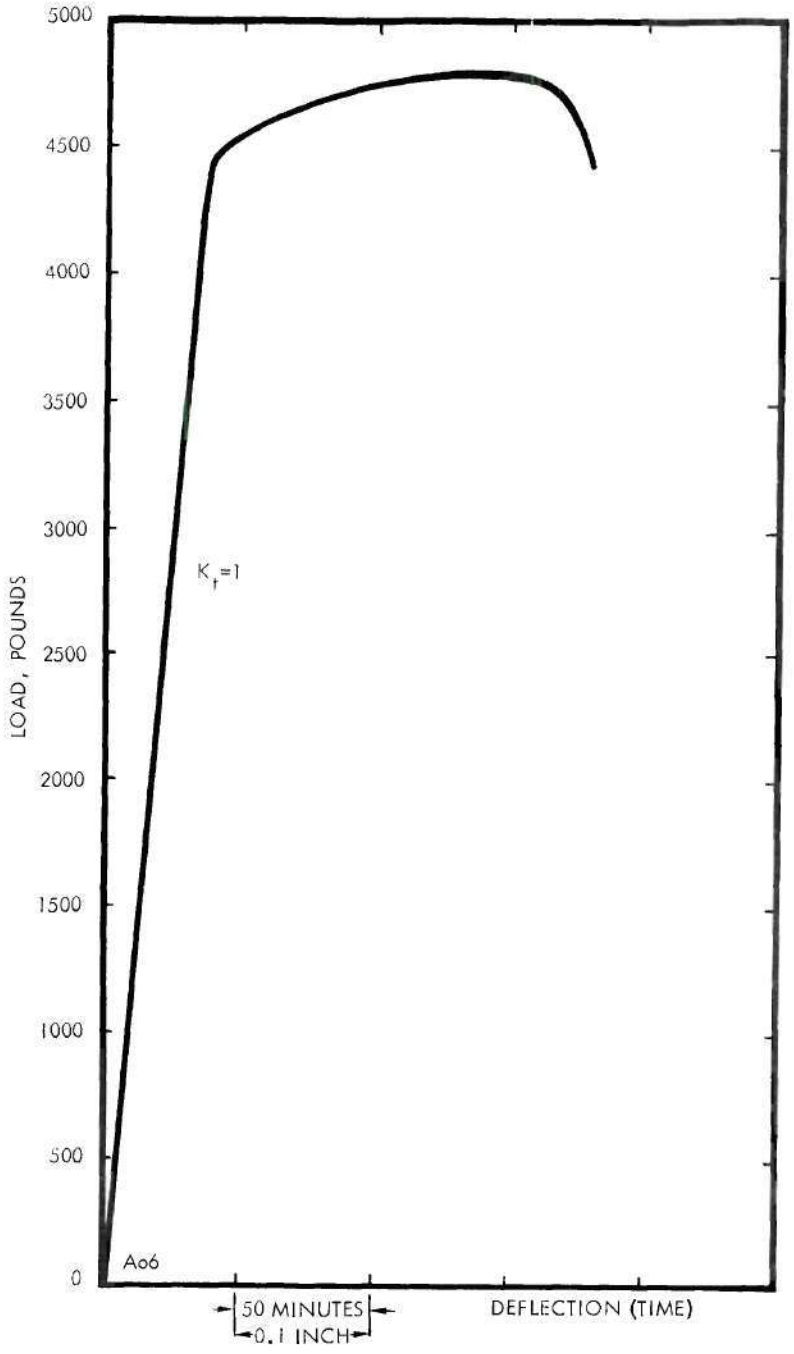

Figure 17. Typical Load-Deflection Curve for 7075-T6 Aluminum Bare Sheet Smooth Specimen Loaded at 0.002 Inch per Minute

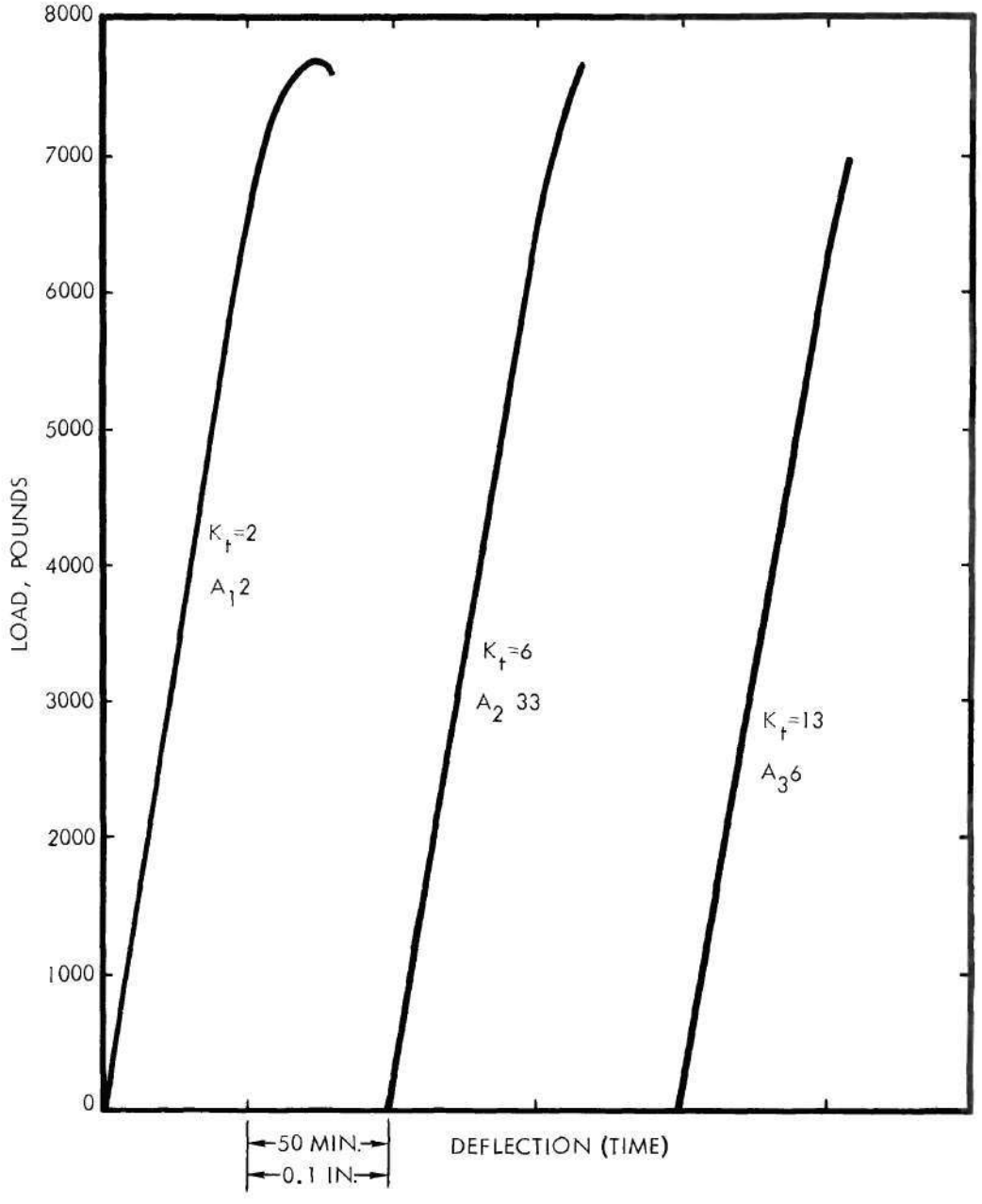

Figure 18. Typical Load-Deflection Curves for 7075-T6 Aluminum Bare Sheet Notched Specimens Loaded at 0.002 Inch per Minute

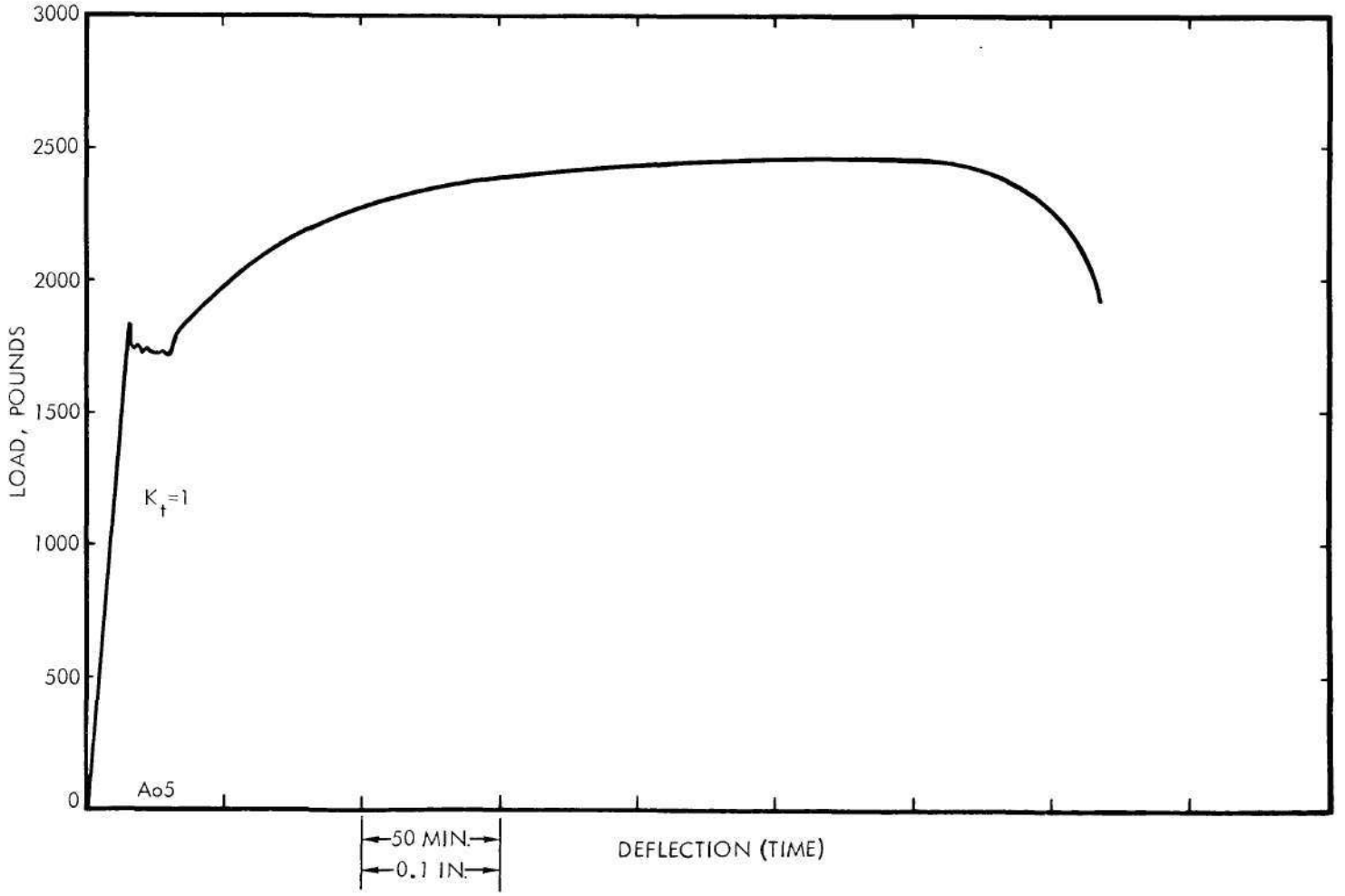

Figure 19. Typical Load-Deflection Curve for Steel Smooth Specimen Loaded at 0.002 Inch per Minute

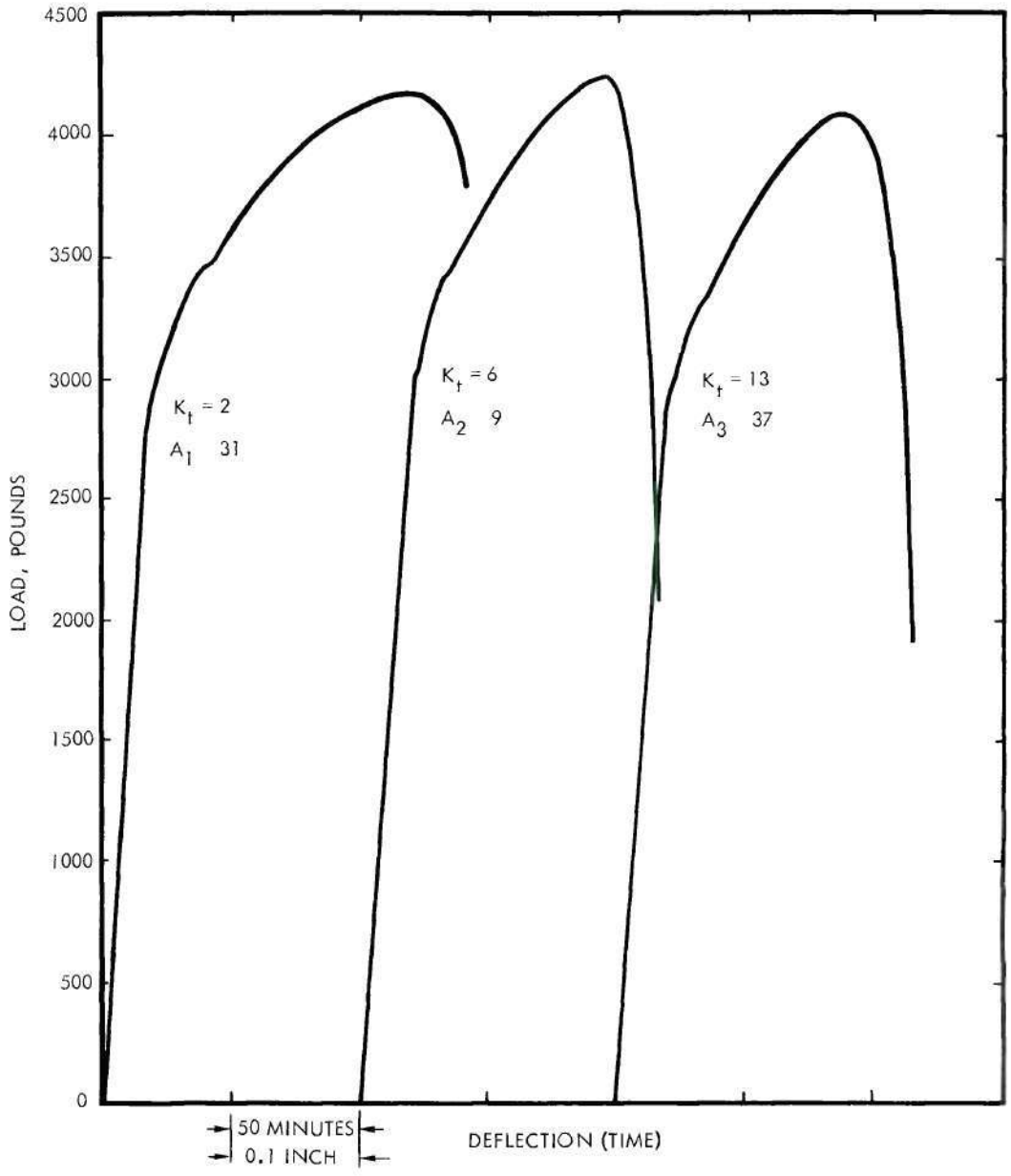

Figure 20. Typical Load-Deflection Curves for Steel Notched Specimens Loaded at 0.002 Inch per Minute

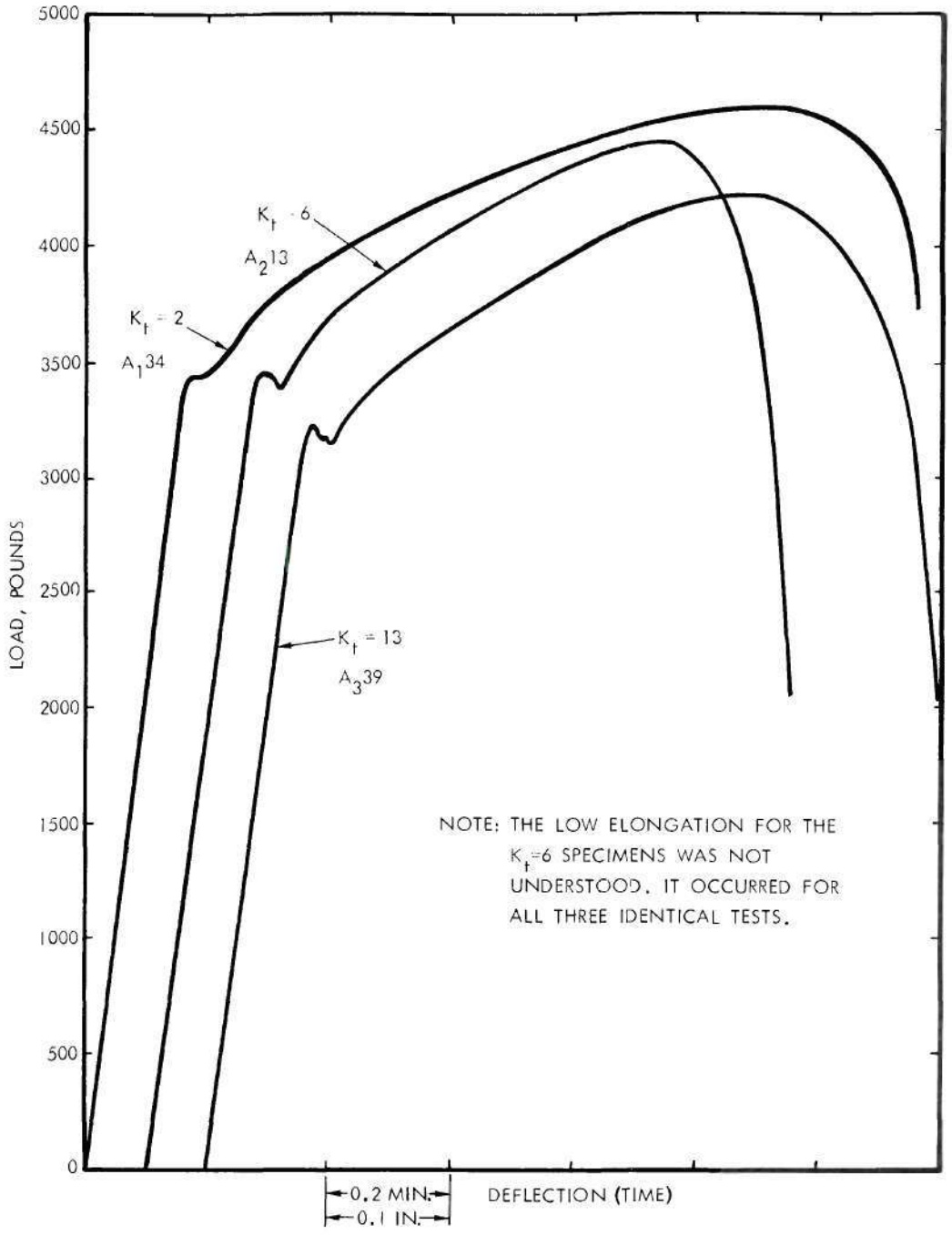

Figure 21. Typical Load-Deflection Curves for Steel Notched Specimens Loaded at 0.5 Inch per Minute

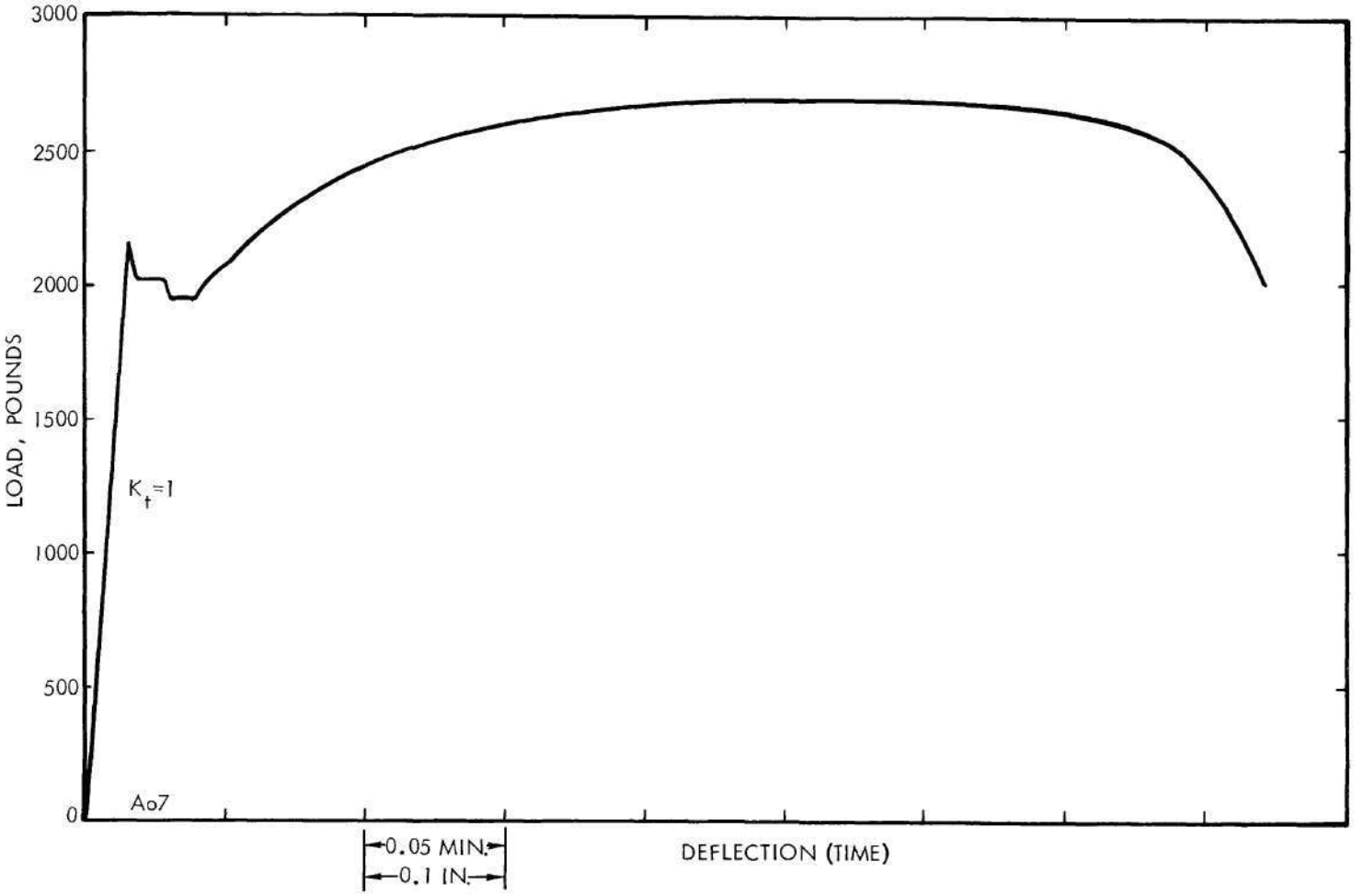

Figure 22. Typical Load-Deflection Curve for Steel Smooth Specimen Loaded at 2 Inches per Minute

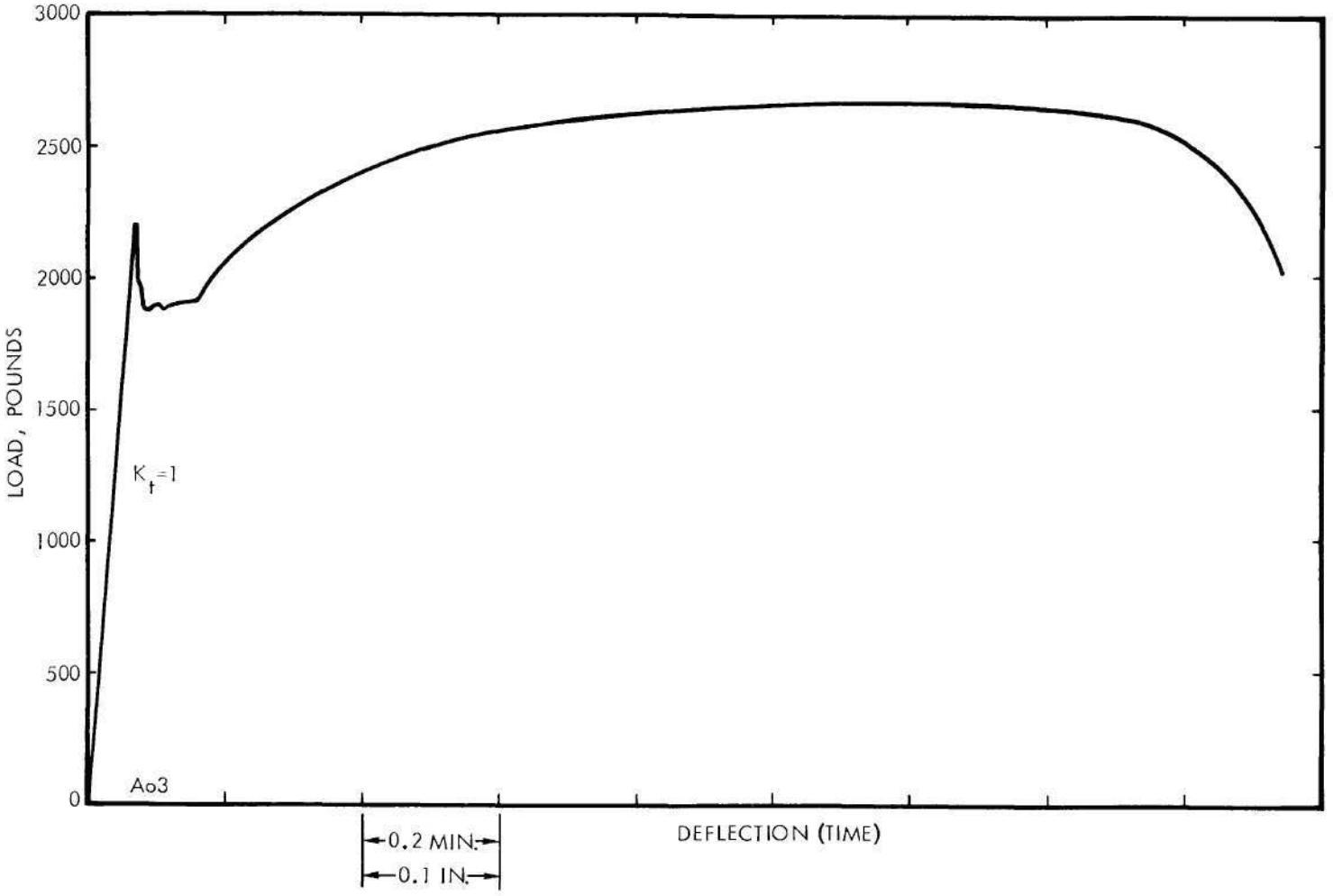

Figure 23. Typical Load-Deflection Curve for Steel Smooth Specimen Loaded at 0.5 Inch per Minute

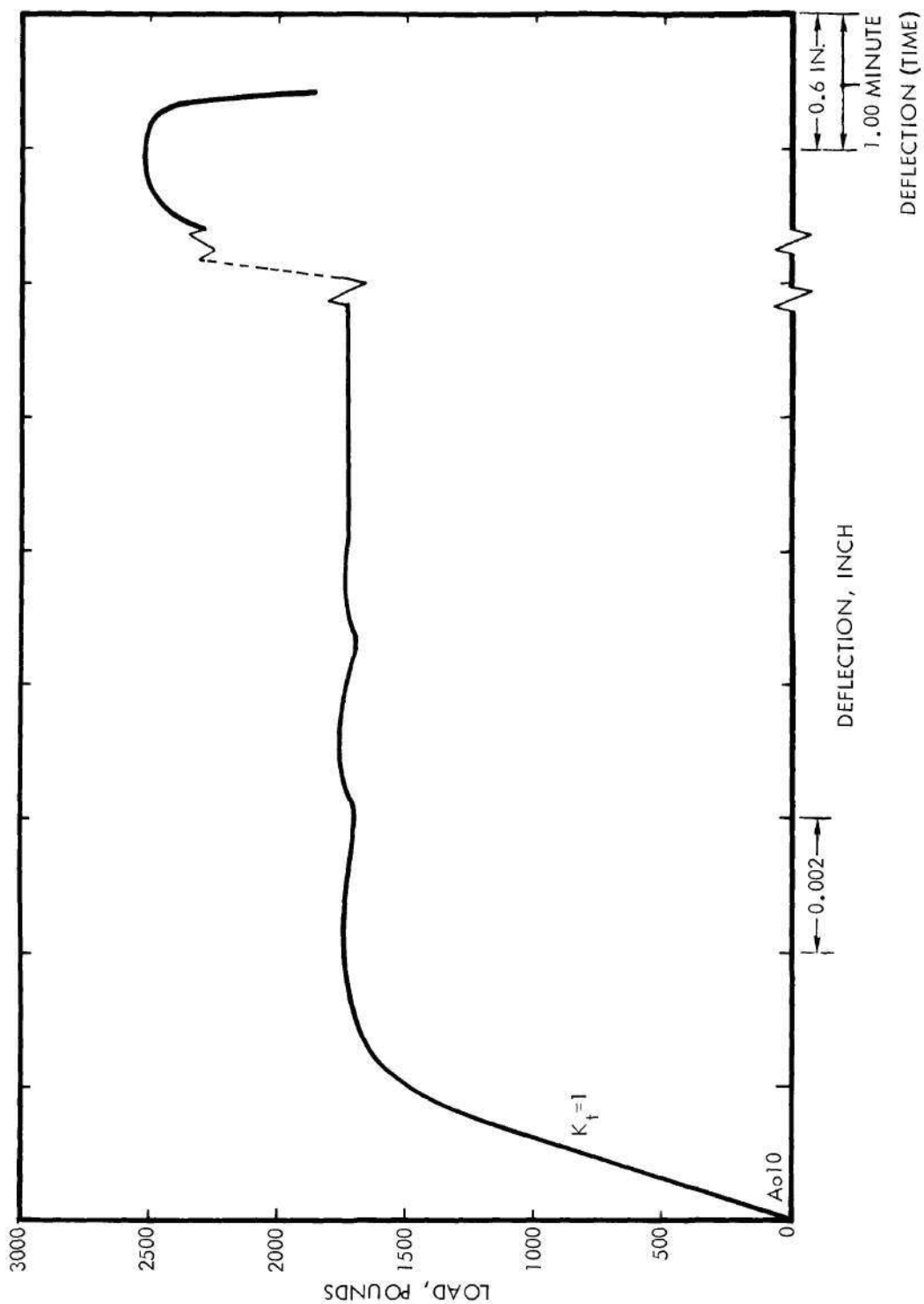

Figure 24. Typical Load-Deflection Curve for Steel Smooth Specimen Loaded at 0.005 Inch per Inch per Minute Past Yield and Same Head Travel Speed to Failure

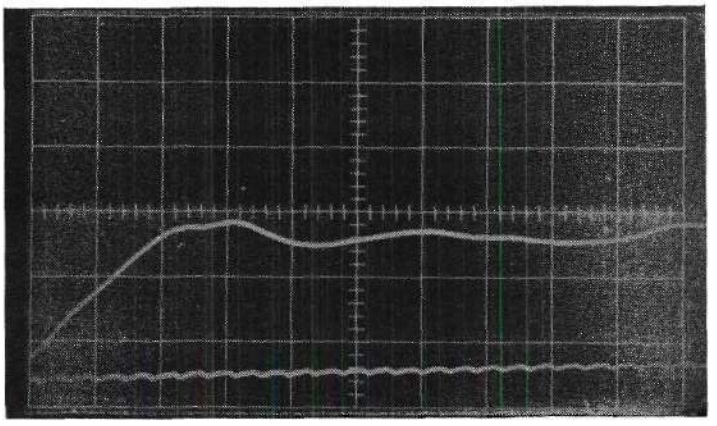

$A_o 16$ → ← 0.001 Second

400 Inches per Minute

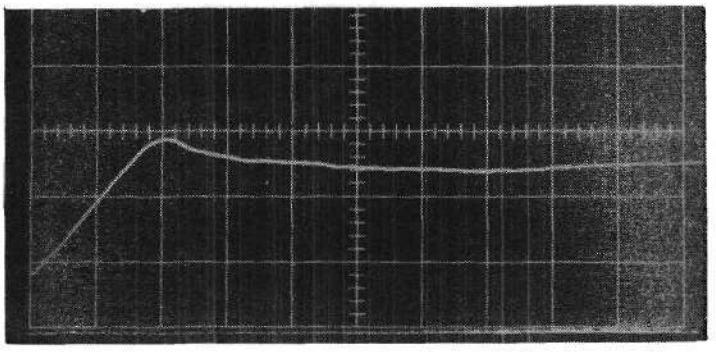

$A_o 19$ → ← 0.005 Second

100 Inches per Minute

Figure 25. Load-Time Curves for 1010 Steel Specimens Loaded at 100 and 400 Inches per Minute, Showing Drop-off Between Upper and Lower Yield Points

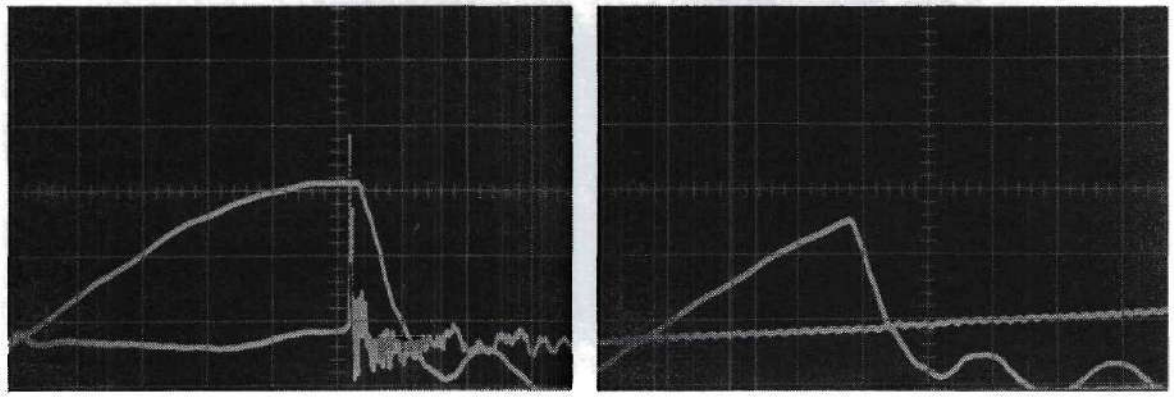

$A_1 16$ $K_t = 2$ $A_3 3$ $K_t = 13$

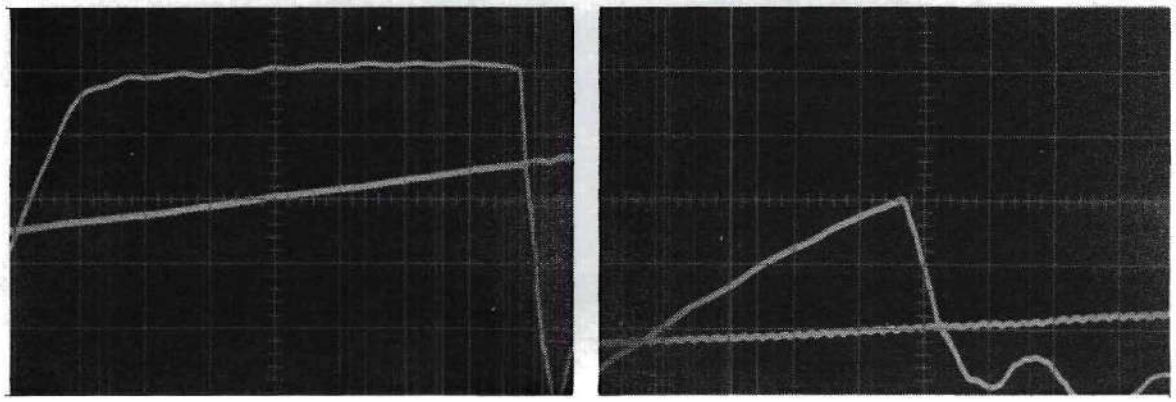

9 $K_t = 1$ $A_2 32$ $K_t = 6$

Figure 26. Typical Load-Time Curves for 7075-T6 Aluminum Loaded at 400 Inches per Minute

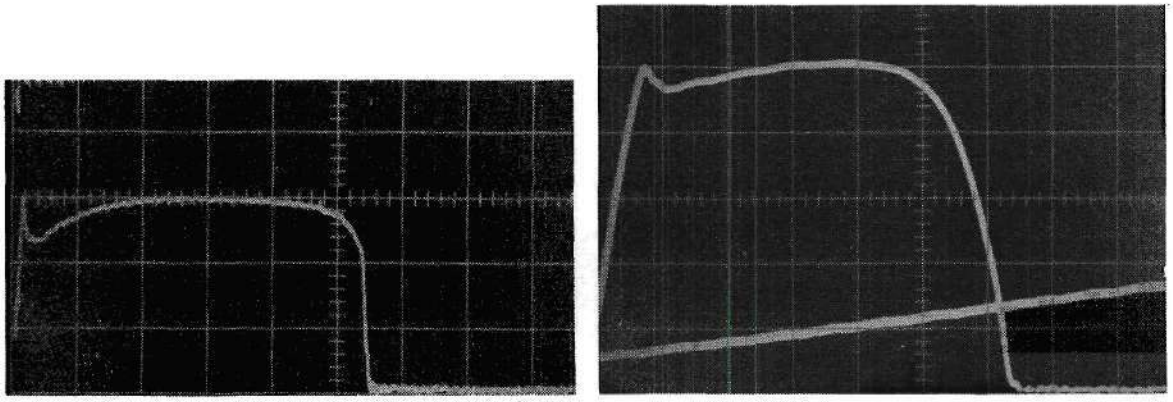

$A_o 18$ $K_t = 1$

$A_3 32$ $K_t = 13$

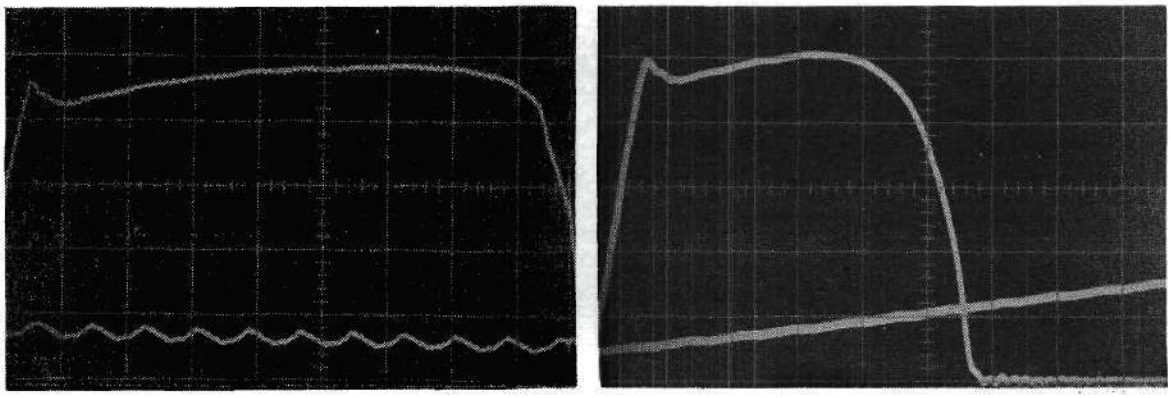

$A_1 41$ $K_t = 2$

$A_2 6$ $K_t = 6$

Figure 27. Typical Load-Time Curves for 1010 Steel Loaded at 100 Inches per Minute

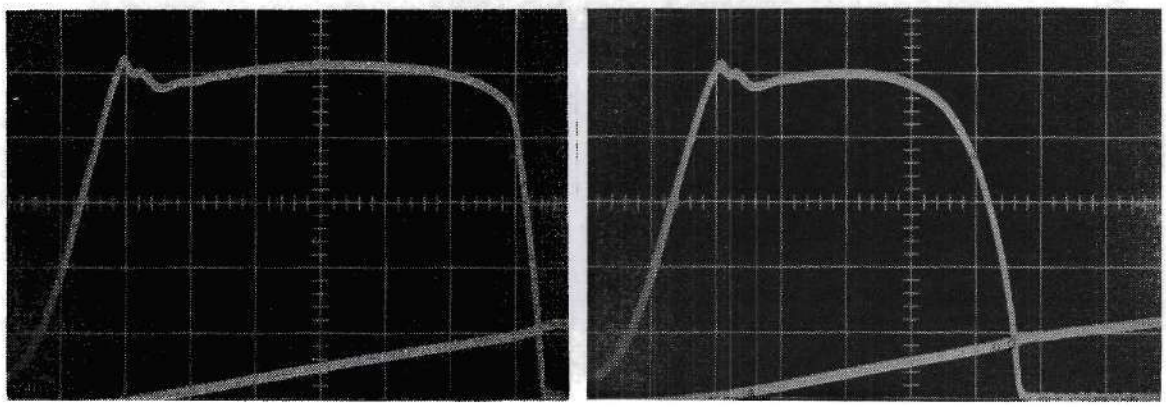

$A_1 59$ $K_t = 2$ $A_3 55$ $K_t = 13$

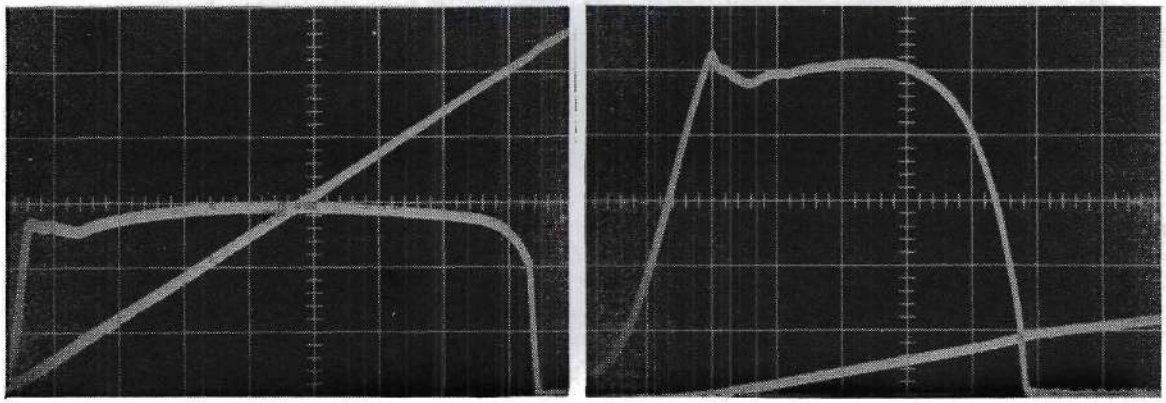

$A_o 28$ $K_t = 1$ $A_2 28$ $K_t = 6$

Figure 28. Typical Load-Time Curves for 1010 Steel Loaded at 400 Inches per Minute

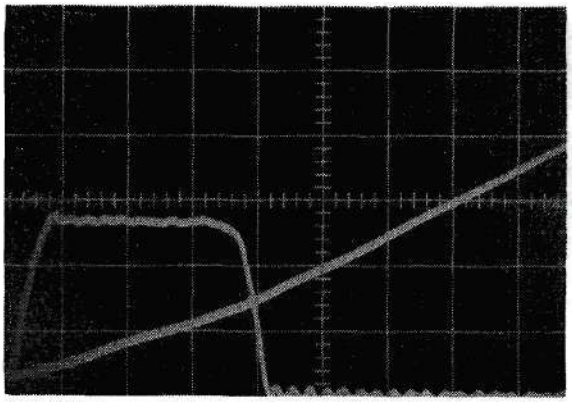

$A_1 49$ $K_t = 2$

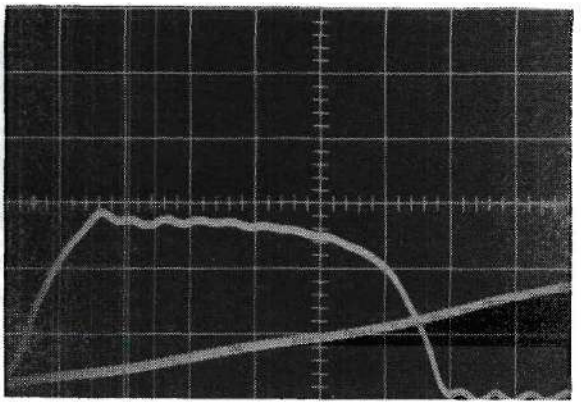

$A_3 50$ $K_t = 13$

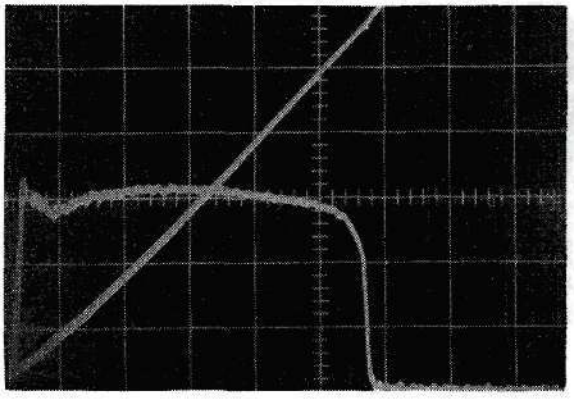

$A_o 27$ $K_t = 1$
(Electronically Filtered)

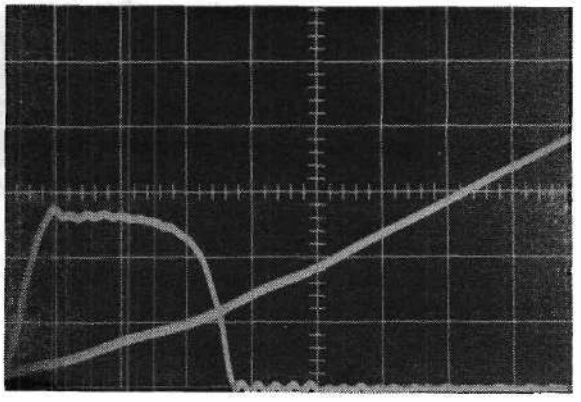

$A_2 21$ $K_t = 6$

Figure 29. Typical Load-Time Curves for 1010 Steel Loaded at 3000 Inches per Minute

(Figure 19) exhibits the normal type of curve with upper and lower yield points; but none of the notched specimens tested at 0.002-inch per minute show discontinuities in the curves that could be considered as distinct yield points. There is some loss in ductility between the specimens containing notches with $K_t = 2$, and $K_t = 6$ (about 20 percent), but no apparent change in ductility between the specimens containing notches with $K_t = 6$ and $K_t = 13$. This behavior was typical of all specimens of these configurations tested.

Typical load-deformation curves of steel for loading rates of 0.5 and 2.0 inches per minute are shown in Figures 21, 22, and 23. Curves obtained from aluminum were all so similar in shape to those shown in Figures 17 and 18 that presentation is unnecessary. At 0.5-inch per minute, the steel mild notch, $K_t = 2$, shown in Figure 21, first showed a slight non-linearity, then a plateau, and finally a very slight drop-off. As the notch acuity increased, the upper and lower yield points became more pronounced.

Increasing the loading rate to 2 inches per minute produced curves for notched specimens with distinct yield points very similar to those produced at 0.5-inch per minute for specimens containing notches with $K_t = 6$ and $K_t = 13$. Presentation of all these curves is unnecessary due to this similarity between curves.

For smooth specimens, as the time scale is increased it becomes obvious that the drop-off from upper tensile yield is not instantaneous. This drop-off is at least two times slower than the response rate of the recorder at 2 inches per minute recorder speed. This was evident in comparing yield drop-off with failure drop-off. It was verified that

time was required for the drop-off by testing specimens at a controlled strain rate of 0.005-inch/inch/minute using a Baldwin PS5M extensometer. Although controlling at this rate was almost impossible due to the speed of the reactions taking place during yielding, the fast drop-off was eliminated, as shown in Figure 24.

Controlled strain rate tests were also conducted on aluminum. The results indicated no measurable differences in σ_{tu}, σ_{ty}, or percent elongation between these tests and the controlled head-travel tests. The results of controlled strain rate tests for both materials are given in Table 4.

The drop-off rate was further investigated at loading rates of 100 and 400 inches per minute. A smooth specimen similar to A_o18 (later shown in Figure 27) was tested under identical conditions except that the oscilloscope time scale was set for 0.005 second per cm, rather than 0.1 second per cm, shown for A_o18. The result, shown in Figure 25, is that the drop-off time is measurable. The time measured from upper yield to lower yield was 0.025 second at a loading rate of 100 inches per minute. At a loading rate of 400 inches per minute a similar curve was obtained. There is no drop-off readily apparent. The curve shows oscillations which were attributed to ringing. However, even if the oscillations shown were interpreted as a lower yield, drop-off would require 0.001 second.

The drop-off time from upper to lower yield points at 100 inches per minute is a significantly large percentage of the test time. For smooth specimens, drop-off required 0.025 second, and the total test time was 0.13 second. For notched specimens, drop-off time was 0.008 second

Table 4. Tensile Properties of 1010 Cold-Rolled Steel Sheet and 7075-T6 Bare Aluminum Sheet Tested at a Controlled Strain Rate of 0.005-Inch Per Inch Per Minute

Spec. No.	σ_{tu}, KSI	σ_{ty},* KSI	σ_{uty}, KSI	σ_{lty}, KSI	Elongation in 2 Inches, Percent	Material
A_o10	83.2	77.4			14.5	Aluminum
A_o11	78.6	71.4			13.5	Aluminum
A_o12	78.2	70.6			13.8	Aluminum
Average	80.0	73.1			13.9	Aluminum
A_o10	43.7		30.0	29.3	39.5	Steel
A_o11	42.8		33.2	31.0	38.0	Steel
A_o12	43.7		34.0	29.1	40.5	Steel
Average	43.4		32.4	29.8	39.3	Steel

* Yield stress was measured at 0.2 percent offset.

as compared to a total test time of 0.020 second. The drop-off time for these two examples is 19 and 40 percent of the total test time, respectively.

At the faster loading rates, 100, 400, and 3000 inches per minute, the load-time curves for aluminum (shown in Figure 26) are similar to those obtained for the slower rates. For the steel, however, the curves obtained at the faster rate show marked differences from those obtained at the slower rates. Typical load-time curves for steel obtained at 100, 400, and 3000 inches per minute are shown in Figures 27, 28, and 29. The upper and lower yield points are very close to the failure loads, and some of the upper yield points are above the failure loads. To evaluate this behavior, the data for upper yield point, lower yield point, and failure stress were plotted in Figures 30 through 33 versus the logarithm of the loading rate. For each configuration tested, the upper yield point exceeded the failure load for some loading rates. The crossover point occurred at a slower loading rate as notch acuity increased. For the sharpest notch (K_t=13), the lower yield point is almost equal to the failure load (Figure 33).

The upper and lower yield stress data versus the loading rate are summarized in Figure 34. An increase in yield stresses with strain rate and stress concentration factor is shown. The highest yield stress values appear to be obtained with the notched specimens where $K_t = 6$, which is reasonable, since the stress versus K_t curves (Figure 14) all show a maximum at some intermediate value of K_t between 2 and 6.

Figures 30 through 34 also show the linear logarithmic relationship of stress as a function of strain rate with a slope change in the approximate range of the transition from Region I to Region II and the

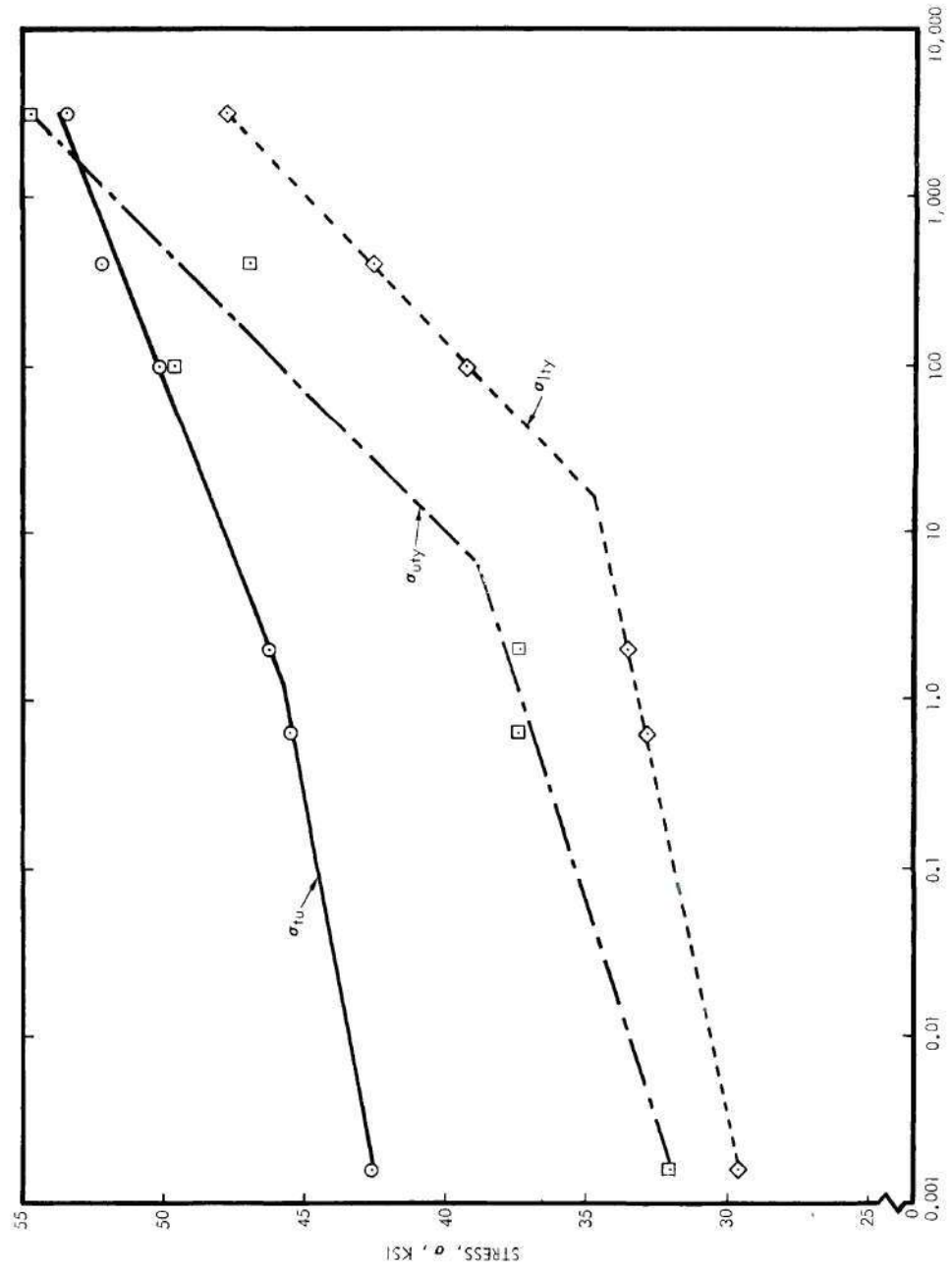

Figure 30. Variation of Tensile Properties of 1010 Steel, Cold-Rolled Sheet, Smooth Specimen, $K_t = 1$, with Strain Rate

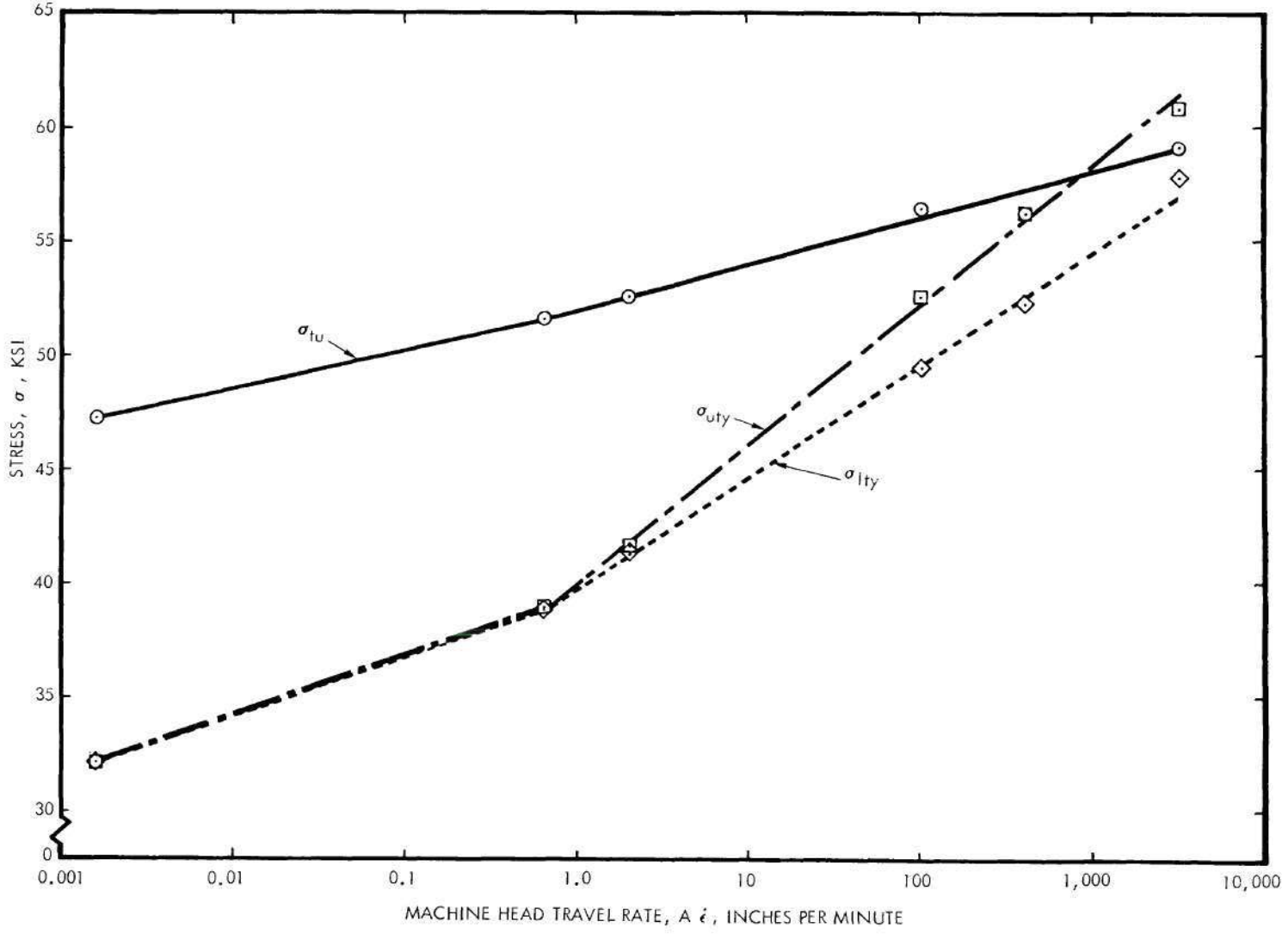

Figure 31. Variation of Tensile Properties of 1010 Steel, Cold-Rolled Sheet, Notched Specimens, $K_t = 2$, with Strain Rate

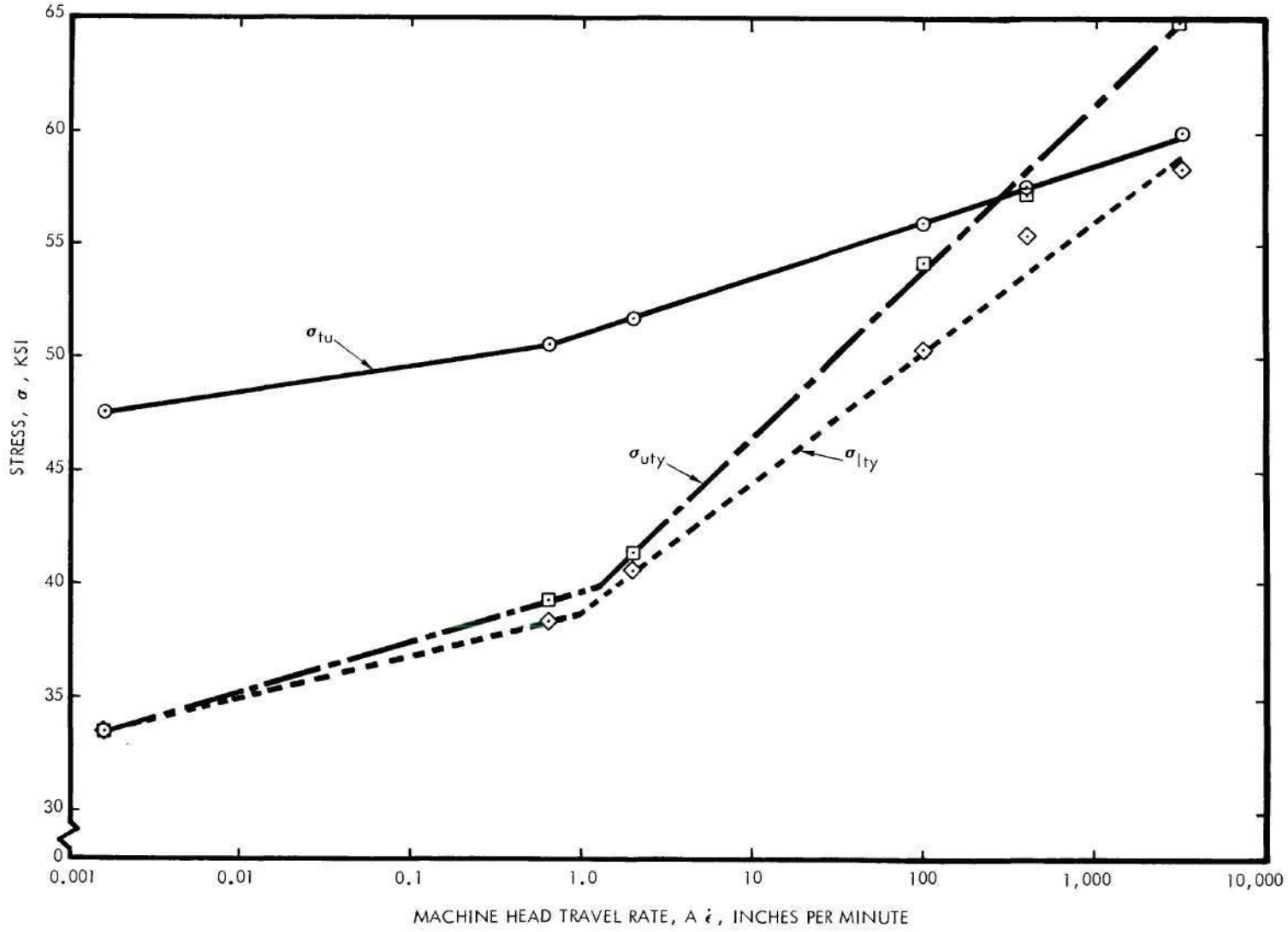

Figure 32. Variation of Tensile Properties of 1010 Steel, Cold-Rolled Sheet, Notched Specimens, $K_t = 6$, with Strain Rate

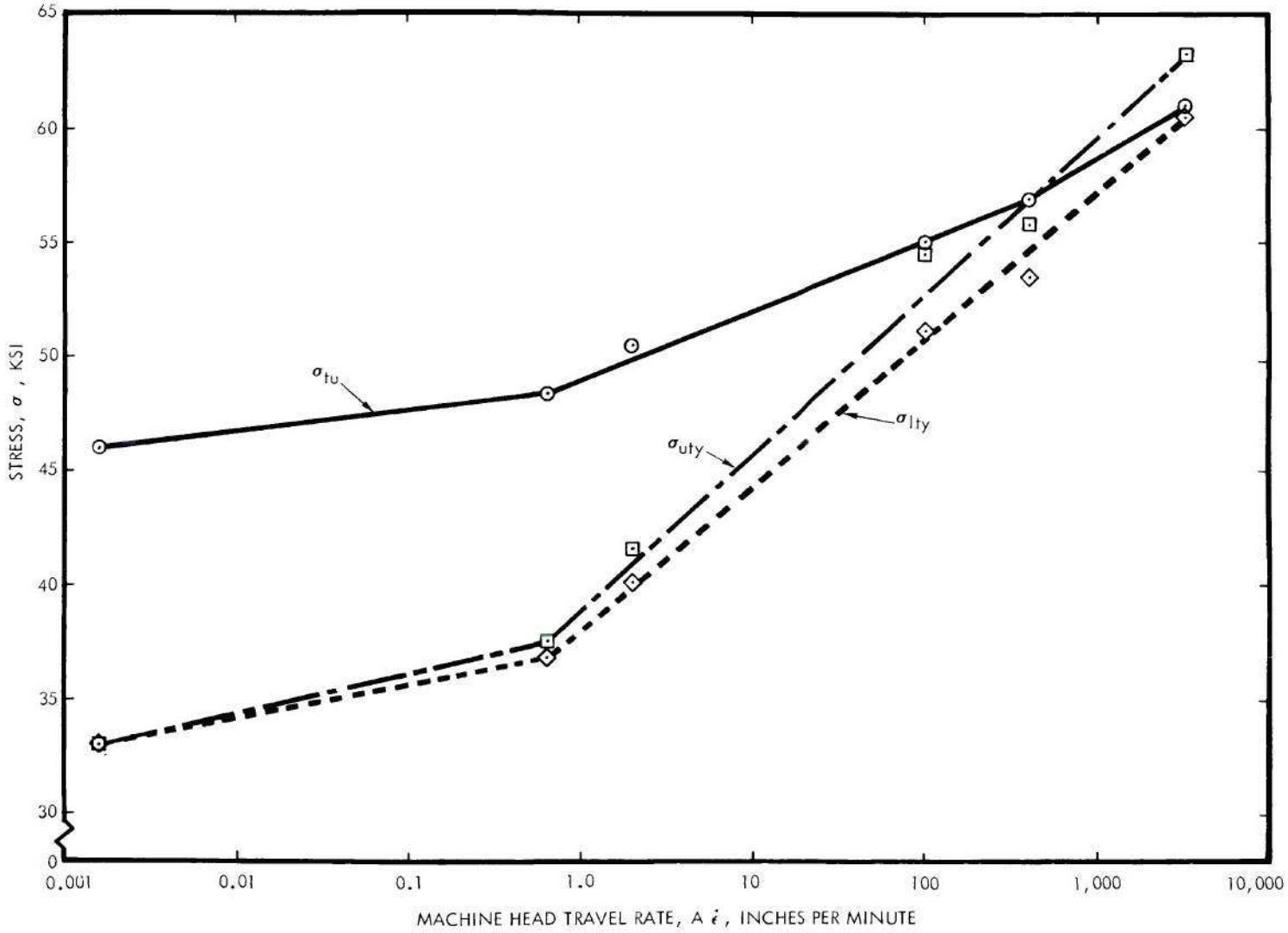

Figure 33. Variation of Tensile Properties of 1010 Steel, Cold-Rolled Sheet Notched Specimens, K_t = 13, with Strain Rate

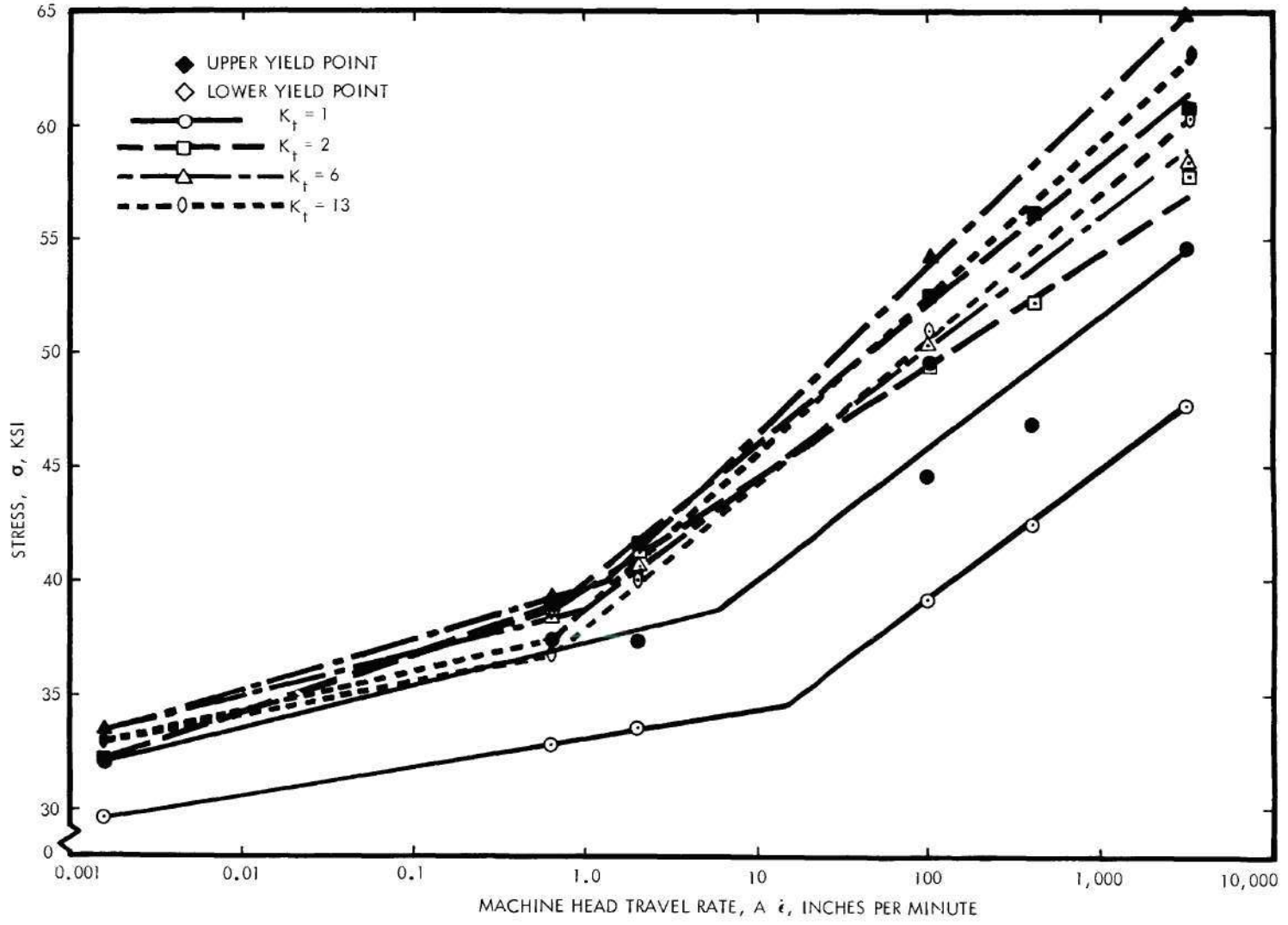

Figure 34. Variation of Upper and Lower Yield Points of 1010 Steel, Cold-Rolled Sheet, with Strain Rate and Stress Concentration

one indication in Figure 33 of a transition from Region II to Region IV.

The elongation in 2-inch gage length for both aluminum and steel are shown in Figures 35 and 36. As would be expected, the percent elongation is reduced drastically in the presence of a notch. No indication of loading rate is evident for the aluminum (Figure 35), but for the steel an increase in elongation is obtained with increasing loading rate for smooth specimens (Figure 36). These data do not indicate a loading rate effect on elongation for notched specimens, although such a dependency may exist and be covered up by experimental error.

The elongations for the smooth specimens are plotted versus the rate parameter in Figure 37. The steel tests exhibit an increase from 34 to 46 percent elongation within the loading rate range examined. Therefore, in addition to increasing the yield stresses and failure stress, the specimen is elongated with increasing rate. This is explainable if the yielding mechanism is again considered. As loading rate is increased, the upper yield point is increased. Thus, the possibility exists that more areas begin to yield at the same time, and instead of slip bands occurring in sequence several occur simultaneously, resulting in a larger elongation.

The data indicate that the aluminum may have a reduction in elongation over the rate range tested. This reduction may appear only as a result of the enlarged elongation scale and may actually be experimental error, although each point is an average of at least three values.

It should be realized that all of the notched specimen results are affected by the plastic zone size ahead of the notch tip. The material tested was all 1/8-inch thick, a size insufficient for develop-

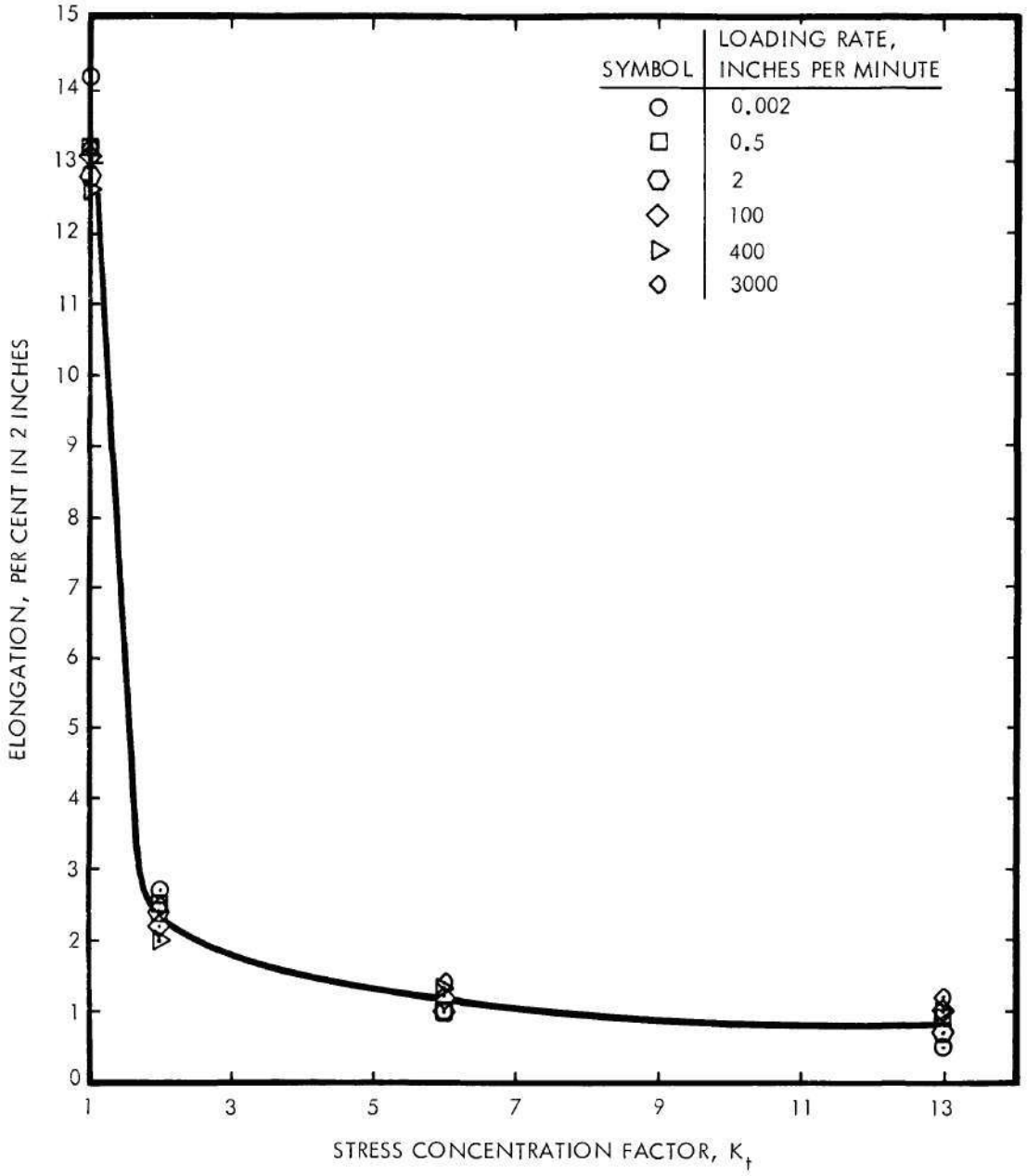

Figure 35. Elongation of 7075-T6 Bare Aluminum Alloy Sheet Versus Stress Concentration Factor for Different Loading Rates

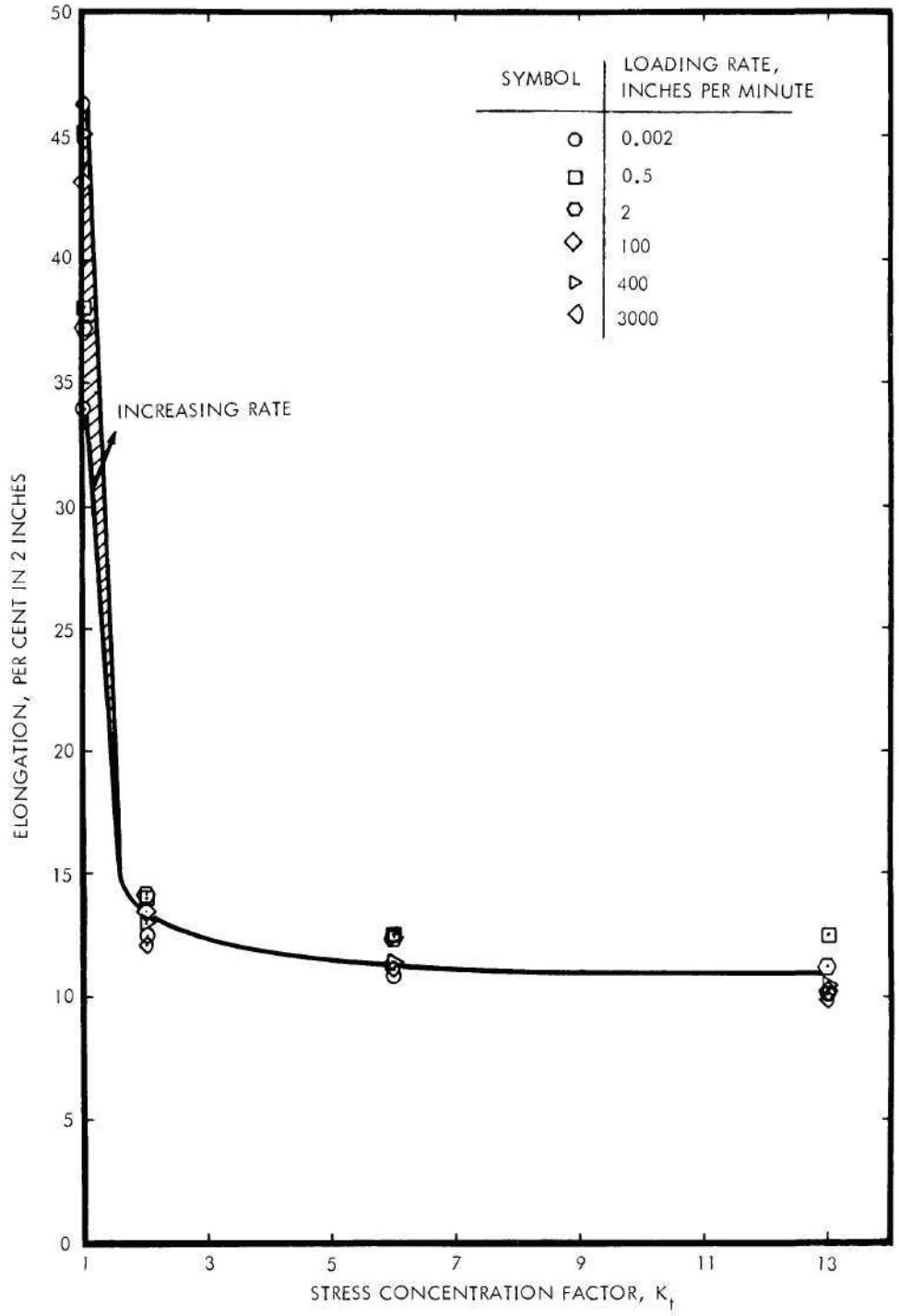

Figure 36. Effect of Stress Concentration and Strain Rate on the Elongation of 1010 Cold-Rolled Steel Sheet

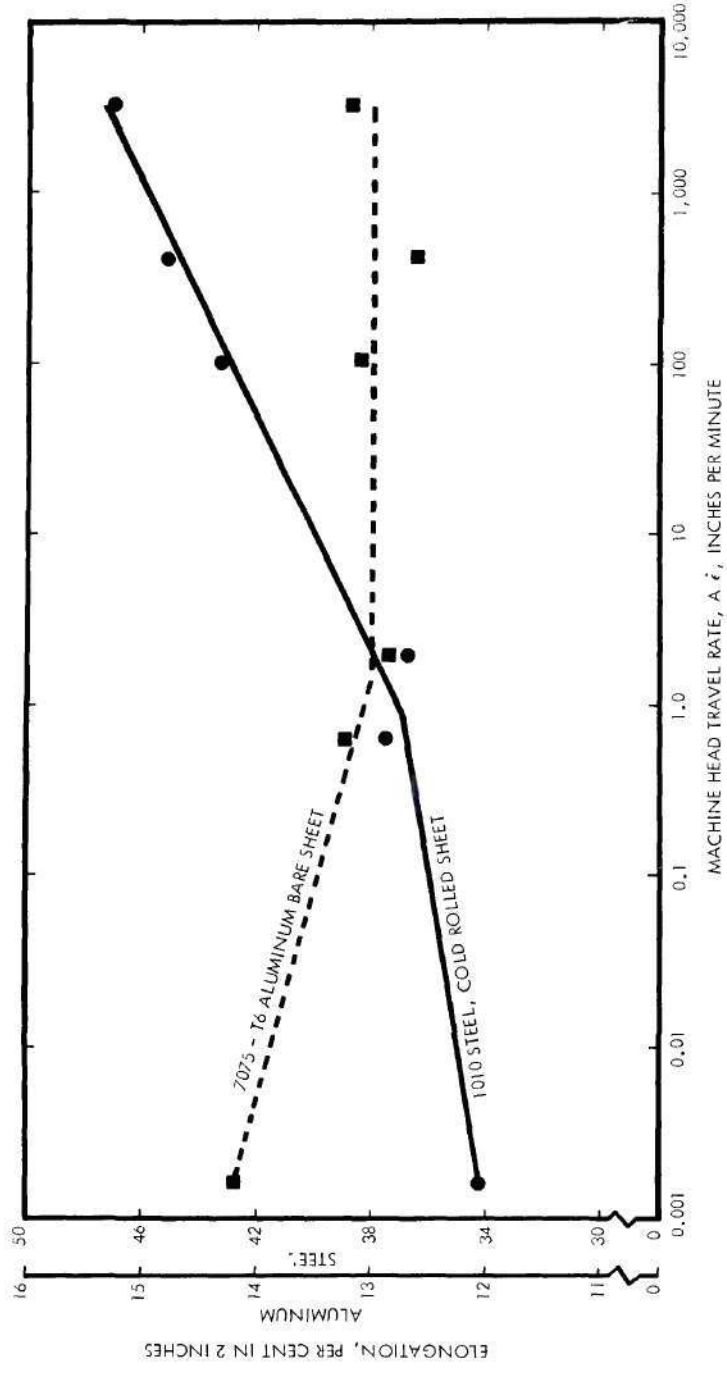

Figure 37. Effect of Strain Rate on the Elongation of Smooth Tensile Specimens of 7075-T6 Aluminum Bare Sheet and 1010 Steel, Cold-Rolled Sheet

ment of plane strain constraint on the notch; hence, gross plasticity was present upon failure. Although the numerical results are only valid for material of this thickness, the trends should apply to any thickness.

CHAPTER V

DISCUSSION

The approach used here for analysis of fracture stress, yield stress, and percent elongation has been to plot the property versus the logarithm of the strain rate. Each property was plotted in the same manner. Rosenfield and Hahn[30] evaluated a differential yield stress, defined as the yield stress at the strain rate being investigated, minus the yield stress obtained at 0.001-inch per inch per second. The results plotted in Figure 30 show that the yield and fracture stress are continuously changing with strain rate below this reference value.

A differential stress value would have no real meaning without including the reference value. Therefore, it appears more straightforward to leave out the reference value and to plot the absolute value of the yield and failure stresses. To compare the techniques, a plot of $\Delta\sigma_{tu}$ versus $\dot{\epsilon}$ for the 1010 cold-rolled steel is shown in Figure 38. It is apparent that the curve for the smooth specimen, $K_t = 1$, looks the same as for the σ_{tu} versus $\dot{\epsilon}$ curve shown in Figure 13. A different shape, however, is obtained for the family of curves analyzed by the two different methods. The value chosen for reference in Figure 38 was 0.002-inch per minute. Since this or any other value chosen for reference is reduced to a single point for all K_t's, all curves will be forced through this point.

The same general conclusions can be drawn from Figure 38 as from

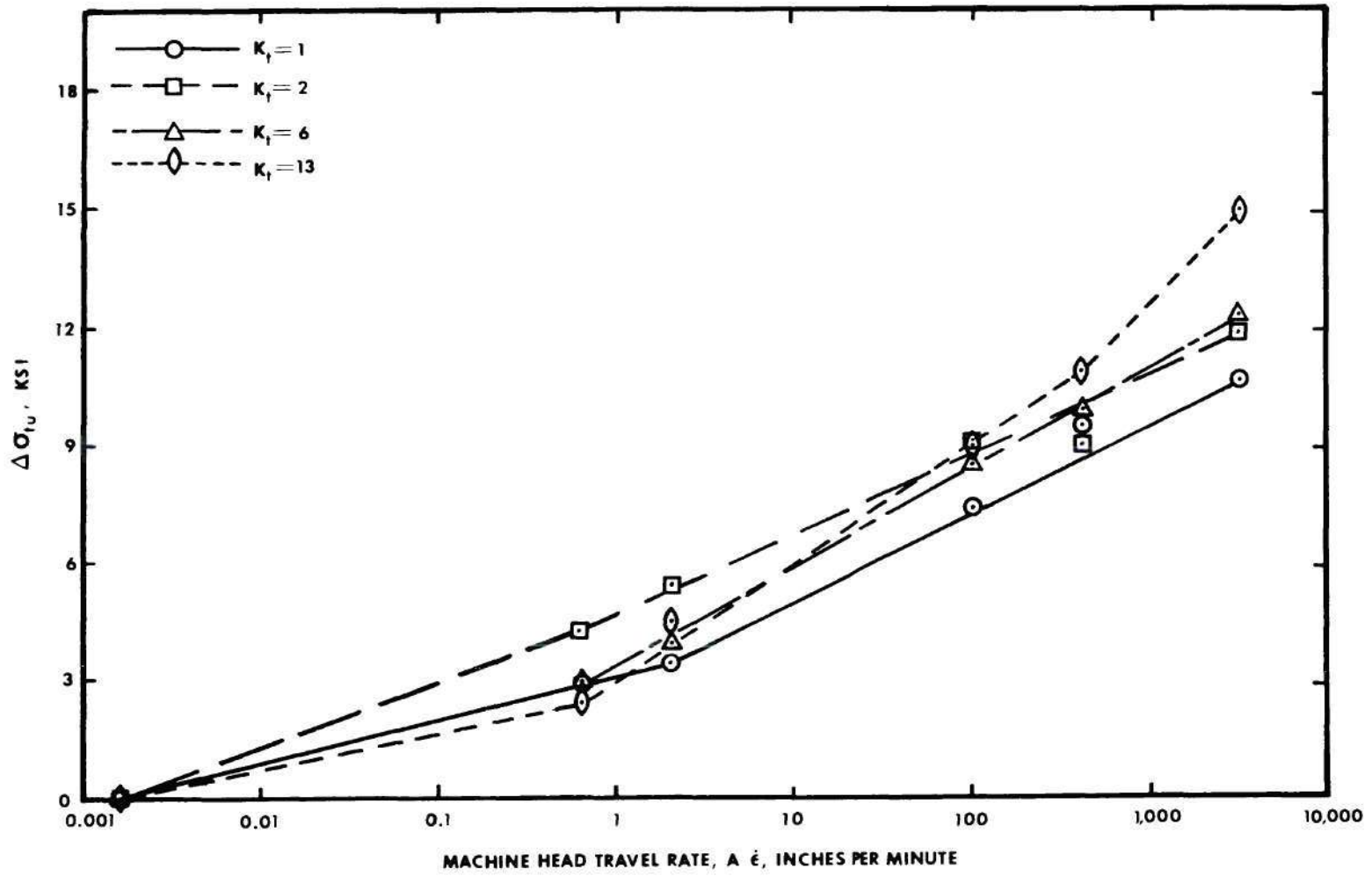

Figure 38. Effect of Stress Concentration and Strain Rate on the Differential Failure Stress of 1010 Cold-Rolled Steel. The differential is between actual failure stress at the indicated rate and the failure stress obtained at 0.002 inch per minute.

Figure 13, but because the curves are forced through a point, interpretation is more difficult than from Figure 13. This difficulty could be eliminated by using a failure stress of the smooth specimen for all references, but there appears to be no advantage of this single reference value over using actual values for σ_{tu} as depicted in Figure 13.

Further insight into the strain rate sensitivity behavior of materials in the presence of stress concentrators can be obtained if plastic deformation at the notch tip is considered. The previous discussion on stress concentration factors uses the concept of elastic stresses or the notch strength ratio to describe material behavior. In the elastic state, the local strain rate in the vicinity of the notch is simply K_t times the gross strain rate $\dot{\epsilon}$, as shown by Hendrickson, et al[37]. However, in the presence of local deformation of the magnitude shown here, the elastic stress concentration factor cannot determine the local strain rate. For this analysis, a plastic stress concentration factor, K_p, is used. Neuber's notch rule[43] could be used here, but the concept of Hardrath and Ohman[44] will be used, since it does not require a mathematical expression of the stress-strain curve. This concept is expressed in the following equation:

$$K_p = 1 + \left(K_t - 1\right)\left(\frac{E_s}{E}\right) \quad , \tag{6}$$

where E_s is the secant modulus at fracture for the notched specimens, and E is the modulus of elasticity of the material.

The local plastic strain rate, $\dot{\epsilon}_p$, will be equal to:

$$\dot{\epsilon}_p = K_p \dot{\epsilon} \quad . \tag{7}$$

The failure stress data for the 1010 steel were re-evaluated on the basis of σ versus $\dot{\epsilon}_p$, and are shown in Figure 39. It now becomes apparent that the curves for the different K_t's are parallel, within experimental error, throughout the strain rate range investigated, with one exception. The specimens with $K_t = 13$ tested at 3000 inches per minute apparently attained an $\dot{\epsilon}$ that is dominated by Region IV behavior as discussed previously. Therefore, it is concluded that the concept of Hendrickson, et al.[37] can be extended to include plastic deformation by the use of Equation (7).

Equations (6) and (7) were applied to the 7075-T6 data, and the resulting curves were so similar in shape to Figure 16 that no conclusions could be drawn. Therefore, analysis of 7075-T6 aluminum by this method is not included.

Although a continuum mechanics approach has been taken thus far in the data evaluation, it is useful in interpretating the shapes of the load-deformation curves to consider dislocation movement. Orowan[45] proposed that, for mild steel, obstacles to slip are reinforced by carbon and nitrogen atoms, and dislocations are not locked but rather blocked or slowed down from free run by these obstacles. In a single crystal of iron without mobile dislocations, the yield point phenomenon is theorized to occur because the production or mobilization of the first dislocations requires a higher stress than their multiplication. In polycrystalline iron, yielding is caused by the subdivision of the specimen into small regions containing few dislocations. (These sub-

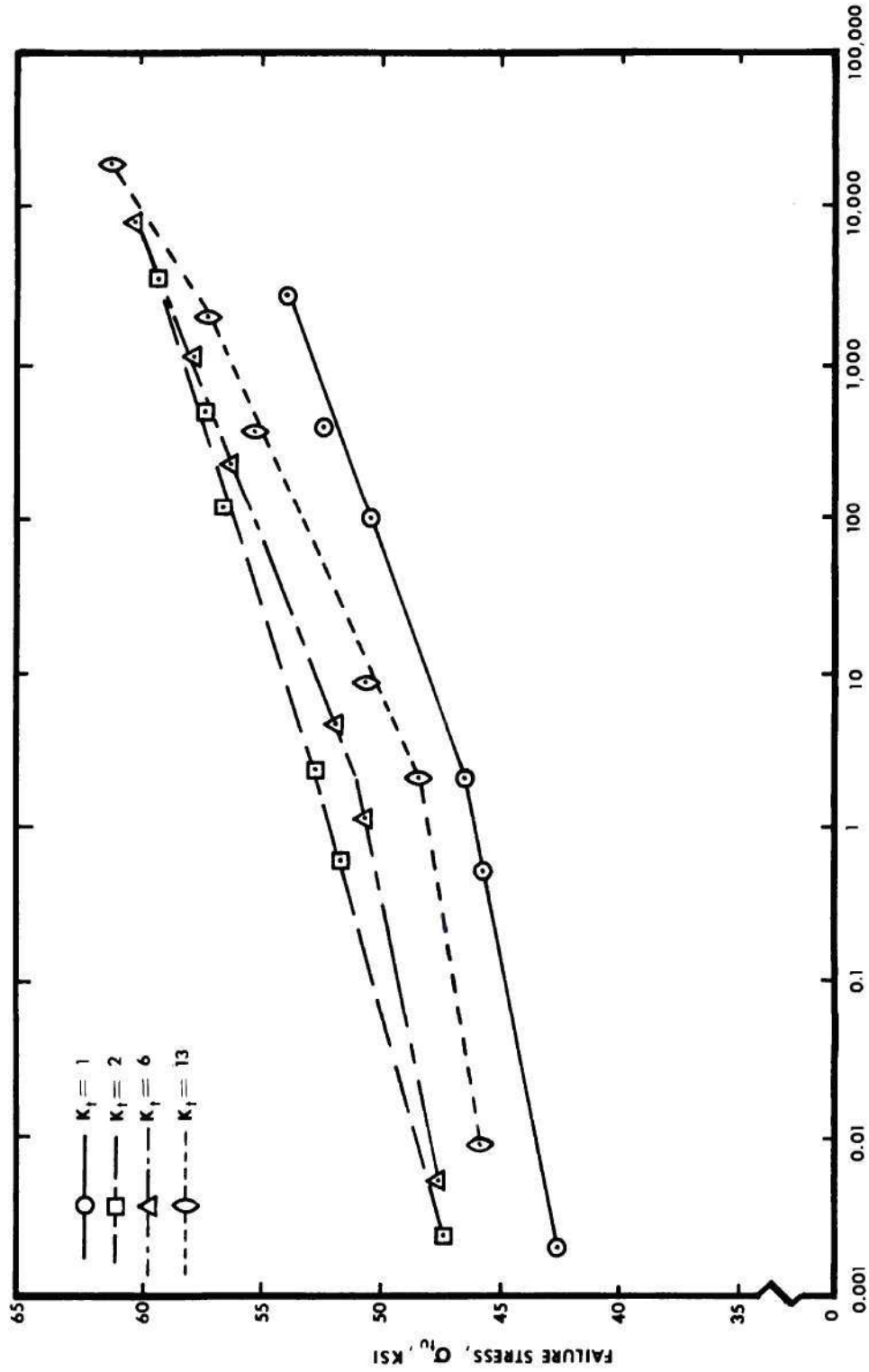

Figure 39. Effect of Stress Concentration and Plastic Strain Rate, as Defined by Equation (7) on the Failure Stress of 1010 Cold-Rolled Steel

divisions are caused by the presence of the following defects: grain boundaries, sub-boundaries, or other strain-hardening obstacles reinforced by impurity atoms, such as bent but not polygonized slip lamallae.) The carbon-reinforced obstacles can prevent initial free run of the dislocations. The upper yield point is then the point where the dislocations reach the velocity needed for breeding into avalanches which break through the reinforced obstacles. A reduced stress or the lower yield stress is the stress required for further breeding and extensive deformation.

A combination of a high stress at a notch and a slow loading rate could cause dislocations to move slowly through the obstacles without ever reaching the velocity required for the avalanche. This condition could feasibly be obtained with smooth specimens, but the loading speed would necessarily be slower since the high stress due to the notch would not be present. As the loading rate is increased, the dislocations begin to move with greater velocities and avalanching occurs. Apparently the combination of $K_t = 2$ and head travel = 0.5-inch per minute appears sufficient to cause dislocation multiplication at a rate approximately equal to the loading rate, and the result is elongation at a stable load.

There is a certain time required for the dislocation multiplication phenomenon to occur. In a smooth tensile coupon loaded at a slow rate, this time is insignificant when compared to the total test time. As the rate is increased this time is a significant percentage of the test time, for instance, about 30 percent at 100 inches per minute, and there is an interaction between the forced elongation rate and the dislocation multiplication rate. This would lead to an increase in the

upper yield point with strain rate, since additional stress is applied to the specimen while the multiplication rate is nearing the critical value for avalanching. Similarly, the lower yield point is raised with increasing strain rate, because the loading rate is large compared to the time required for the avalanche to reach equilibrium. Due to the quickly imposed strain rate, the specimen is being forced apart fast enough to prevent avalanche equilibrium. The failure stress would not be expected to increase as much with strain rate as the yield points, because strain hardening would have more time to reach a terminal velocity.

CHAPTER VI

CONCLUSIONS

From this research, the following conclusions are drawn.

1. The stress concentration factor corrected for plasticity as suggested by Hardrath and Ohman[44] appears to have better validity than the theoretical elastic stress concentration factor K_t, in predicting the strain rate behavior of 1010 cold-rolled steel.

2. When stress concentrators exist, there is an effective strain rate (greater than the nominal strain rate) which is equivalent to $K_p \dot{\epsilon}$, and consistent with the brittle material correction, $K_t \dot{\epsilon}$, as suggested by Hendrickson, et al[37].

3. The NSR versus K_t behavior of a material is an effective indication of the rate sensitivity of notched specimens of 1010 cold-rolled steel and 7075-T6 aluminum, in that, if NSR < 1 due to the presence of a notch, a high strain rate will cause additional strength reduction. Conversely, notch strengthening, NSR > 1, indicates strain rate strengthening in the presence of a notch.

4. The absence of an apparent strain rate effect found with smooth specimens of 7075-T6 aluminum is not an indication of the strain rate behavior in the presence of a notch.

5. The Orowan theory for yielding in iron[45] offers a logical explanation for observed behavior of notched and unnotched 1010 steel.

APPENDICES

APPENDIX A

LINEAR ELASTIC FRACTURE MECHANICS

The stress analysis of material containing a natural crack is the basis of linear elastic fracture mechanics. This concept was originated by Griffith[46] for use in analyzing the fracture of glass specimens containing a crack. Griffith assumed that equilibrium existed between the strain energy available for crack propagation (creation of a new surface) and the elastic strain energy available to the specimen. Catastrophic failure occurred when the total strain energy decreased with increasing crack length. This is shown schematically in Figure 40, where the total energy is the sum of the strain energy contained in a part under load (negative) and the surface energy required to form a new surface (positive). A crack will grow when the decrease in strain energy due to the growth of a crack exceeds the surface energy required for crack propagation.

$$\Delta U_T = \Delta U_\gamma - \Delta U \quad , \tag{8}$$

where

ΔU_T = total energy change in the system

ΔU_γ = surface energy change required for crack formation

ΔU = decrease in strain energy due to presence of crack

Substituting in Equation (8) the equations for these energy terms yields

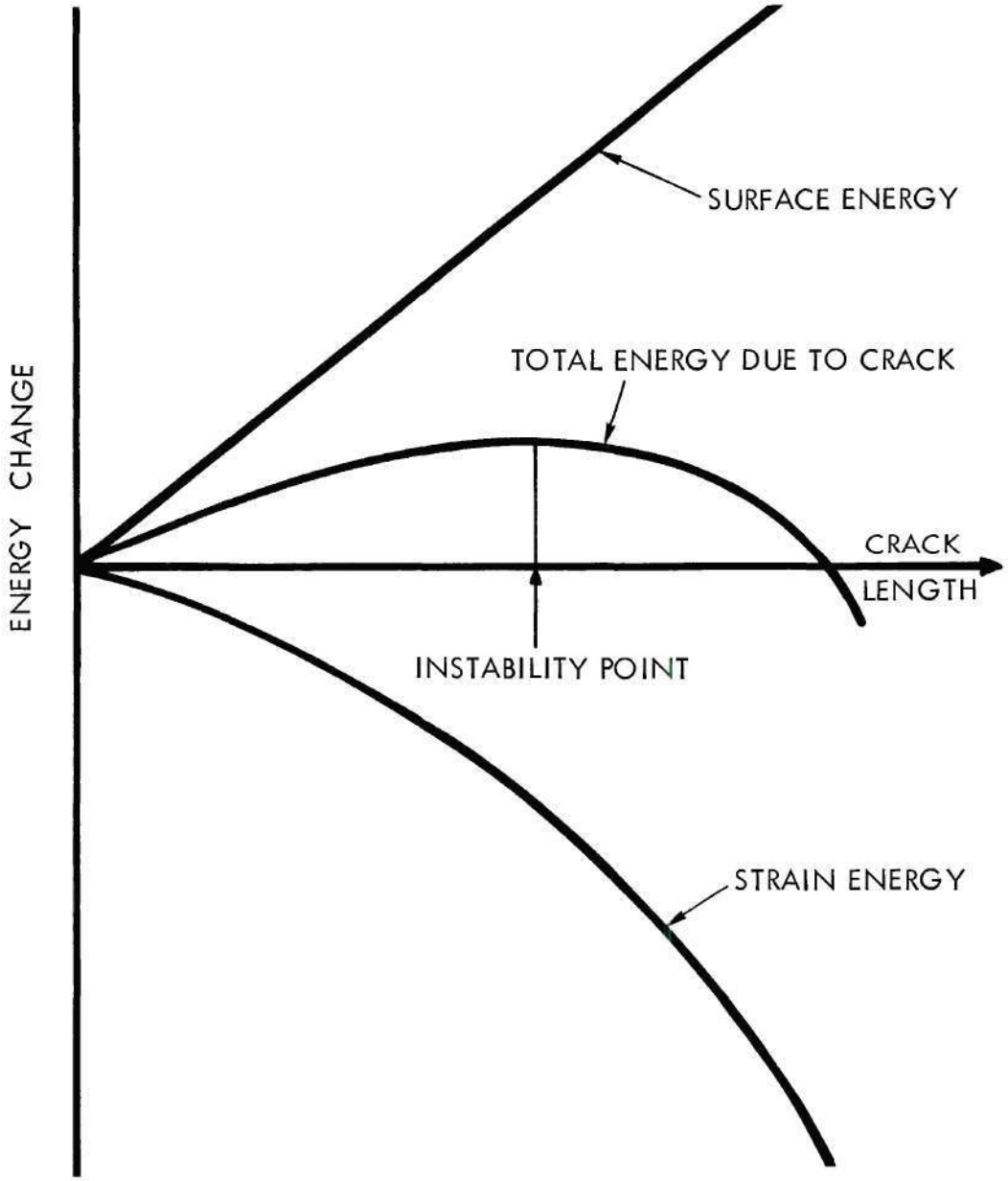

Figure 40. Energy Balance for Crack in Infinite Elastic Plate

$$\Delta U_T = 4 c \gamma - \frac{\pi \sigma^2 c^2}{E} \quad ,$$

where

c = half crack length

γ = surface energy of the material

σ = stress on the part

E = Young's modulus

The instability point (crack propagation with no increase in load) occurs when the slope of the critical total energy curve is zero, as shown in Figure 40. This occurs when

$$\frac{\partial(\Delta U_T)}{\partial c} = 0 \quad ,$$

or when

$$0 = 4 \gamma - \frac{2 \pi \sigma^2 c}{E} \quad ,$$

or

$$\sigma = \sqrt{\frac{2 E \gamma}{\pi c}} \quad . \qquad (9)$$

Griffith was able to predict the failure stress for glass, using Equation (9), from the measurements of the crack length and surface energy.

Two difficulties are encountered when Equation (9) is applied to engineering materials: (1) the surface energy at room temperature is very difficult to measure, and (2) deformation in the vicinity of the

crack is not considered.

Orowan[47] added a plastic work term, W_p, proportional to the crack length, to the surface energy term, γ, to obtain the modified Griffith equation:

$$\sigma = \sqrt{\frac{2\,E(\gamma+W_p)}{\pi\,c}} \quad .$$

At about the same time, Irwin[48] suggested that $2(\gamma+W_p)$ could be replaced by a single term $\mathcal{G}$, which is a material constant.

$$2(\gamma+W_p) = \mathcal{G} \quad .$$

Experimental tests for $\mathcal{G}$ could then be made, the value of $2(\gamma+W_p)$ obtained directly, and γ would not be needed as an independent variable. The equation suggested by Irwin is:

$$\sigma = \sqrt{\frac{E\,\mathcal{G}}{\pi\,c}} \quad . \tag{10}$$

Irwin further postulated that failure would occur when $\mathcal{G}$, or the strain energy release rate, reached a critical value, $\mathcal{G}_c$. Failure would, therefore, occur when:

$$\mathcal{G}_c = \frac{\sigma^2 \pi\, c}{E} \quad , \tag{11}$$

or

$$E\,\mathcal{G}_c = \sigma^2 \pi\, c \quad .$$

Each of the preceding analyses does not consider the stress distributior in the vicinity of the crack, but rather the thermodynamics of the system. The thermodynamics provides a necessary condition for fracture, in that the total energy of the system and crack growth will proceed catastrophically. However, it is clear that the Griffith criterion need not be sufficient for fracture if the local stress at the tip of the crack is not sufficiently high to cause the atomic bonds to break. Orowan showed that, using the stress concentration concept with a sharp notch, the local stresses were sufficiently high to cause fracture, thus establishing both the necessary and sufficient conditions for fracture. However, the stress analysis used was that for an ellipse in an infinite body and not that for a true crack.

Westergaard[49] developed a complex potential function that would determine the stresses associated with a crack tip. These were first given by Irwin as:

$$\left.\begin{aligned} \sigma_x &= K \frac{\cos\frac{\theta}{2}}{\sqrt{2r\pi}}\left(1-\sin\frac{\theta}{2}\sin\frac{3\theta}{2}\right) \\ \sigma_y &= K \frac{\cos\frac{\theta}{2}}{\sqrt{2r\pi}}\left(1+\sin\frac{\theta}{2}\sin\frac{3\theta}{2}\right) \\ \sigma_{xy} &= K \frac{\cos\frac{\theta}{2}}{\sqrt{2r\pi}}\sin\frac{\theta}{2}\cos\frac{3\theta}{2} \quad , \end{aligned}\right\} \qquad (12)$$

in terms of the coordinates r and θ from the crack tip, as shown in Figure 41, where K is a crack shape factor, $K \propto \sigma\sqrt{c}$.

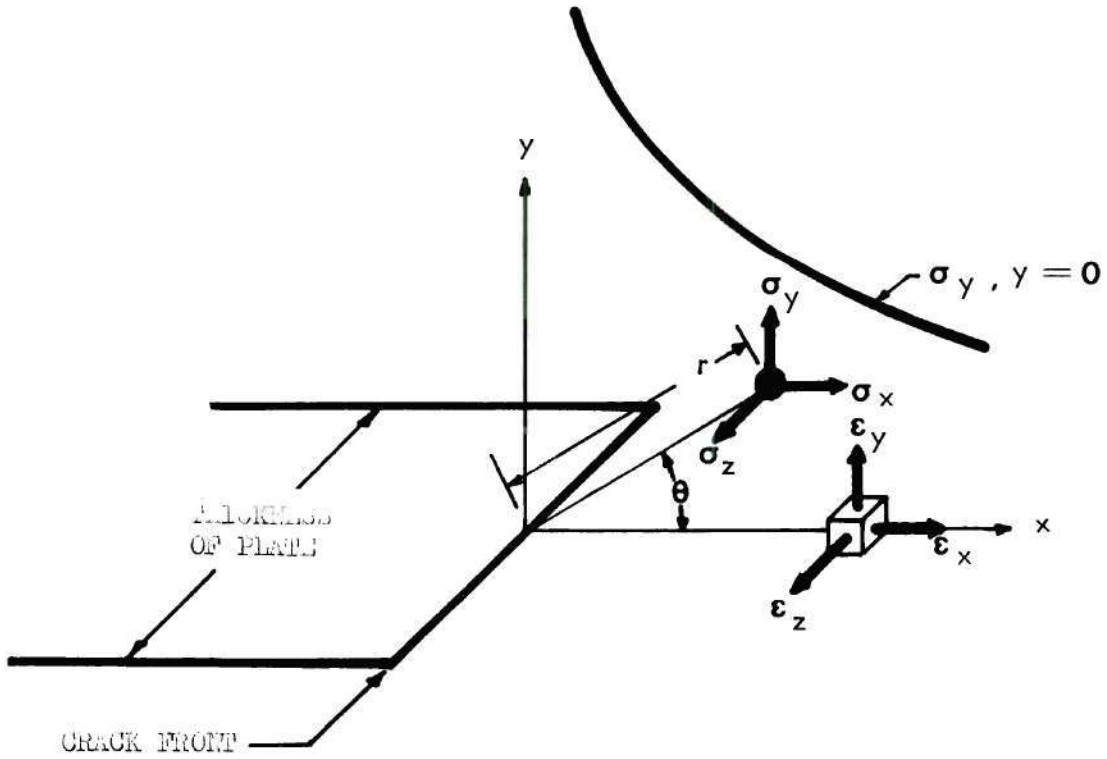

Figure 41. Elastic Stress Distribution in the Vicinity of a Sharp Crack

When $\theta = 0$, $\sigma_y = \frac{K}{\sqrt{2\pi r}}$, or $\sigma_y\sqrt{2\pi r} = \sigma\sqrt{c} \propto K$, then

$$\sigma_y^2 \, 2\pi r = \sigma^2 c \propto K^2 \quad . \tag{13}$$

The similarity to Equation (11) is noted with $E\mathcal{G}$ equivalent to K^2. The K at the crack tip is then equal to

$$K^2 = \sigma^2 \pi c \quad , \tag{14}$$

and from Equation (11)

$$E\mathcal{G} = K^2 \alpha \quad . \tag{15}$$

The factor α accounts for the stress condition at the crack tip and will be either of two values:

$$\alpha = 1 \text{ for plane stress}$$

$$\alpha = 1 - \nu^2 \text{ for plane strain}$$

where ν = Poisson's ratio.

The term K is referred to as a stress intensity factor. Researchers in this field began to determine K rather than $\mathcal{G}$, since the inclusion of Young's modulus with a fracture toughness measurement simplified comparison of materials.

The term K_c was used for critical stress intensity factor, i.e., the value of K when failure would occur. At first, $\mathcal{G}_c$ and K_c were considered to be material constants; however, variations with specimen size were noted in determinations of the values. Irwin[50] reported a variation of K_c with material thickness for 7075-T6 aluminum, shown in Figure 42.

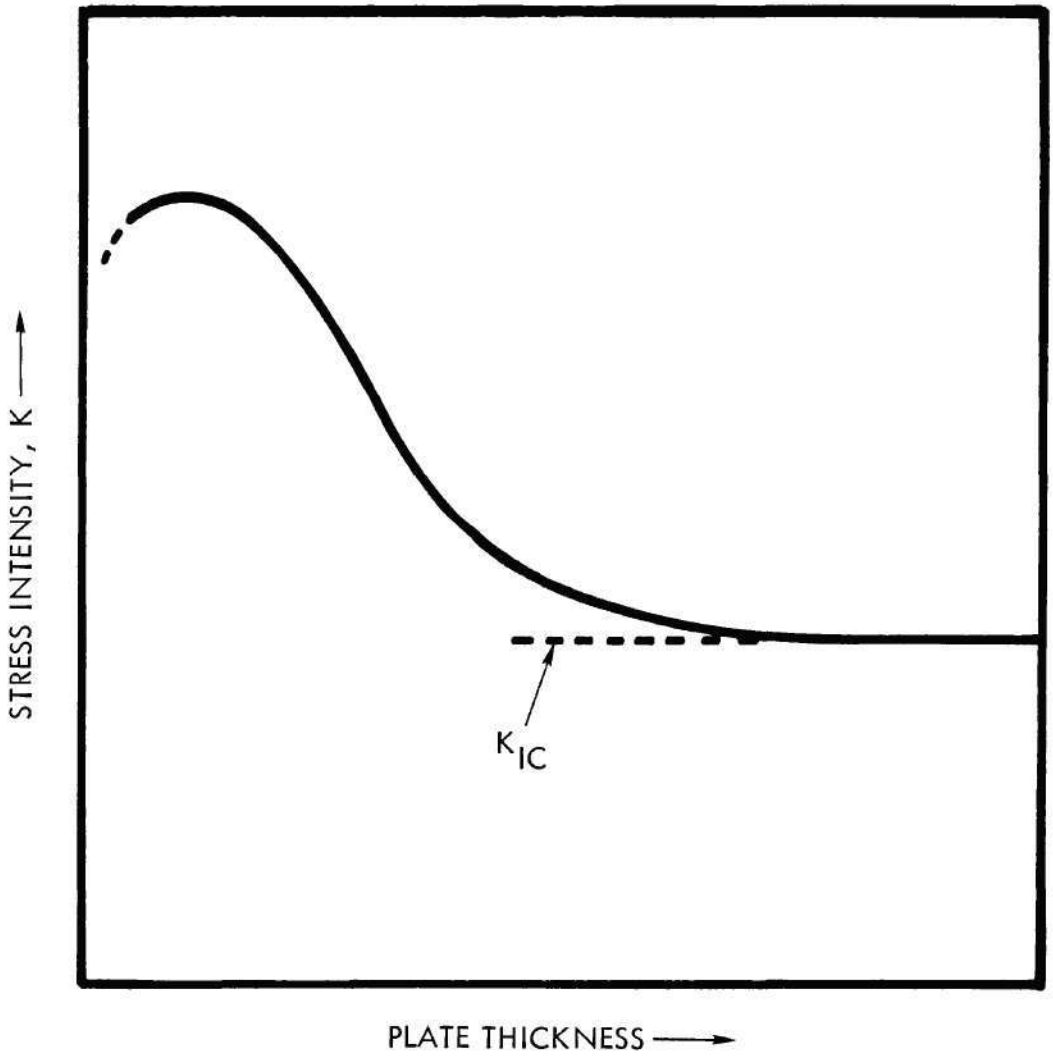

Figure 42. Variation of Stress Intensity with Plate Thickness

Hanna and Steigerwald[51] have verified the thickness variation for other materials. The lowest value of K_c is obtained on thick specimens where constraint at the crack tip in the thickness direction (z) is at a maximum, i.e., $\epsilon_z \rightarrow 0$. Using "constraint at the crack tip" to characterize the stress state, in general, the minimum constraint in a thin material is associated with plane stress, $\epsilon_z \equiv \nu(\epsilon_x+\epsilon_y)$, and maximum constraint in a thick material is associated with plane strain, $\epsilon_z \rightarrow 0$.

The minimum K_c (or $\mathscr{G}_c$) value associated with thick sections (plane strain) was designated K_{Ic} (or $\mathscr{G}_{Ic}$). The I stands for the first opening mode of the crack, a crack in a material loaded so that all displacements of the crack faces are normal to the plane of the crack ($\epsilon_y > 0$, $\epsilon_z \rightarrow 0$, $\epsilon_x \rightarrow 0$) (cf. Figure 41).

The thickness of material required for plane strain conditions to be present depends on the extent of plastic deformation at the crack tip. The plastic zone size is found by setting σ_y in Equation (12) equal to σ_{ty} for $\theta = 0$, and solving for r:

$$r_p = \frac{1}{\beta\pi}\frac{\sigma_{ty}^2}{K_{Ic}^2} \quad , \tag{16}$$

where

r_p = the radius of the plastic zone

σ_{ty} = yield stress of the material in uniaxial tension

$\beta = 6$ for plane strain

$\beta = 2$ for plane stress .

The criterion that $2\,r_p$ must be less than the plate thickness has

been established for the plane strain analysis to be valid. Research in linear elastic fracture mechanics testing has been concentrated on K_{Ic} testing rather than the testing of thinner materials, where $K_c(B)$ would be established. $K_c(B)$ symbolizes K_c as a function of the thickness B. This has come about because $K_c(B)$ is much more difficult to analyze theoretically and because the primary interest in brittle fracture was concentrated in areas where thick materials are used extensively. Consequently, most data available on variation of fracture toughness with strain rate are in terms of K_{Ic}.

APPENDIX B

DETERMINATION OF STRESS CONCENTRATION FACTOR FOR TEST SPECIMENS

Stress concentration theory is usually not specific enough to allow the application of formula to a configuration of interest and to determine a K_t value. This is so primarily because the assumption of an infinite specimen is made in development of the theory. In many cases, the configuration of interest will have dimensions large enough with respect to a discontinuity that the infinity assumption does not introduce a measurable error. The configuration of a tension member containing a notch is solved theoretically by the combination of two solutions, each for an infinite member. The solution as described by Peterson[13] based on the solutions of Neuber[14] is as follows.

1. Shallow Elliptical Notch in Infinite Body (Figure 43)

   For these boundary conditions, Neuber develops

$$K_{te} = \frac{\sigma_1}{\sigma_{nom}} = 1 + 2\sqrt{\frac{t}{r}} \quad , \tag{17}$$

where

K_{te} = theoretical stress concentration factor for a shallow notch

σ_1 = stress for the notch root

σ_{nom} = nominal stress in the bulk material

t = depth of the notch

r = minimum radius at the notch root.

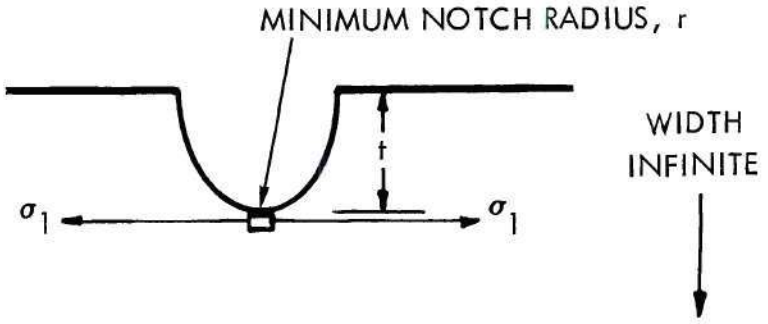

Figure 43. Shallow Elliptical Notch in Infinite Member

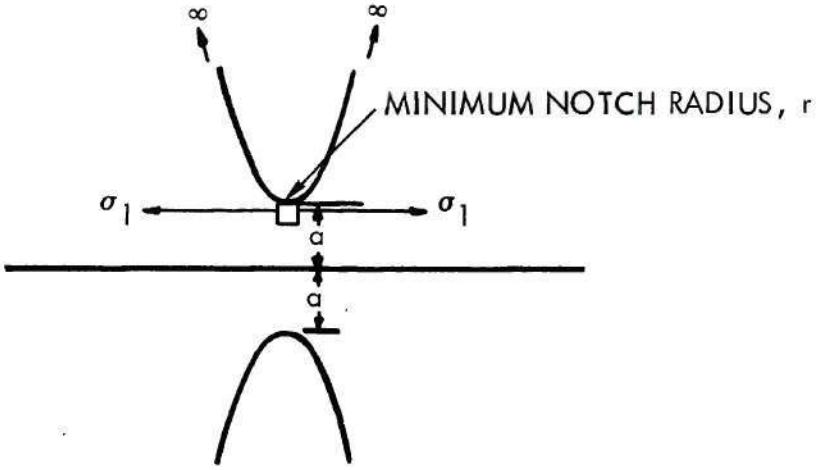

Figure 44. Deep Hyperbolic Notch in Infinite Member

2. Deep Hyperbolic Notch in Infinite Body (Figure 44)

For these boundary conditions, Neuber develops

$$K_{th} = \frac{\sigma_1}{\sigma_{nom}} = \frac{2\left(\frac{a}{r} + 1\right)\sqrt{\frac{a}{r}}}{\left(\frac{a}{r} + 1\right)\tan^{-1}\sqrt{\frac{a}{r}} + \sqrt{\frac{a}{r}}} \quad , \tag{18}$$

where

K_{th} = theoretical stress concentration factor in an infinite body

σ_1 = stress at the notch root

$\sigma_{nom} = \frac{P}{2ah}$

P = load

a = half minimum width

h = thickness

r = minimum radius at the notch root.

Neuber assumed that, for a finite member, some relationship between K_{te} and K_{th} exists. He proposed the following:

$$\frac{1}{(K_t-1)^2} = \frac{1}{(K_{te}-1)^2} + \frac{1}{(K_{th}-1)^2} \quad ;$$

hence,

$$K_t = 1 + \frac{(K_{te}-1)^2 \quad (K_{th}-1)^2}{(K_{te}-1)^2 + (K_{th}-1)^2} \quad . \tag{19}$$

This relation, shown in Figure 45, agrees with the end conditions of both solutions, and Peterson[13] states that it will be reasonably

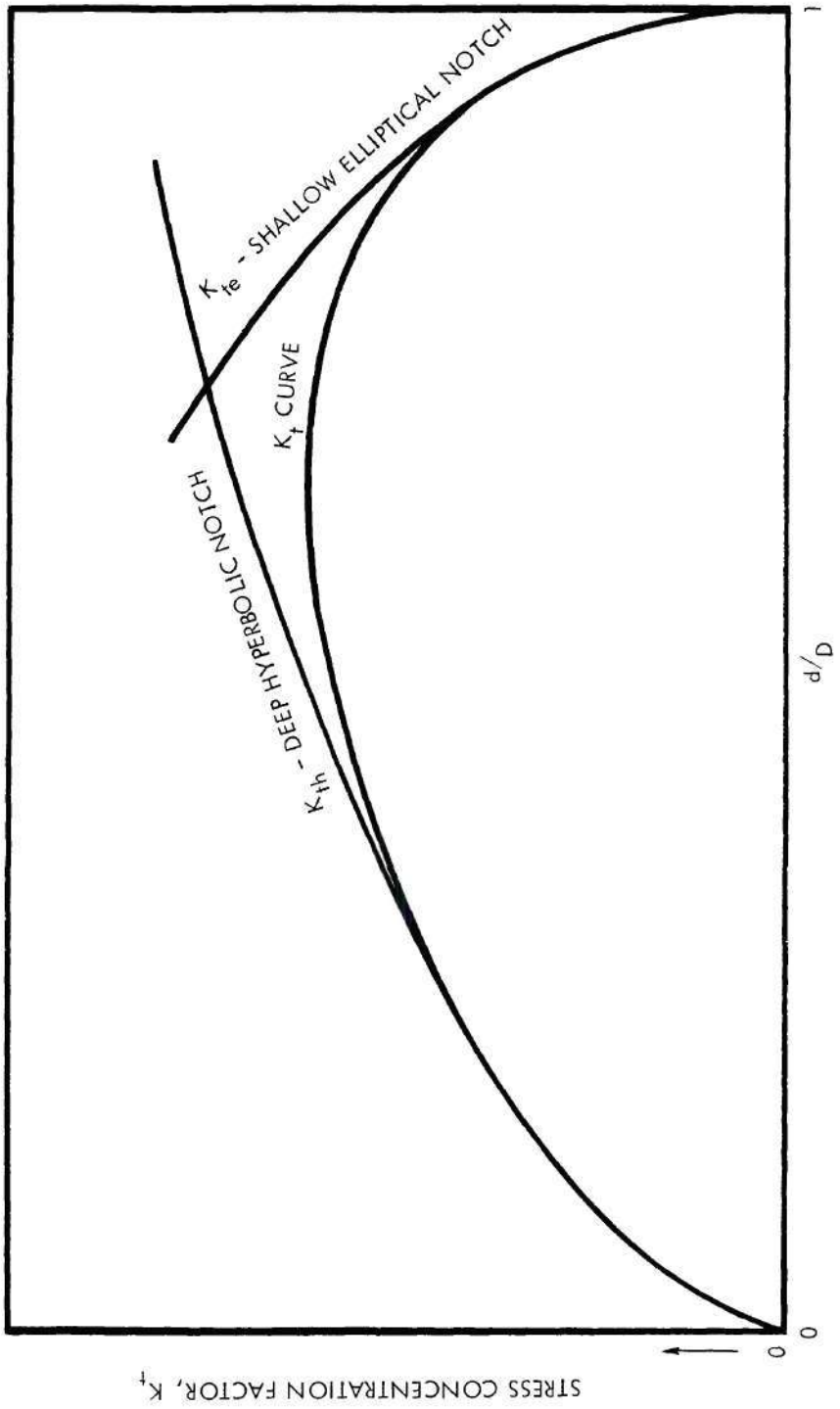

Figure 45. Neuber Analysis for Notched Flat Bars Loaded in Tension

accurate in the intermediate region. Peterson's reasoning is based in part on the experimental results of Durelli and Jacobson[52].

The quadratic relation, Equation (19), could be solved for each case in question; however, Peterson developed a family of curves which are solutions to Equation(19) for a wide variation of specimen dimensions. This family of curves given in Figure 46 was used to determine the K_t's reported herein.

One additional factor must be considered. The solutions discussed are for hyperbolic and elliptical notches, and most notches encountered in practice are not of these shapes. The radius at the tip of the hyperbola or ellipse and the depth of penetration were the only dimensions that entered into the equations for K_t. It is assumed then that Equation (19) is valid for any notch shape and that the only critical dimensions are the depth and the tip radius. Leven and Frocht[53] have shown that this assumption is valid unless the flank angle is too large. The flank angle is the included angle between the notch sides. If this angle does not exceed 60°, Equation (19) may be used with reasonable accuracy.

From the experimental evidence of Leven and Frocht showing deviations at large K_t values, there was reason to doubt that a $K_t = 14.7$ notch was really obtained in this test program. The actual K_t was assumed to be about 10 percent lower than the calculated value: $K_t = 14.7 - 0.10\ (14.7) = 13.2$, or $K_t \cong 13$. The fact that the sharpest notch could have a slightly higher or lower K_t does not change any conclusions or trends shown here.

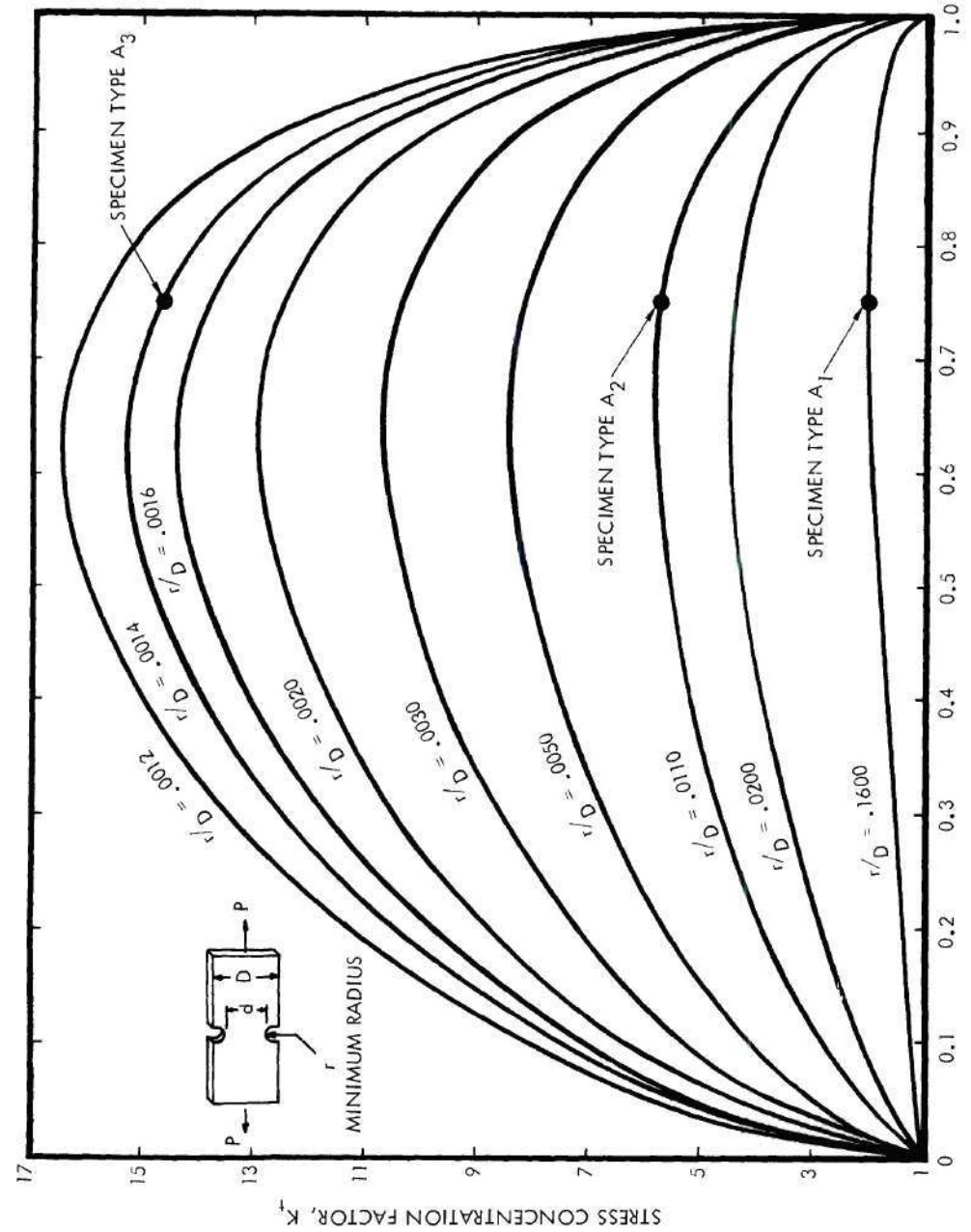

Figure 46. Stress Concentration Factor for a Notched Flat Bar Loaded in Tension

BIBLIOGRAPHY

1. P. Ludwik, "Deformation Speed and Its Influence on the After Effects," Physikalische Zeitschrift, Vol. 10, June 15, 1909, pp. 411-417.

2. W. P. Roe and J. R. Kattus, "Tensile Properties of Aircraft-Structural Metals at Various Rates of Loading After Rapid Heating," Southern Research Institute, WADC TR 55-199, Part I, May, 1955, Part II, August, 1956, and Part III, July, 1957.

3. T. A. Trozera, O. D. Sherby, and J. E. Dorn, "Effect of Strain Rate and Temperature on the Plastic Deformation of High Purity Aluminum," Transactions of the American Society for Metals, Vol. 49, 1957, pp. 173-188.

4. P. E. Duwez, D. S. Wood, D. S. Clark, "Dynamic Tests of the Tensile Properties of SAE 1020 Steels, ARMCO Iron and 2017 Aluminum Alloy," NRDC Report No. A182, May, 1943.

5. "Short Time Elevated-Temperature Mechanical Properties of Metals Under Various Conditions of Heat Treatment, Heating, Exposure Time, and Loading," Contract No. DA-01-009-ORD-491, Summary Report to ABMA, Southern Research Institute, July 17, 1959.

6. H. E. Dedman, E. J. Wheelaham, and J. R. Kattus, "Tensile Properties of Aircraft Structural Metals of Various Rates of Loading After Rapid Heating," Southern Research Institute, WADC TR 58-440, Part I, October, 1958, and Part II, February, 1959.

7. F. R. Schwartzberg, "Effects of High Strain Rates and Rapid Heating on the Tensile Properties of Titanium Alloys," Defense Metals Information Center, DMIC Memorandum 4, December 29, 1958.

8. J. B. Preston and J. R. Kattus, "Determination of the Mechanical Properties of Aircraft-Structural Materials at Very High Temperatures After Rapid Heating," WADC TR 57-649, Part II, Southern Research Institute, April, 1960.

9. J. G. Kaufman, "Summary Report of the Effects of High Strain Rates on the Mechanical Properties of Aluminum Alloys," Aluminum Company of America, Alcoa Research Laboratory Report No. 9-60-31, August 15, 1960.

10. D. P. Moon and J. E. Campbell, "Effects of Moderately High Strain Rates on the Tensile Properties of Metals," Defense Metals Information Center, DMIC Memorandum 142, December 18, 1961.

11. Metallic Materials for Aerospace Vehicle Structures, Mil-HDBK-5A, February 8, 1966, Department of Defense, Washington 25, D. C.

12. W. L. Cowell, "Dynamic Tests of Structural Aluminum Alloys," U. S. Naval Civil Engineering Laboratory, Port Hueneme, California, Technical Report R478, AD 640369, September, 1966.

13. R. E. Peterson, Stress Concentration Design Factors, John Wiley & Sons, Inc., New York, 1953.

14. H. Neuber, Theory of Notch Stresses: Principles for Exact Calculation of Strength with Reference to Structural Form and Material, Translation by U.S.A.E.C. Office of Technical Information, AEC TR-4547, 1961, of Second German Edition, 1958.

15. G. V. Savin, Stress Concentration Around Holes, Translated from the Russian, Pergamon Press, New York, 1961.

16. M. M. Frocht, Photoelasticity, Vol. I and Vol. II, John Wiley & Sons, Inc., New York, London, 1941, 1948.

17. A. J. Durelli and W. F. Riley, Introduction to Photomechanics, Prentice-Hall, Englewood Cliffs, N. J., 1965.

18. G. Sachs and J. G. Sessler, "Effects of Stress Concentration on Tensile Strength of Titanium and Steel Alloy Sheet at Various Temperatures," American Society for Testing and Materials, STP 287, p. 122.

19. P. F. Packman, "Crack Initiation in Crystalline Materials," Ph.D. Dissertation, Syracuse University, July, 1964.

20. V. Weiss, J. Sessler, P. Packman, and G. Sachs, "The Effect of Several Geometrical Variables on the Notch Tensile Strength of 4340 Steel Sheet Heat Treated to Three Strength Levels," WADD Technical Report 60-310, June, 1960.

21. C. Zener and J. H. Hollomon, "Plastic Flow and Rupture of Metals," Transactions of the American Society for Metals, Vol. 33, 1944, p.163.

22. C. Zener and J. H. Hollomon, "Effect of Strain Rate Upon the Plastic Flow of Steel," Journal of Applied Physics, American Institute of Physics, Vol. 15, 1944, p. 22.

23. J. H. Hollomon and C. Zener, "Conditions of Fracture of Steel," Transactions of the American Institute of Mining and Metallurgical Engineers, Vol. 158, 1944, p. 283.

24. J. H. Hollomon, "The Mechanical Equation of State," Transactions of the American Institute of Mining and Metallurgical Engineers, Vol. 171, 1947, p. 535.

25. H. Conrad and S. Frederick, "The Effect of Temperature and Strain Rate on the Flow Stress of Iron," ACTA Metallurgica, Vol. 10, November, 1962, p. 1013.

26. H. Conrad, "Comment on 'The Effect of Carbon on the Strain Rate Sensitivity of Iron Single Crystals,'" ACTA Metallurgica, Vol. 15, 1967, p. 147.

27. D. L. Davidson, U. S. Lindholm, and L. M. Yeakley, "The Deformation Behavior of High Purity Polycrystalline Iron and Single Crystal Molybdenum as a Function of Strain Rate at 300°K," ACTA Metallurgica, Vol. 14, June, 1966, p. 703.

28. P. G. Gillis, "Dislocation Dynamics and Strain Rate Effects," Applied Polymer Symposia, No. 1, 1965, p. 1-12.

29. J. A. Hendrickson and D. S. Wood, "The Effect of Rate of Stress Application and Temperature on the Upper Yield Stress of Annealed Mild Steel," Transactions of the American Society for Metals, Vol. 50, 1957, p. 498.

30. A. R. Rosenfield and G. T. Hahn, "Numerical Descriptions of the Ambient Low-Temperature, and High-Strain Rate Flow and Fracture Behavior of Plain Carbon Steel," Transactions of the American Society for Metals, Vol. 59, 1966, p. 962.

31. C. M. Glass, J. I. Misey, S. K. Golaski, and G. L. Moss, "A Metallurgical Study of High Strain Rate Deformation," U. S. Army Ballistic Research Laboratories, Aberdeen Proving Ground, Maryland, Report No. AFWL-TR-66-7, AD 629921, March, 1966.

32. J. E. Dorn, J. Mitchell, and F. Hauser, "Dislocation Dynamics," Experimental Mechanics, November, 1965, p. 353.

33. W. C. Leslie and R. J. Sober, "The Strength of Ferrite and Martensite as Functions of Composition, Temperature, and Strain Rate," Transactions of the American Society for Metals, Vol. 60, 1967, pp. 459-484.

34. A. R. Rosenfield, E. Votava, and G. T. Hahn, "Dislocations and the Ductile-Brittle Transition," Battelle Memorial Laboratories, Columbus, Ohio, Report prepared for American Society for Metals Weekend Seminar, "Ductility-Limitations and Utilization," October, 1967, National Metal Congress, Cleveland, Ohio.

35. J. F. Knott, "On Stress Intensifications in Specimens of Charpy Geometry Prior to General Yield," Journal of Mechanics and Physics of Solids, Vol. 15, Pergamon Press, Ltd., 1967, pp. 97-103.

36. A. Gilbert and B. A. Wilcox, "Further Investigation of Notch Sensitivity of Refractory Metals," Technical Report AFML-TR-65-286, 1965.

37. J. A. Hendrickson, D. S. Wood, and D. S. Clark, "The Initiation of Brittle Fracture in Mild Steel," Transactions of the American Society for Metals, Vol. 50, 1958, p. 56.

38. V. Weiss and J. G. Sessler, "Analysis of Effects of Test Temperature on the Notch Strength of High-Strength Sheet Alloys," American Society for Testing and Materials, STP 302, 1961.

39. H. T. Corten and A. K. Shoemaker, "Fracture Toughness of Structural Steels as a Function of the Rate Parameter T ln $A/\dot{\epsilon}$," American Society for Testing and Materials, STP 302, 1961, p. 122.

40. J. M. Krafft and A. M. Sullivan, "Effects of Speed and Temperature on Crack Toughness and Yield Strength in Mild Steel," Naval Research Laboratory Report No. 5776, April 30, 1962.

41. G. R. Irwin, "Basic Concepts for Dynamic Fracture Testing," Presented at AWS-ASME Metals Engineering Session, 49th Naval Meeting of the American Welding Society, April, 1968, Chicago, Illinois.

42. "High-Rate Testing at Reynolds," Closed-Loop, Vol. 1, No. 6, Published by MTS Systems Corporation, 1968.

43. H. Neuber, "Theory of Stress Concentration for Shear-Strained Prismatic Bodies with Arbitrary Nonlinear Stress-Strain Law," Transactions of the American Society of Mechanical Engineers, December, 1961.

44. H. F. Hardrath and L. Ohman, "A Study of Elastic and Plastic Stress Concentration Factors Due to Notches and Fillets in Flat Plates," NACA-TR 1117.

45. E. Orowan, "Theory of the Yield Phenomenon in Iron," MIT Preprint No. 879, December 18, 1967.

46. A. A. Griffith, "The Phenomena of Rupture and Flow of Solids," Philosophical Transactions of the Royal Society (London), Series A, Vol. 221, 1920, pp. 163-198.

47. E. Orowan, "Energy Criteria of Fracture," Welding Research Supplement, Vol. 20, 1955, p. 157.

48. G. R. Irwin, "Onset of Fast Crack Propagation in High Strength Steel and Aluminum Alloys," NRL Report 4763, Proceedings, 1955 Sagamore Conference on Ordnance Materials, Vol. II, Syracuse University Press, N. Y., 1956.

49. H. M. Westergaard, "Bearing Pressures and Cracks," Transactions of American Society of Mechanical Engineers, Vol. 61, 1939, A49-A53.

50. G. R. Irwin, "Fracture Mode Transition for a Crack Traversing a Plate," Journal of Basic Engineering, June, 1960.

51. G. L. Hanna and E. A. Steigerwald, "Influence of Work Hardening Exponent on Crack Propagation in High Strength Steels," AFML TR-66-139, October, 1966.

52. A. J. Durelli and R. H. Jacobson, "Discussion, Factors of Stress Concentration in Bars with Deep Sharp Grooves and Fillets in Tension," Proceedings of Society of Experimental Stress Analysis. Vol. 8, No. 2, 1951, p. 163.

53. M. M. Leven and M. M. Frocht, "Stress Concentration Factors for a Single Notch in a Flat Bar in Pure and Central Bending," Transactions of the American Society of Mechanical Engineers, Vol. 74, 1952, Applied Mechanics Section, p. 560.